REPORT DOCUMENTATION PAGE

Form Approved
OMB No. 0704-0188

1. REPORT DATE *(DD-MM-YYYY)*	2. REPORT TYPE	3. DATES COVERED *(From - To)*
05-10-2013		

4. TITLE AND SUBTITLE	5a. CONTRACT NUMBER
The Effect of Unsteady Wakes on Turbine Tip Gap Leakage	5b. GRANT NUMBER
	5c. PROGRAM ELEMENT NUMBER

6. AUTHOR(S)	5d. PROJECT NUMBER
Galvin, Christopher Dean	5e. TASK NUMBER
	5f. WORK UNIT NUMBER

7. PERFORMING ORGANIZATION NAME(S) AND ADDRESS(ES)	8. PERFORMING ORGANIZATION REPORT NUMBER

9. SPONSORING / MONITORING AGENCY NAME(S) AND ADDRESS(ES)	10. SPONSOR/MONITOR'S ACRONYM(S)
U.S. Naval Academy Annapolis, MD 21402	
	11. SPONSOR/MONITOR'S REPORT NUMBER(S)
	Trident Scholar Report no. 414 (2013)

12. DISTRIBUTION / AVAILABILITY STATEMENT

This document has been approved for public release; its distribution is UNLIMITED.

13. SUPPLEMENTARY NOTES

14. ABSTRACT

Gas turbines are found in military and civilian aircraft, ships, and power plants. Because of this widespread use, relatively small improvements in efficiency can have a large cumulative impact on energy use. The most significant source of loss and inefficiency in a gas turbine engine is tip gap leakage. Tip gap leakage occurs when flow travels across the top of the turbine blade through the small clearance space between the blade tips and the turbine casing, instead of along the length of the turbine blades. Tip gap leakage reduces the amount of force on the turbine blades, and the flow that is leaked across the tip gaps is wasted. Additionally, tip gap leakage leads to vortices that result in dissipated rotational kinetic energy and can disrupt the flow in the next stage of the turbine. In this project, experimental methods were used to study the effects of unsteadiness on gas turbine tip gap leakage. A case with steady flow and no tip gap was used as a baseline to compare to the results of the other cases. The flow patterns were studied for each of the cases and compared to see the effects of unsteadiness on tip gap vortices and end wall flows. Particle Image Velocimetry, PIV, was used to collect velocity fields upstream of the blades, inside the blade passage and in planes perpendicular to the flow downstream of the blades. These data will be used to help limit the negative effects of tip gap leakage and make gas turbine engines more efficient.

15. SUBJECT TERMS

Gas Turbine, Tip Gap Leakage, Vortex, PIV, Wakes

16. SECURITY CLASSIFICATION OF:			17. LIMITATION OF ABSTRACT	18. NUMBER OF PAGES	19a. NAME OF RESPONSIBLE PERSON
a. REPORT	b. ABSTRACT	c. THIS PAGE		65	19b. TELEPHONE NUMBER *(include area code)*

Standard Form 298 (Rev. 8-98)
Prescribed by ANSI Std. Z39.18

U.S.N.A. --- Trident Scholar project report; no. 414 (2013)

The Effect of Unsteady Wakes on Turbine Tip Gap Leakage

by

Midshipman 1/C Christopher D. Galvin
United States Naval Academy
Annapolis, Maryland

_____

Certification of Adviser(s) Approval

Professor Ralph J. Volino
Mechanical Engineering Department

_____

_____

Assistant Professor Cody J. Brownell
Mechanical Engineering Department

_____

_____

Acceptance for the Trident Scholar Committee

Professor Maria J. Schroeder
Associate Director of Midshipman Research

_____

_____

USNA-1531-2

Abstract

Gas turbine engines are an essential source of power in the modern world. Gas turbines are found in military and civilian aircraft, ships, and power plants. Because of this widespread use, relatively small improvements in efficiency can have a large cumulative impact on energy use. The most significant source of loss and inefficiency in a gas turbine engine is tip gap leakage. Tip gap leakage occurs when flow travels across the top of the turbine blade through the small clearance space between the blade tips and the turbine casing, instead of along the length of the turbine blades. Tip gap leakage reduces the amount of force on the turbine blades, and the flow that is leaked across the tip gaps is wasted. Additionally, tip gap leakage leads to vortices that result in dissipated rotational kinetic energy and can disrupt the flow in the next stage of the turbine. Tip gap vortices also interact with the rest of the flow moving through the turbine passage, further complicating the flow pattern. In order to study to the full effects of tip gap leakage, the flow through a turbine must be modeled, including the effect of wakes from blades in upstream stages of the engine.

Experimental methods are used to study the effects of unsteadiness on gas turbine tip gap leakage. A case with steady flow and no tip gap is used as a baseline to compare to the results of the other cases. The flow patterns are studied for each of the cases and compared to see the effects of unsteadiness on tip gap vortices and end wall flows.

The total pressure loss is found for each case and related to the energy dissipated by secondary aerodynamic losses. Additionally, the dynamic pressure is recorded at various places along the blades. The effects of the wakes on the velocity of the flow are shown by phase averaging velocity data. The velocity and turbulence of phases in and out of the wake are compared to find the effect of the wake. Additionally these phases are compared to a case with steady flow. Finally, the effects of wakes on total pressure loss are found by comparing cases with wakes to cases without wakes. Particle Image Velocimetry, PIV, was used to collect velocity fields upstream of the blades, inside the blade passage and in planes perpendicular to the flow downstream of the blades. The study shows that the locations of vortices are not affected by the passing of the wake. The locations of vortices were correlated to the regions of high pressure loss showing that the vortices were the cause of the pressure loss. Additionally the tip gap vortex was the leading cause of pressure loss studied and the pressure loss increased as the tip gap size increased. These data will be used to help limit the negative effects of tip gap leakage and make gas turbine engines more efficient.

Keywords: Gas Turbine, Tip Gap Leakage, Vortex, PIV, Wakes

Acknowledgements

Table of Contents

Introduction

Gas turbine engines are an essential means of power conversion in the modern world. Gas turbines are found in military and civilian aircraft, ships, and power plants. Because of this widespread use, relatively small improvements in efficiency can have a large cumulative impact on energy use.

A gas turbine engine has three main components: a compressor, a combustion chamber, and a turbine, as shown in Fig 1. The engine depicted in Fig 1 is a turbo fan, a type of gas turbine engine used in modern aviation where the mechanical work from the turbine powers a fan for propulsion. This study will focus on the high pressure turbine component of the gas turbine engine. A schematic of these components is shown in Fig 2. Air enters the gas turbine engine and travels to the compressor. The compressor squeezes the air through the use of rotating blades and stationary vanes, which results in an increase in both air temperature and pressure. The air then enters the combustion chamber, where fuel is injected and a chemical reaction occurs. This process creates a high temperature, high pressure, and high velocity flow that then passes through the turbine. The flow drives the turbine blades, causing the blades and the shaft to which they are attached to rotate. A turbine stage with blades on the rotor is shown in Fig 3. This rotation is used as mechanical work to power the compressor, and it can also drive mechanical elements such as a propeller shaft or an electric generator.
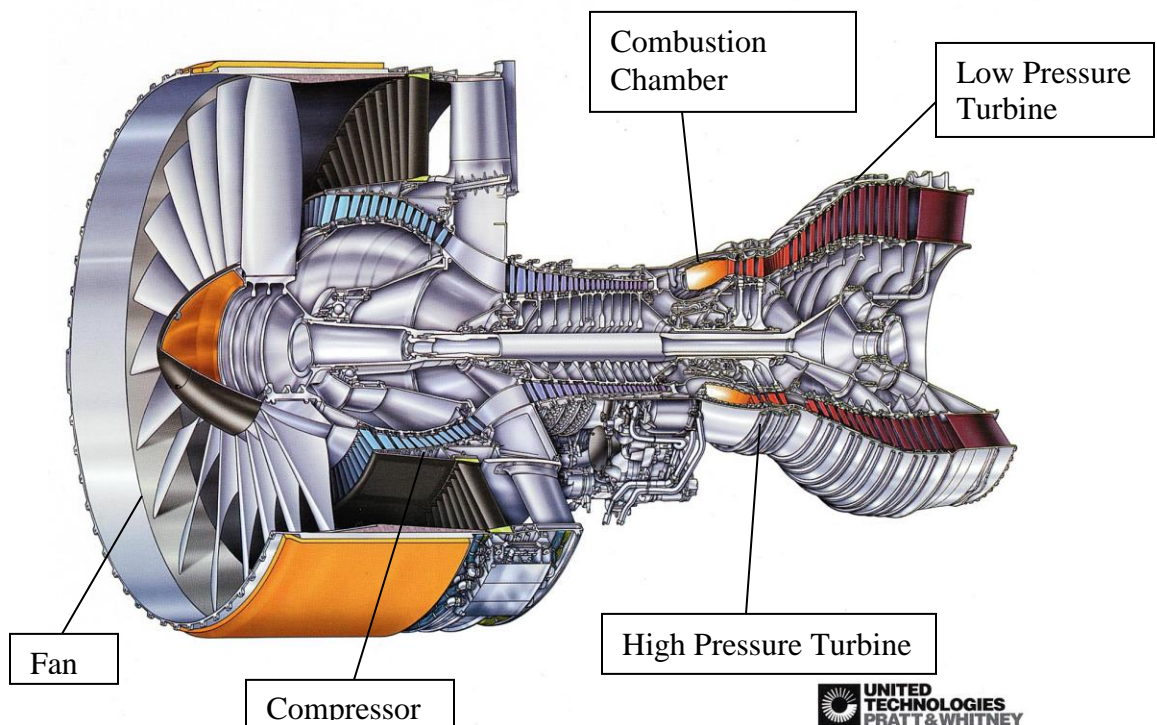

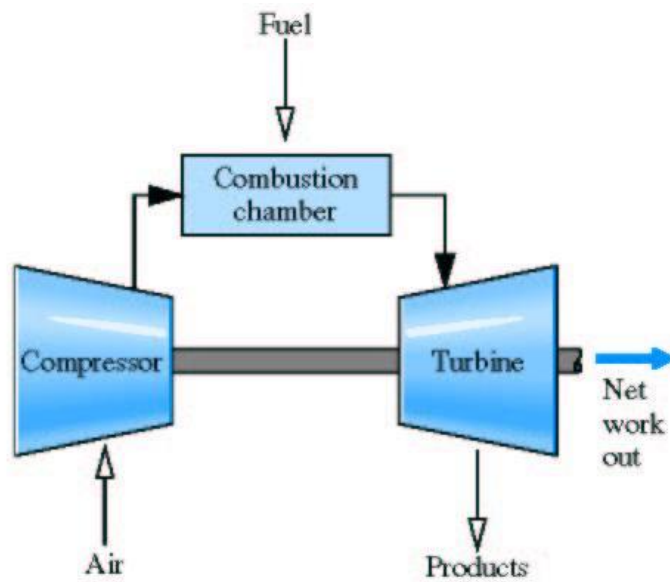**Figure 1: Cutaway of a turbine engine - Pratt and Whitney (2002).**

Figure 2: The gas turbine thermodynamic system - Cengel and Boles (2002).

The stationary vanes (all but four vanes have been removed for the photograph)

Blades attached to the rotor

Figure 3: Turbine blades on a rotor – European Commission (2004).

An increase in turbine efficiency would decrease energy costs and allow the use of smaller engines in vehicles. One method to improve the efficiency of gas turbine engines is to increase the combustion chamber's operating temperature. This method has been extensively pursued, and gas turbines now run at such high temperatures that the melting temperatures and thermal creep of the turbine blades limit further increase of temperature. The introduction of film cooling for turbine blades helps prevent thermal creep and other damage to turbine blades operating at high temperatures. Film cooling is blowing of bleed air from the compressor through holes in the turbine blades. The bleed air creates a film of cooler air around the turbine blades and lowers the impact of hot exhaust flowing across the blades.

 A second method to increase the efficiency of turbine engines is to reduce irregularities in the flow over the turbine blades. These irregularities, where the flow creates vortices, eddies, or separates from the turbine blades, cause the gas turbine engine to produce less work, reducing efficiency. One major location of flow irregularity is the endwall boundary layer. In fluid dynamics a boundary layer is a region of the flow near a surface where the fluid's viscosity greatly affects the flow. Fluid directly in contact with a surface has a relative velocity with respect to the surface of zero. This is known as the "no slip" condition at the wall. The boundary layer is the thin layer of fluid where the relative velocity increases from zero at the surface to the freestream velocity. In a turbine, the endwall boundary layer is the portion of the flow that is affected by contact with the turbine casing, at one end of the blade, or hub, at the other end as shown in Fig 4.   The endwall boundary layer flow is driven by the main flow through the passage between two blades combined with the pressure gradient across the passage. The pressure gradient drives a flow across the endwall from the high pressure (concave) side of the blade toward the suction (convex) side of the adjacent blade on the opposite side of the passage. The pressure difference between the two sides of each blade also provides the force which causes the turbine to rotate. Figure 4 shows the complicated flow structure of the endwall flow. The endwall shown is the surface of the hub where the blades are mounted. In reality the hub has curvature, but is depicted flat to make it easier to see the flows.   Endwall flows contribute to secondary losses as the kinetic energy in the vortices is eventually dissipated and cannot be used to produce useful work. Vortices are portions of the flow that undergo rotation or spin because of frictional forces as the flows moves over a surface.

Another major complication in turbine engines is the unsteadiness caused by the turbine vanes and blades moving in relation to one another. The wakes and vortices created by a turbine blade interact with the blades and vanes downstream. This creates an even more complex flow as vortices from unsteadiness interact with the endwall boundary layer.

The last main cause of losses in gas turbine engines is tip gap leakage. Unshrouded airfoils have a gap between the tip of the turbine blades and the casing of the turbine. Each blade is attached at its base to the hub endwall as shown in Fig 3, but is not attached to the opposite endwall at the tip as shown in Fig 5. Flow leaks from the high pressure side of the turbine blade to the low pressure side through the tip gap. Ideally the tip gap clearance is small to minimize leakage, but some clearance is necessary to allow for thermal expansion of the blades under hot engine conditions and to prevent the blades from rubbing against the casing.
Figure 5 shows the tip gap vortices caused by tip gap flow. The flow around the tip of the turbine blade reduces the loading on the turbine blade by reducing the mass flow of air traveling along the full length of the blade, thereby reducing the lift of the airfoil. This means less force on each blade to rotate the turbine, resulting in less power output.
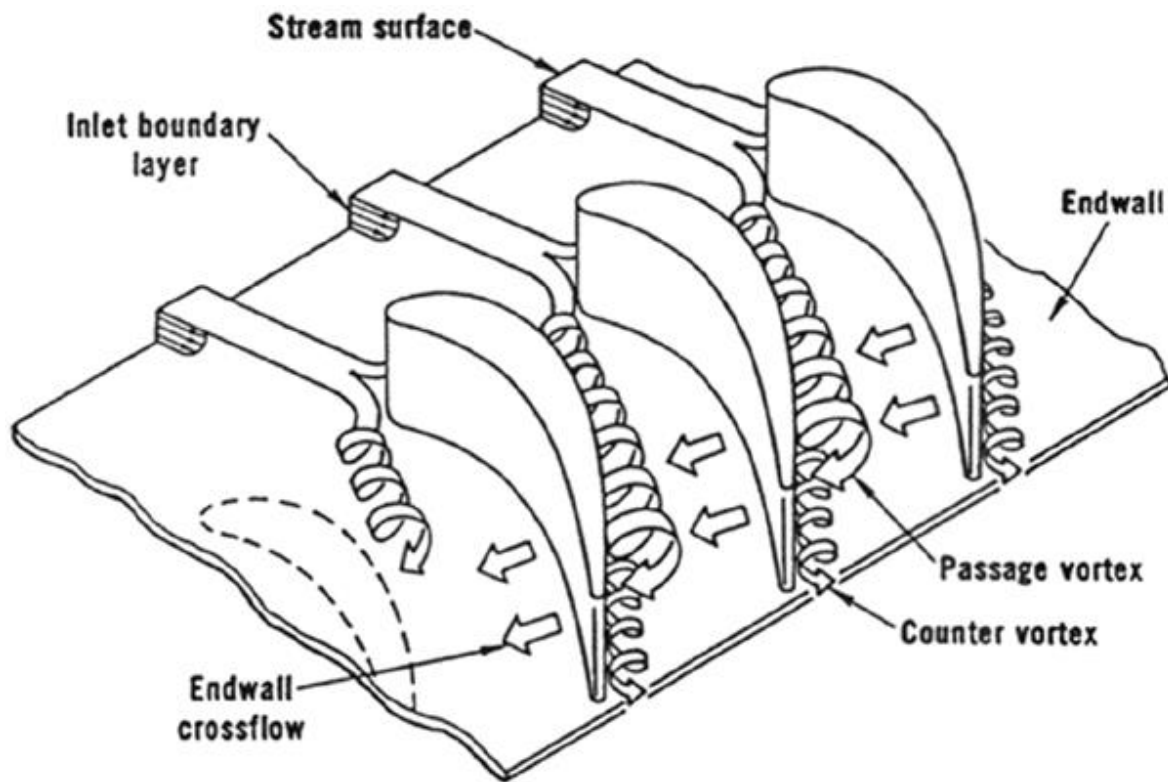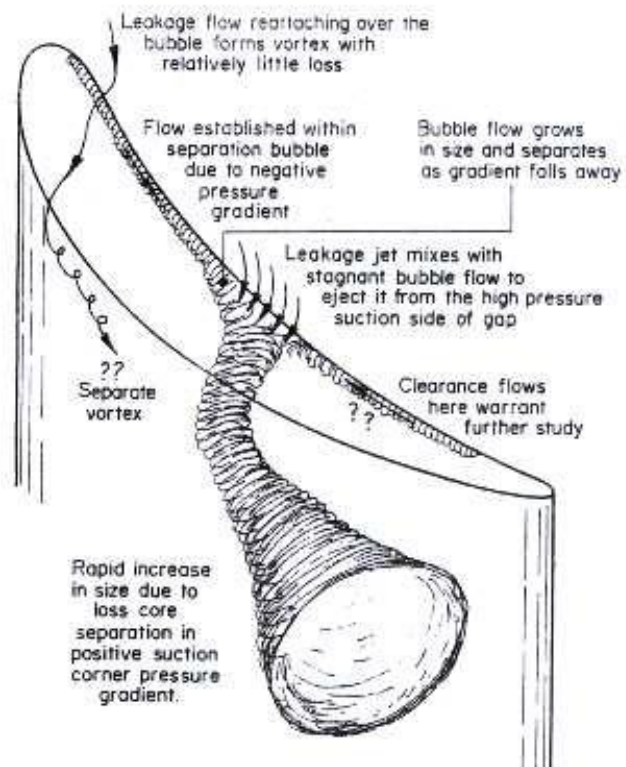
Figure 4- Endwall flow – Langston (1980)

Figure 5 - Tip gap vortices- Bindon (1989)

Langston (1980) noted that the flow interaction between the endwall boundary layer and the leading edge of the turbine blades created horseshoe vortices. The pressure gradient between the suction and pressure sides of the turbine blades interacts with the boundary layer and produces the passage vortices. The losses caused by endwall flows cause a large percentage of the aerodynamic losses in turbines. Sharma and Butler (1987) noted that endwall flows can account for 30-50% of the total losses in a turbine and that the effects are greater in low aspect ratio turbines where the endwall layer makes up a large portion of the turbine's total volume. The aspect ratio of a turbine blade is the span of the blade, the distance from hub to tip, divided by the chord length, the distance from leading edge to trailing edge. The studies described above had static airfoils and steady flow, meaning that the blades did not rotate and there was no disruption of the flow by upstream airfoils. Static airfoils under steady flow conditions ignore the important effects of unsteadiness in turbines. Because vanes and rotors move in relation to each other, their flows interact creating new sources of vorticity and further complicating the flow inside a turbine. Hodson and Howell (2005) describe the effects of wakes on airfoil rows. The vortices created by an airfoil can interact with the flow around a downstream airfoil. These vortices typically persist and interact with the endwall flow. Behr (2007) describes the interaction between airfoil rows and lists a number of previous studies that duplicated the effect of upstream airfoils through various systems. Studies have utilized rotating facilities with multiple stages and others have used a more simplified method involving cascades, a row of blades representing a part of a rotor stage, with moving upstream bars. The effects of unsteadiness are compounded with the introduction of tip gap leakage.

Denton (1993) analyzed the effects of tip leakage and determined that the flow around the tip of the turbine blade alters the mass flow on the contour of the airfoil and reduces loading on the airfoil, diminishing lift. As the flow travels around the tip of the airfoil, it enters the endwall boundary layer on the suction side of the passage, creating a shear force that creates a tip gap vortex. The energy in this vortex is eventually dissipated and is lost. Harvey (2004) also showed that the vortices from tip leakage could persist and affect downstream rows of airfoils, illustrating the need to reduce the effect of tip gap leakage. Payne (2003) showed that there were four primary sources of loss: (1) tip gap leakage, (2) wake vortex, (3) upper and (4) lower passage vortex. The results of this study showed that tip gap leakage was the largest cause of loss and that a 0.25 mm reduction in tip gap height could result in 1% reduction in fuel consumption.

Experimental Methods

To study the flow through a turbine, a model of a section of a turbine was constructed and placed in a wind tunnel where pressure and velocity measurements were recorded. Detailed measurements are much easier to make in a wind tunnel than in an actual operating engine, but the flow inside a gas turbine engine is hotter and faster than in the testing apparatus used in the experiment. In order to ensure similitude between the flow in the testing apparatus and the flow in a gas turbine engine, the Reynolds numbers were made similar. The Reynolds number is a dimensionless term that gives a ratio of inertial forces to viscous forces for the flow of a fluid. By keeping this ratio constant between two different cases, dynamic similitude in fluid flows can be ensured. The Reynolds number is calculated using (1):

$$(1) \qquad\qquad Re = \frac{u\,l}{v}$$

Where u is the velocity of the air, l is the length of the chord of the turbine blade and v is the kinematic viscosity of the air. The air velocity was chosen to maintain a Reynolds number of approximately 30,000, a value similar to the Reynolds number of the flow in a turbine. Another important property to match is the flow coefficient. The flow coefficient is a ratio of the fluid's flow speed to the speed of the blades moving relative to the vanes. As previously stated vanes are stationary, and blades rotate. In this linear cascade the blades are stationary and the vanes which are modeled by carbon fiber rods move. The relative motion between the blades and the vanes is maintained in this manner. The flow coefficient was maintained at 1. Finally the geometry of the blade passages of a gas turbine engine was similar to the geometry of the testing apparatus.

Experimental Apparatus

The apparatus used to conduct the experiments, shown in Fig 6, consists of a single cascade of turbine blades mounted in a corner test section in a low speed wind tunnel. The turbine blade shape for the experiment was the GE E^3 high pressure turbine stage 1 blade (Halila et al. 1982). The E^3 airfoil was a blade designed by General Electric for NASA to be an efficient airfoil that is available in the public domain. The use of this blade allows the airfoil dimensions used to be published without restrictions. This blade is a high pressure turbine blade design for highly loaded uses. In order to vary the tip gap height, the endwall height was designed to be adjustable.
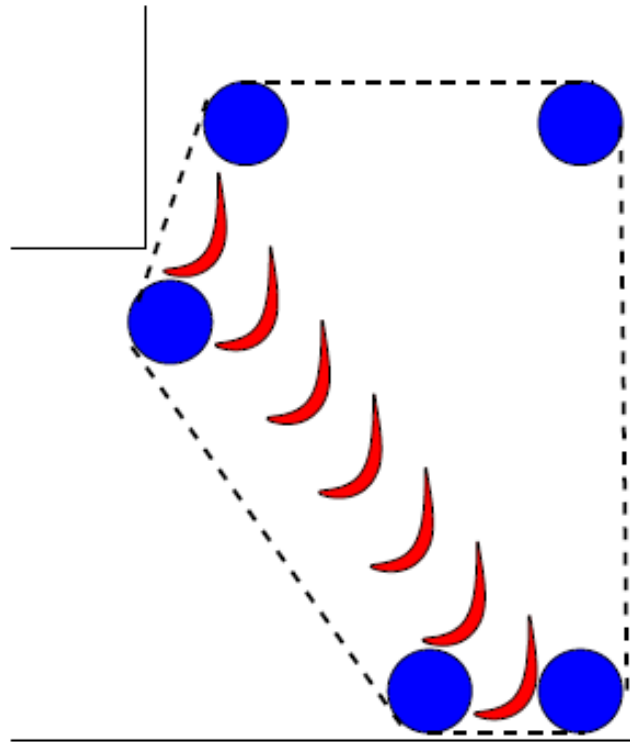

Figure 6 – Chain path around sprockets and cascade blades (red)

   To simulate the effect of wakes from upstream vanes, a wake generator from a previous study was used (Volino, 2010). The wake generator utilizes two parallel chains, which form closed loops around the cascade, extending around a series of sprockets, as shown in Fig 7 and 8. The chains pass just upstream of the airfoils and then loop back downstream. Attached to the chains are slender carbon fiber rods that extend from the top chain to the bottom chain, parallel to the span of the turbine blades. The rods are spaced at 127 mm, approximately a 1 to 1 ratio with the blade spacing. The chains are driven by two sprockets linked by a common axle. This set up ensures that the upper and lower chains and the rods move in unison. The axle is connected to a variable speed motor that drives the chains and allows for multiple speeds to be used. Because the blades are stationary in this experiment, the flow coefficient is defined as the ratio of the freestream air speed in the axial direction to the speed of the rods. The axial direction is the direction along the axis of the turbine.
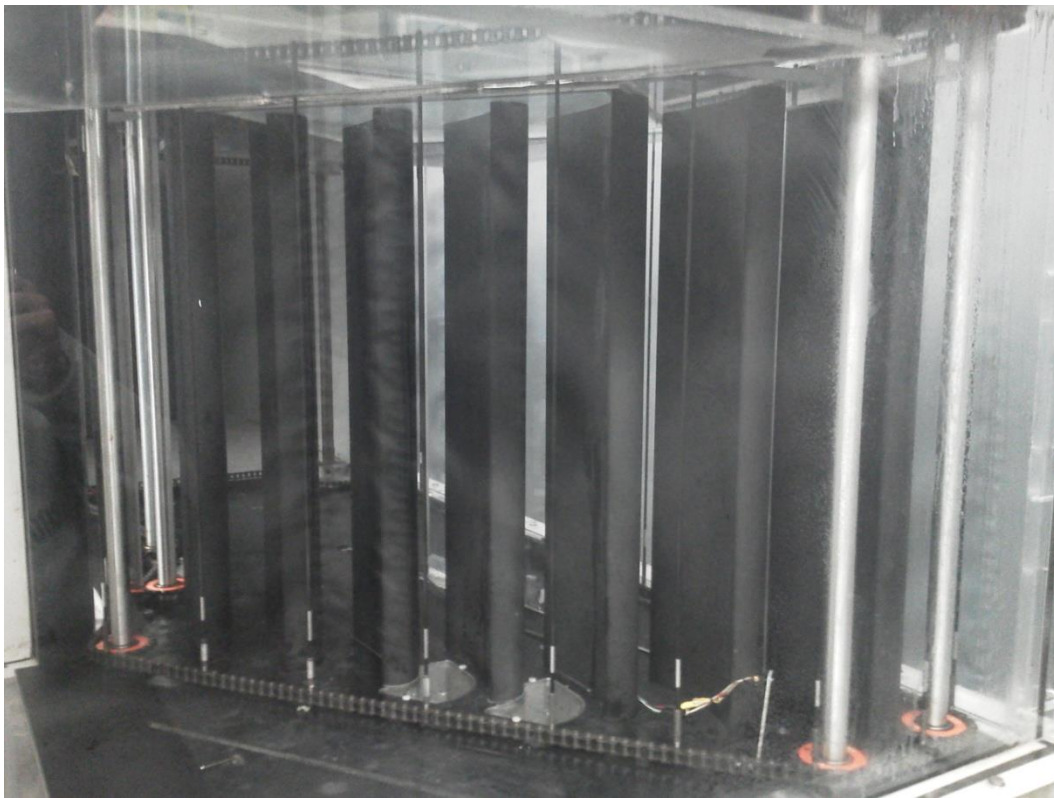

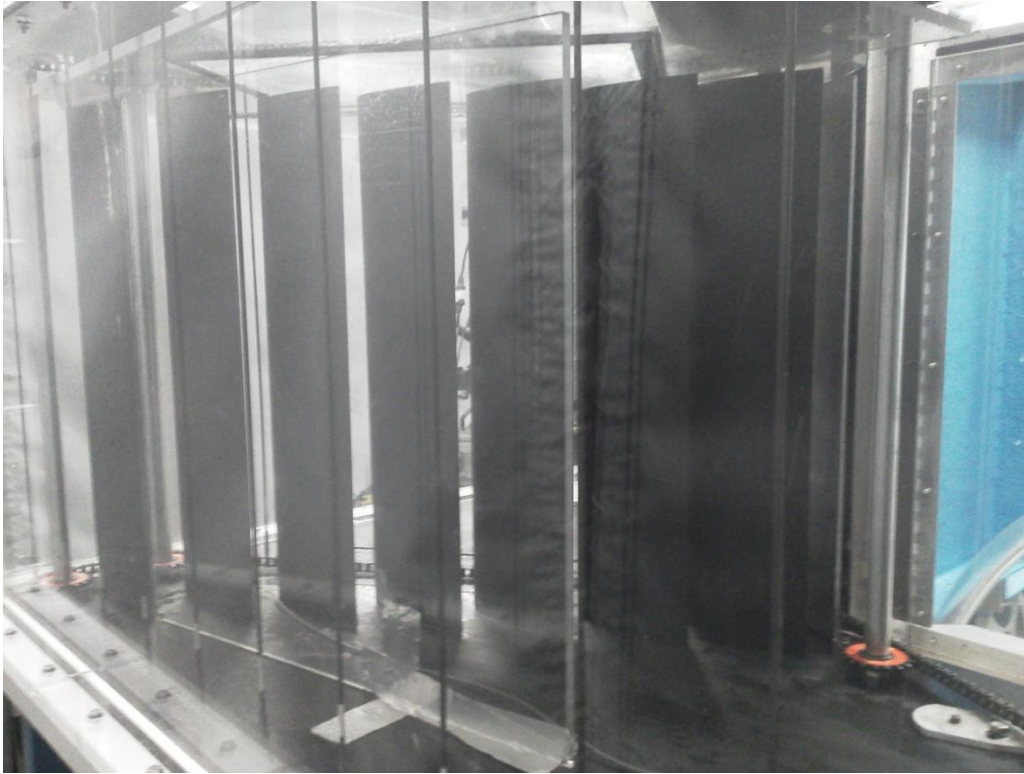**Figure 7 – Upstream of the Testing Apparatus**

Figure 8 – Downstream of the Testing Apparatus

The background freestream turbulence intensity, or FSTI, is a measure of the turbulence inherent in the flow. FSTI is the standard deviation of the velocity of the freestream as it varies in time normalized on the mean freestream velocity. In order to increase the FSTI to simulate turbine conditions in the apparatus, a grate with coarse openings was placed upstream of the blades. This grate imparts a background freestream turbulence intensity of approximately 4%. While the FSTI does not have a large effect on the flow compared to upstream wakes, 4% is typical of conditions inside gas turbine engines.

Instrumentation

The losses through the cascade are determined by measuring the drop in total pressure between the inlet and exit of the cascade. The total pressure is the pressure the flow would have if it were brought to a stop. The inlet total pressure is found by using a pitot tube placed upstream of the cascade. A pitot tube is a probe that has two ports, one that measures the total pressure and one that measures the static pressure of the flow. The dynamic pressure is the difference between the total pressure and the static pressure. The dynamic pressure from the pitot tube is used to measure the inlet velocity. A Kiel probe placed downstream of the cascade is used to measure the exit total pressure. Kiel probes, like pitot tubes also measure total pressure. However Kiel probes have a wide inlet which allows them to measure flow that is up to 20 degrees off the normal of the probe. The ability to measure flow over a wider angle is important because the exact direction of the flow leaving the cascade is unknown. Because of the complexity of the

flow downstream of the blades, the Kiel probe was traversed in a two dimensional grid parallel to the exit plane of the blade row as shown in Fig 9. Measurements were made in the endwall region and also at the midspan of the blades for comparison as shown.

The three blades that make up the center two passages have pressure taps installed at their midspan and near the tip. These pressure taps measure the static pressure at different points along the pressure and suction sides of the blades. The pressure difference between the pressure and suction side of the blade is proportional to the force of loading on the blade. In order to adjust pressures in the passages there is an acrylic tail board as shown in Fig 8. The position of the acrylic tail board, which controls flow around the outside corner of the wind tunnel, was adjusted until the pressures of the center two passages were as similar as possible. The similarity between the center two passages is necessary because flow through the passages in a turbine stage should be the same. The flow through the outer passages interacts with the walls of the wind tunnel as well as the axels for the wake generator chain drive and therefore is not similar to the flow in an engine. These outer passages serve to create proper boundary conditions for the center two passages.

Hot wires are used to measure the velocity of the flow upstream of the cascade. Hot wires are probes with a small wire placed perpendicular to the flow. The wire has a resistance and when an electric current is applied to it, the wire generates heat. The air flow cools the wire and the wire temperature is held constant. The voltage required to maintain the wire temperature is proportional to the velocity of the flow over the wire. Hot wire velocity measurements were taken upstream of the rods, upstream of the blades but behind the rods, and downstream of the blades. Velocity profiles in the endwall boundary layer show the boundary layer thickness at the inlet of the cascade. Hot wires have a fast response time and therefore were used to measure velocity differences cause by wakes from the rods. Phase averaging the velocity profiles downstream of the rods shows the effect of the rod wakes on the flow.

To understand the flow mechanisms that result in aerodynamic losses, the fluid velocity field was measured using a technique called particle image velocimetry, or PIV. PIV was used to determine two components of the local, instantaneous fluid velocity within a 2D image plane. By providing access to the spatial variations in a fluid flow, PIV can show the structures (i.e., vortices) which cause, or are caused by, aerodynamic losses. In PIV measurements particles are illuminated by a pulsed laser sheet. A camera captures two images of the illuminated particles in rapid succession. The velocity field can be mapped by tracking the movement of particles between the pair of images. The calculation of a velocity vector field from an image pair uses a spatial correlation technique and was done using commercial software. Figure 10 is a visual explanation of the PIV system showing the laser system and particle movement between the images. The tracer particles used in the system were olive oil droplets, a substance used with success in this facility previously. The laser sheet and the PIV camera were triggered by a photo detector, which senses the passing of each wake rod. The trigger delay was varied to capture the flow at different times after the wake passage. Measurements were collected for a number of timings relative to the wake to determine how the flow responds to a wake disturbance and recovers after the wake passes. For each measurement plane, several hundred PIV image pairs were collected.
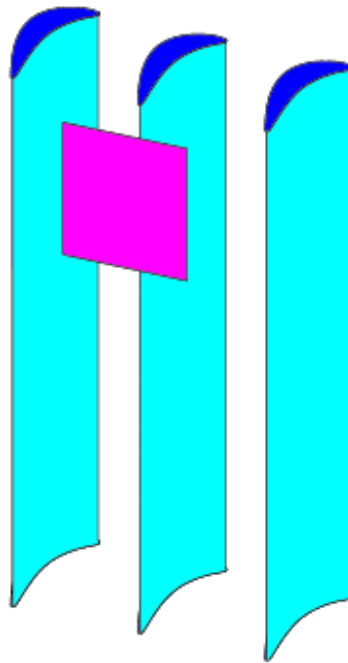
Figure 9- Kiel probe two dimensional movement grid

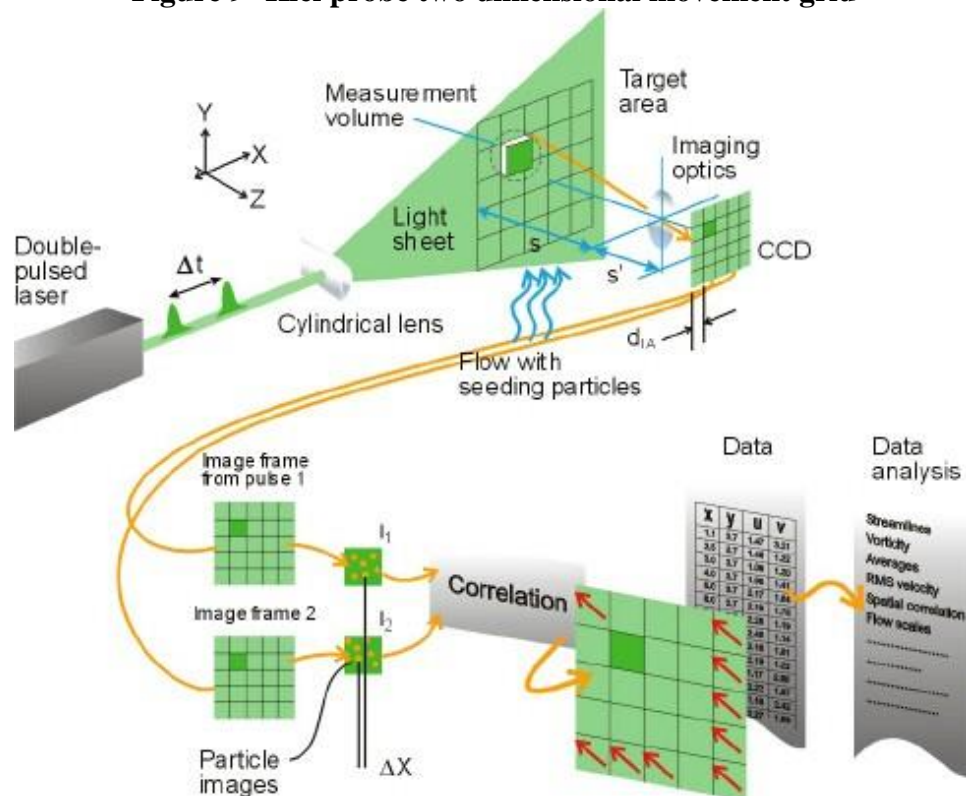**Figure 10-PIV visual explanation- Dantec Dynamics (2012)**

Table 1 shows the experimental matrix. The first two cases are cases with and without wakes with no tip gap. Next, a 2 mm tip gap was introduced and the velocity fields were

measured with and without wake generation. Finally a 5 mm tip gap was introduced and the velocity fields were measured with and without wake generation. For each case the total pressure loss was measured, and the velocity field was documented using PIV. The gap heights of 2 mm and 5 mm compare to the blade chord length of approximately 13 cm. The first image plane, the 1 plane, shown in Fig 11 was used to analyze endwall and tip gap vortices in the plane perpendicular to the flow. The 2 plane shown in Fig 12 is perpendicular to the flow and further downstream. The third imagine plane, the 3 plane, shown in Fig 13 is parallel to the blade exit and was used to collect velocity fields in the same plane as the pressure loss grids.

Table 1 – Test Matrix

Trial Number	Tip Gap	Wake Generation
1	No	No
2	No	Yes
3	2 mm	No
4	2 mm	Yes
5	5 mm	No
6	5 mm	Yes

The velocity fields collected using PIV were used to calculate other fluids properties. The vorticity of the fluid, a measure of the local angular rate of rotation was calculated using (2):

$$\vec{\omega} = \vec{\nabla} \times \vec{v}$$
(2)

The vorticity is the curl of the velocity. The turbulence intensity was measured at different points in the flow by computing the standard deviation of the velocity at each location. The standard deviation is calculated by (3):

$$u' = \left(\frac{\sum_{i=1}^{N}(u-\bar{u})^2}{N}\right)^{1/2}$$
(3)

Where u is the instantaneous velocity, $\bar{u}$ is the average velocity and N is the number of points. The vorticity of the flow and the turbulence intensity were compared to the total pressure loss or loss coefficient, which is given by (4):

$$\psi = \frac{P_1 - P_2}{\frac{1}{2}\rho u_1^2}$$
(4)

Where P_1 is the total inlet pressure, P_2 is the total exit pressure, ρ is the density of the fluid, in this case air, and u_1 is the inlet velocity. By comparing the loss coefficient to the vorticity and turbulence intensity of the flow, a relationship between the flow structure and losses can be found. Comparing the effects of tip gap size and geometry on the flow structure could then provide a direct link between tip gap design and losses.
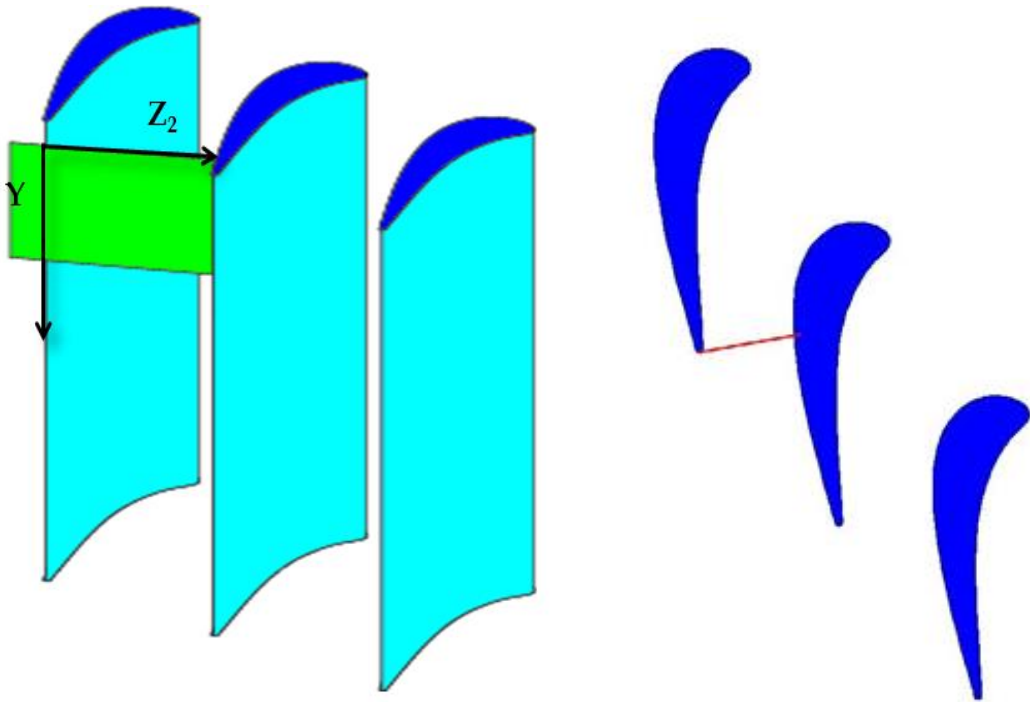
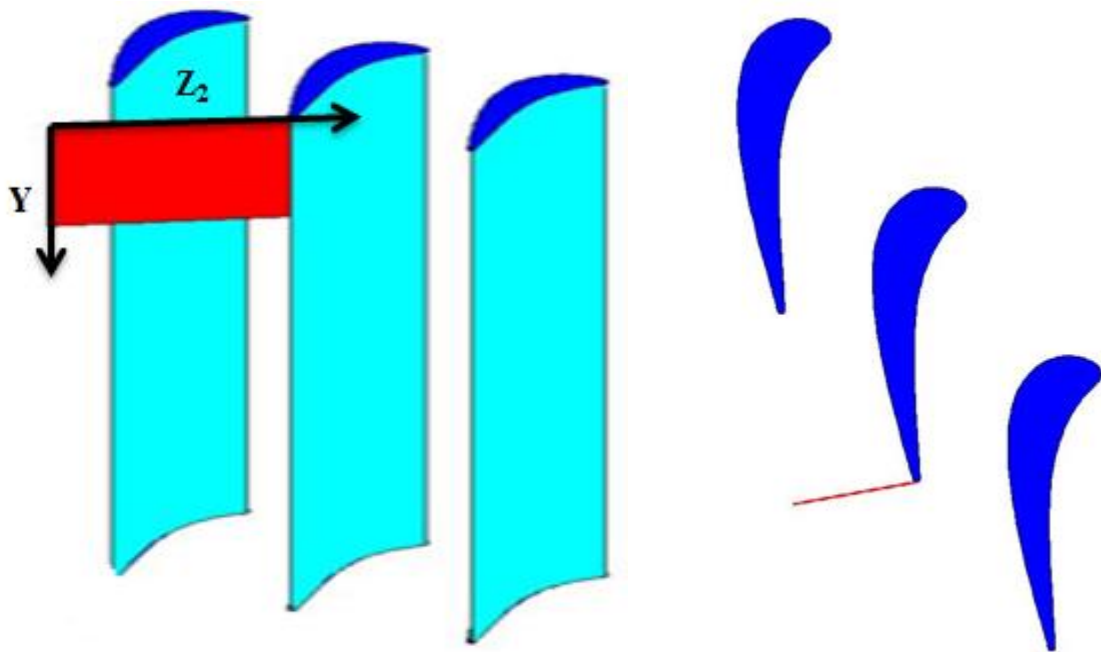**Figure 11- Image Plane 1 as seen from behind the blades and above the blades**

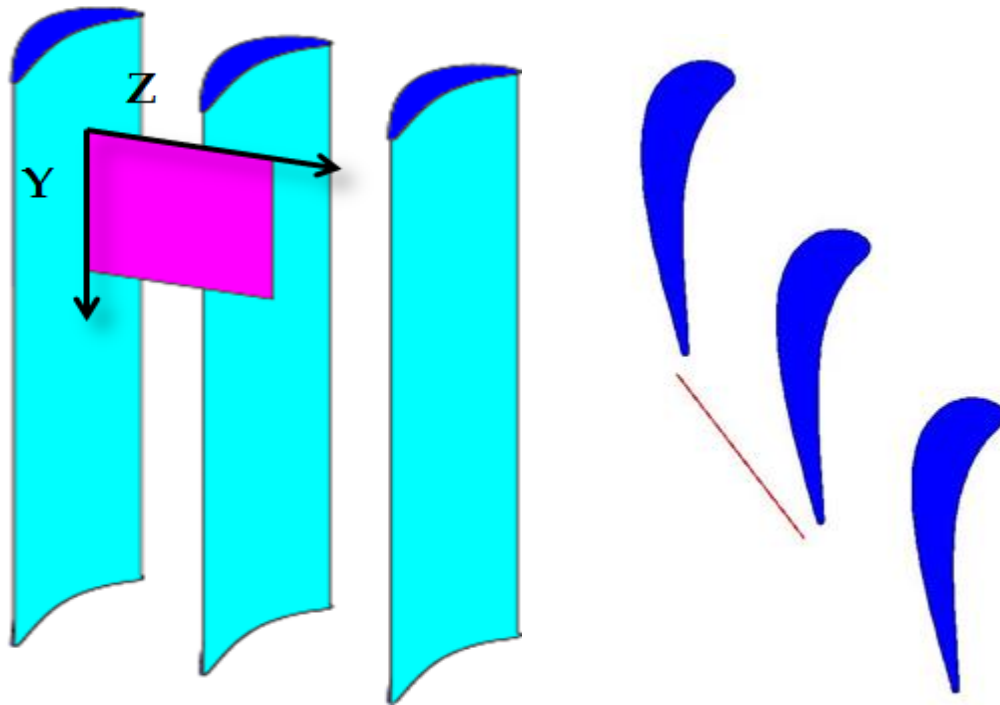**Figure 12- Image Plane 2 as seen from behind the blades and above the blades**

Figure 13- Image Plane 2 as seen from behind the blades and above the blades. This image plane is parallel to the blade exit row and is same plane where the pressure loss measurements were taken

Results

Pressure Distributions on Airfoil

      The majority of the experiments focus on the center two passages of the turbine cascade. The side passages were designed to create the correct flow pattern through the center passages. The flow through the center two passages must be similar for the experimental set up to properly match a real turbine. The dynamic pressure was measured at a series of locations along the blades of the center two passages as the difference between the upstream total pressure measured with the pitot tube and the local static pressure measured on the blade. The pressure taps located $0.1x_c$ from the tip of the blades measure the pressure in the endwall boundary layer. The axial chord, X_c, is the distance in the axial direction from the inlet plane of the blade row to the exit plane. The pressure taps at the midspan of the blades measure the pressure outside of the endwall boundary layer. The dynamic pressure is normalized to the pressure coefficient Cp by (5):

$$(5) \qquad Cp = \frac{P_1 - P}{\frac{1}{2}\rho\, u_1^2}$$

Where P is the measured pressure, P_1 is the inlet stagnation pressure, ρ is the density of the fluid and u_1 is the inlet velocity. Cp is a ratio of the dynamic pressure at the measured point to the inlet dynamic pressure. Figure 14 shows Cp for the two passages at the midspan and at the tip of the

blades. x is distance into the passage in the axial direction. Cp is essentially the same for the two passages at the midspan with a maximum value of approximately 5 for the first passage and 4.66 for the second passage. Cp at the trailing edge of the blade is 2.76 for each passage. The difference in maximum Cp of 0.34 indicates that the first passage may have slightly more flow entering it than the second passage. However Cp at the trailing edge of the blade is very similar for both passages indicating that flow leaving each passage is similar. Because Cp is a measurement of the dynamic pressure at each point, it can be used as a metric to make sure the flow has not separated from the blade and to compare two passages.

The maximum dynamic pressure is lower at the tip of blades which is expected because the velocity of the flow in the endwall boundary layer is slower than the velocity of the flow in the freestream. The Cp differs more between the two passages at the top of the blade. The maximum Cp differs by approximately 0.5 between the two passages. The flow is more complex in the endwall region because the boundary layer creates turbulence. The Cp at the trailing edge of the tip of the blades is 2.76.
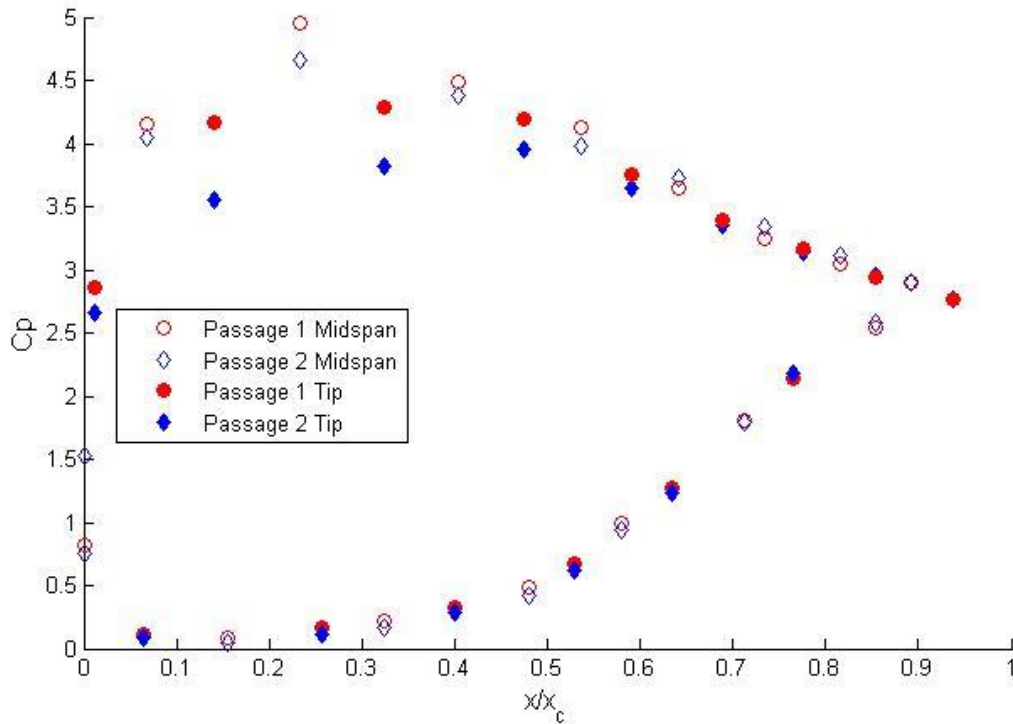

Figure 14 -Cp along the blades for both passages

Figure 15 shows Cp through both passages at the midspan of the blades with steady flow and with the rods generating wakes. The time averaged Cp are similar for each case. The wakes have no effect on the time averaged Cp. The wakes created by the rods do not cause separation or greatly disrupt the flow across the blades. In order to find the effects on the flow of the rod at different phases, the hot wire data were acquired and analyzed.
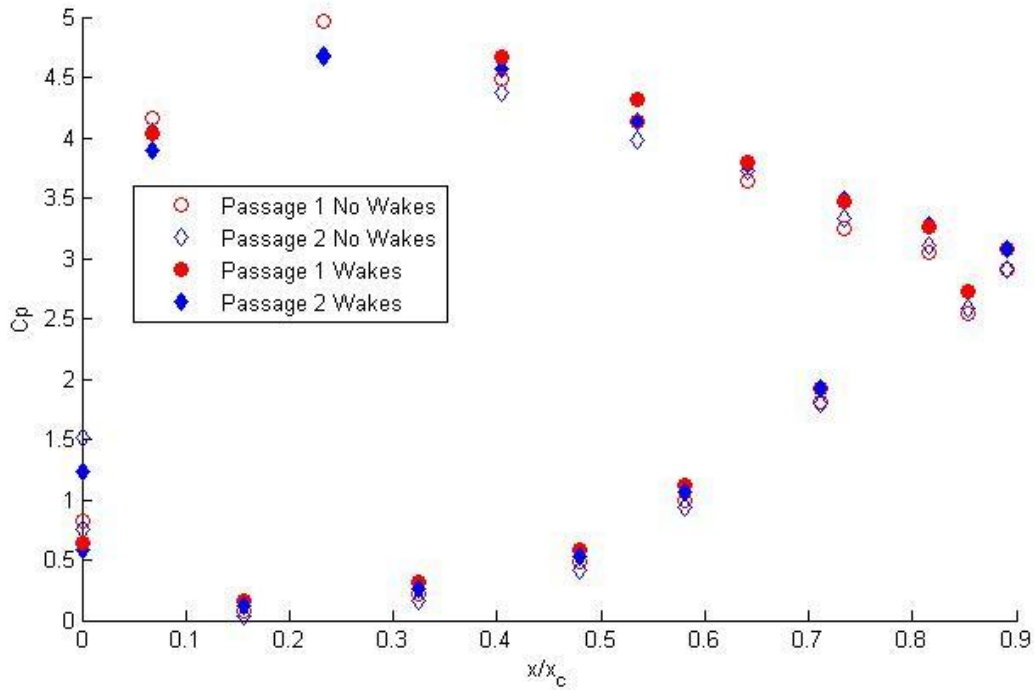
Figure 15 -Cp for both passages at the midspan with and without wakes

Figure 16 shows the Cp at the midspan and at the tip of the blades for cases for steady flow with different tip gap heights. Passage 1 is plotted because previous tests showed that passage 1 and passage 2 had similar dynamic pressures along the blade profile and the majority of the remainder of the data were collected from passage 1. There is no difference between the Cp for the cases with no tip gap, 2 mm tip gap and 5 mm tip gap at the midspan of the blade. The effects of the tip gap vortex and the endwall flows do not reach the midspan of the blade. The Cp measured at the pressure taps near the tips of the blade change for the three cases. The dynamic pressure is higher in the case with no tip gap than in the other two cases when X/X_c is 0.5 or less. The dynamic pressure on the suction side of the blade is higher for the cases with tip gap when X/X_c is 0.6 or greater. Similarly the Cp on the pressure side of the passage for cases with tip gap were lower than for the no tip gap case when X/X_c is 0.6 or greater. This shows that there is flow through the tip gap from the pressure side to the suction side. The effect was larger for the case with the larger tip gap. The Cp for the 5 mm tip gap case is 0.6 greater than for the case with no tip gap at $X/X_c = 0.6$ while the Cp for the case with 2 mm tip gap is only 0.3 greater than the case with no tip gap. This indicates that there is more tip gap flow in the case with larger tip gap. The load on the tip of the blade decreased 7.2% from the midspan load for the case without tip gap. Similarly the load on the tip of the blade decreased 8.2% from the midspan load for the case with 2 mm tip gap. The load only decreased by 2.7% from the midspan loading to the tip loading for the case with 5 mm tip gap. The difference in loading is within the experimental error.
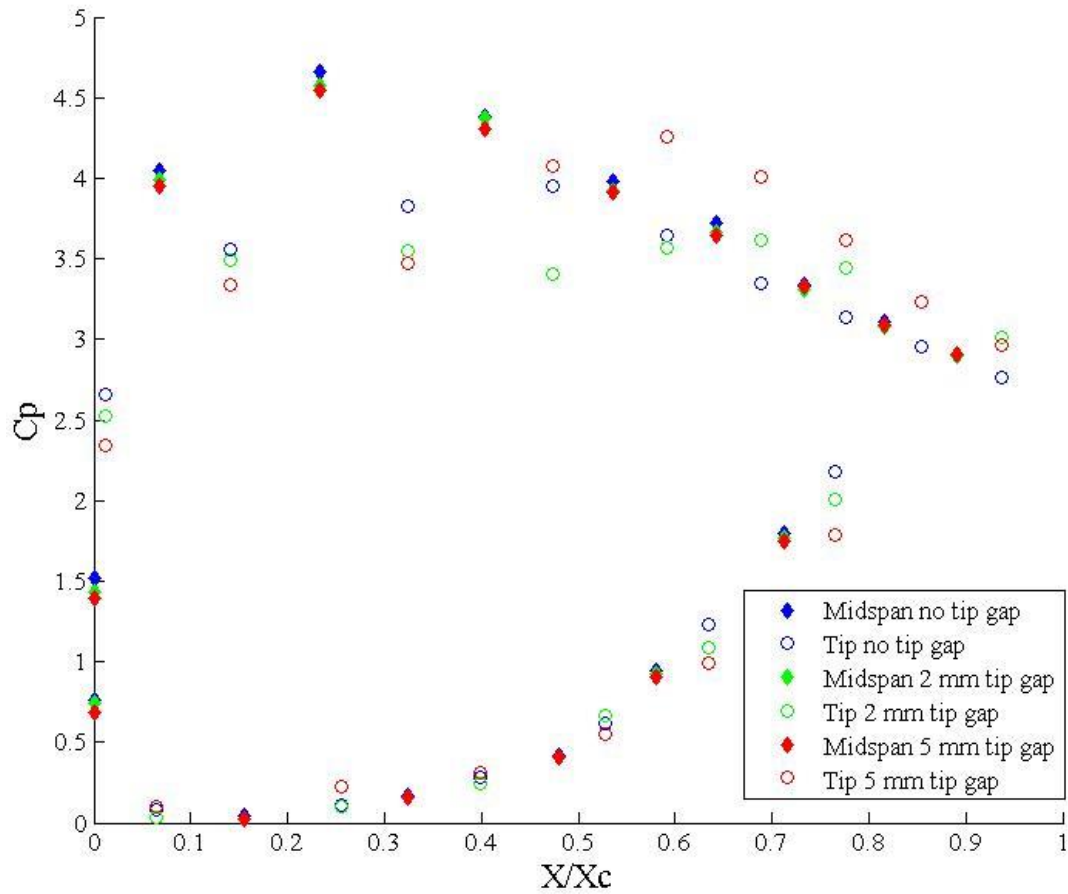
Figure 16 – Cp for passage 1 at the midspan and the tip with different tip gap sizes

Figure 17 shows the effect of wakes on the Cp measured at the tip of the blades for cases with different tip gap sizes. The Cp are similar for each case. The wakes have no effect on the time averaged Cp. The wakes created by the rods do not change the time averaged Cp for cases with tip gaps. In order to find the effects on the flow of the rod at different phases, the hot wire data were acquired and analyzed.
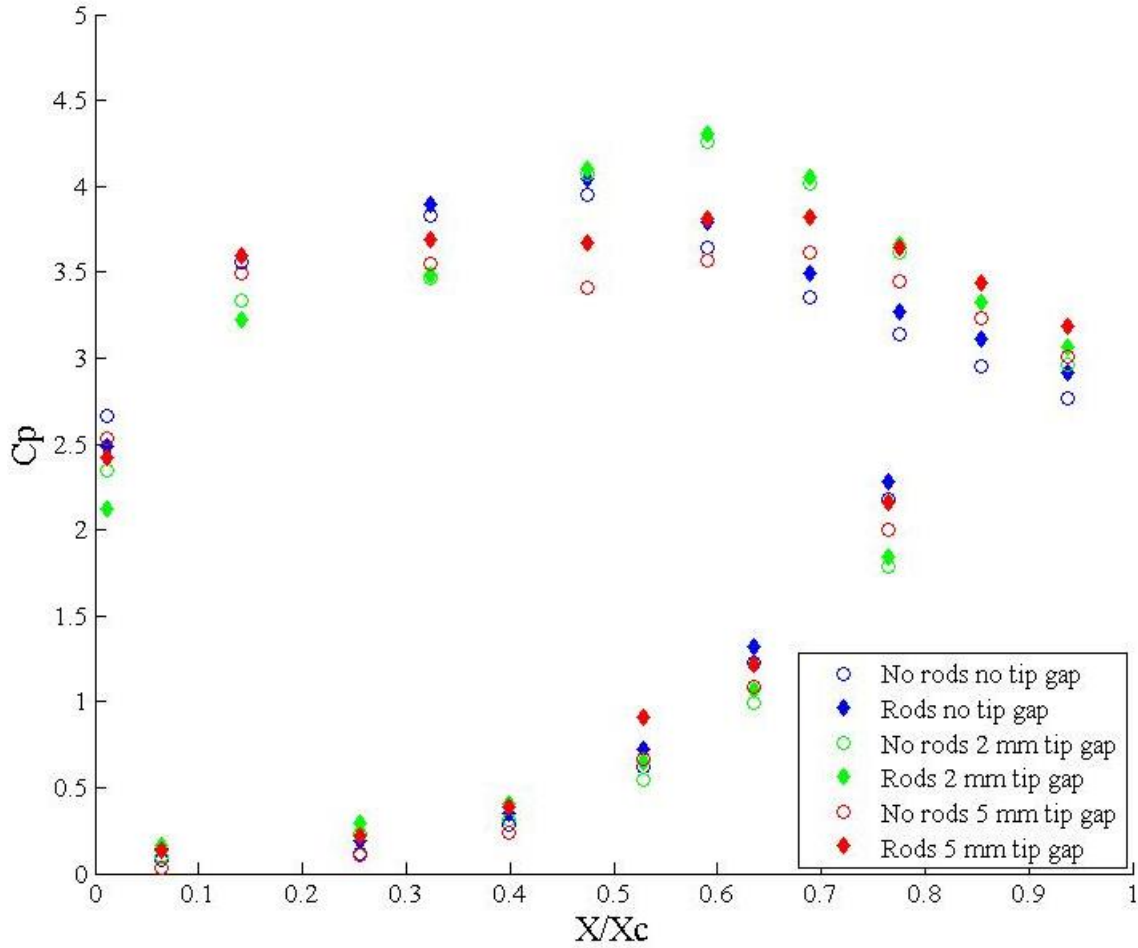
Figure 17 – Cp for passage 1 at the tip with different tip gap sizes with and without rods

Inlet flow Conditions

The inlet flow conditions are documented to ensure the experimental set up has the proper flow conditions. The boundary layer thickness and turbulence are analyzed as well as the turbulence caused by the wake generation system. A hot wire probe was mounted on a traverse and positioned downstream of the wake generation system in the inlet of passage 1. The hot wire was positioned at the endwall and then traversed toward the freestream stopping to collect velocity data at 56 points over approximately a chord length. Figure 18 shows the velocities normalized to the local freestream velocity, u_∞, as a function of distance from the endwall normalized by chord length for cases with wakes and without wakes. The variable y is the distance from the endwall in the vertical direction. The data for both cases are time averaged at all points to produce the case without rods and the time averaged case with rods. The velocity data illustrate the no slip condition as the velocity of the flow near the endwall is recorded to be approximately

0.17 of u_∞. The boundary layer thickness was determined by the location where the velocity reached 99% of u_∞, computed as an average of the last five velocities in the profile. The boundary layer thickness is $0.41x_c$ or approximately 55 mm. The time averaged velocity data of the case with wakes is similar to the case with no wakes. In order to see the effect of a rod passing, the data were phase averaged. A sensor was used to determine when a rod passed. Data from the hot wire and data from the rod sensor were collected simultaneously. Phase averaging involved dividing the data into 24 equal phases from when a rod passed to when the next rod passed. These phases show the velocity at different time intervals from the rod's passing. The velocities for each phase were averaged for every rod passing. The average velocities of a phase inside of the wake and outside of the wake are plotted to show the effect of the wake. The velocity profile for a phase inside the wake of a rod has a maximum velocity of approximately 0.9 u_∞. The flow in the wake of the rod is slower. Conversely the flow outside of the wake of the rod has a maximum velocity 1.06 u_∞. The faster flow outside of the wake and the slow flow in the wake average to a similar velocity profile as in the case without rods.
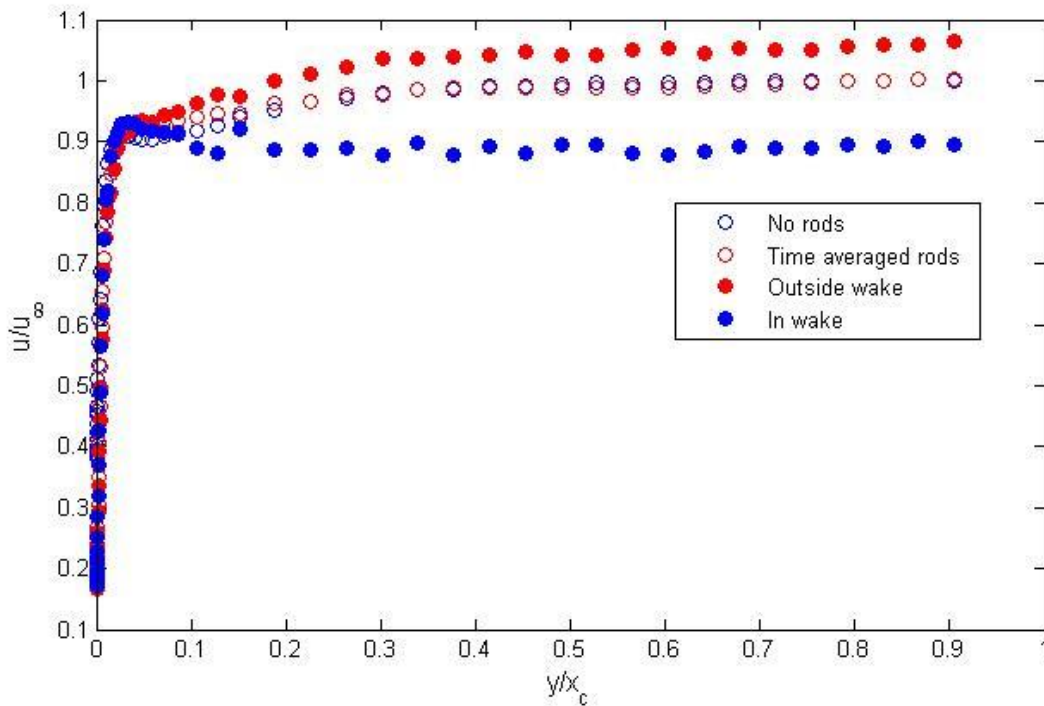

Figure 18- Hot wire velocity profile in the endwall boundary layer

The standard deviation of velocity is a measure of turbulence. Figure 19 shows the standard deviations of velocity at different distances from the endwall for cases with without wakes. For the case with wakes, results are shown for the time average of all the data and for phases in the wake and outside of the wake. The variable u' is the standard deviation of the velocity. Turbulence is a function of the velocity gradient and the shear stress. All of the cases have a peak turbulence of approximately $0.16u_\infty$ at $0.01x_c$. This is the near wall shear peak. The turbulence is driven by the shear, which is the gradient of

velocity. Thus as the velocity begins to change more slowly beyond $0.01x_c$ from the endwall the turbulence drops despite higher velocities. The turbulence from the case with no wakes and the phase outside the wake is approximately the same with a freestream turbulence intensity of $0.04u_\infty$. This value is the expected FSTI caused by the metal grate upstream of the testing corner. The case inside the wake has the highest turbulence with a freestream turbulence intensity of $0.135\ u_\infty$. The time average of the case with rods has a $u' = 0.12u$, which is due to the fact that it contains the high turbulence in flow in the wakes and the low turbulence in flow outside of the wakes.
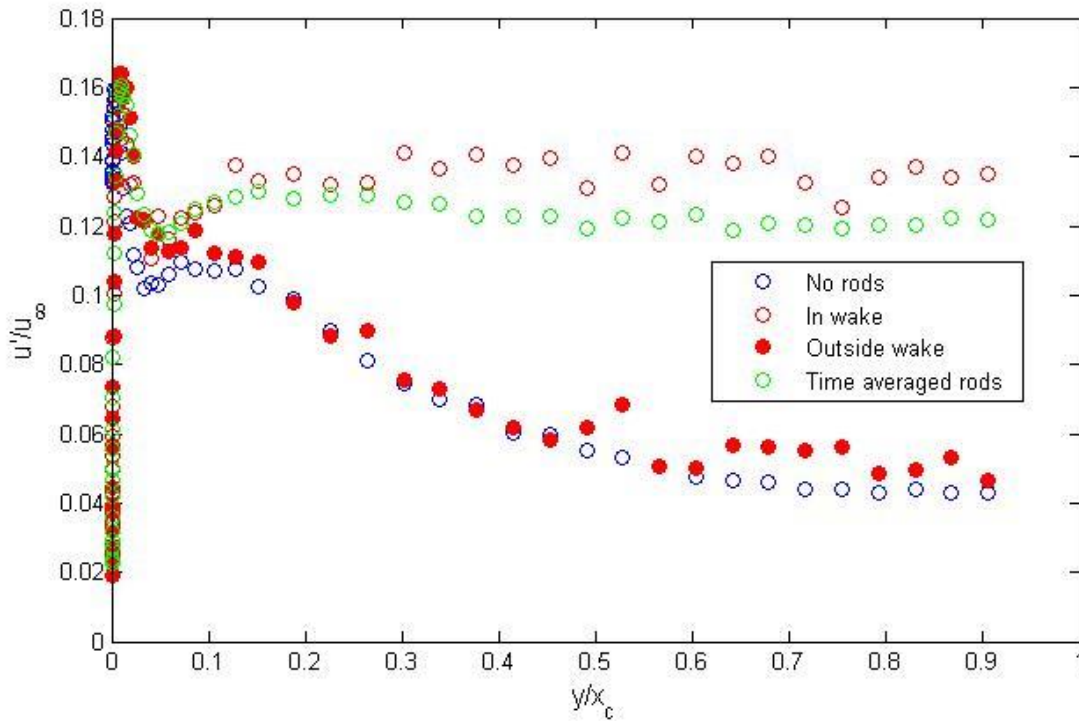
Figure 19- Standard deviation of velocity in the endwall boundary layer

Figure 20 shows the phase averaged normalized velocity, u/u_∞, of the flow at different times, t, over two rod periods, T, at different distances from the endwall. The plot shows the data repeated to show the periodicity of the rods passing. The two low velocity areas at $t/T = 0.2$ and 1.2 are the velocity in the wake of the rod. The high velocity region shows the flow velocity outside of the wake. The period of time over which the wake affects the velocity begins to shift later in time near the endwall because the fluid velocity in the endwall boundary layer is slower and therefore the wake takes longer to reach the hot wire sensor.

Figure 21 shows the phase averaged u'/u_∞ over a rod passing at different distances from the endwall. The times when the flow is affected by the wake and the flow is outside of the wakes are the same as in the mean velocity plot because they are taken from the same case. The freestream turbulence intensity for the flow unaffected by the wakes is approximately $0.04u_\infty$ which is the same as in the case without rods. The FSTI during the phases affected by the wakes is approximately $0.16u_\infty$. The wake affects the flow for

approximately 0.4T which is similar to the result from the mean velocity plot. Thus the wake of a rod both decreases the velocity and increase the turbulence intensity.
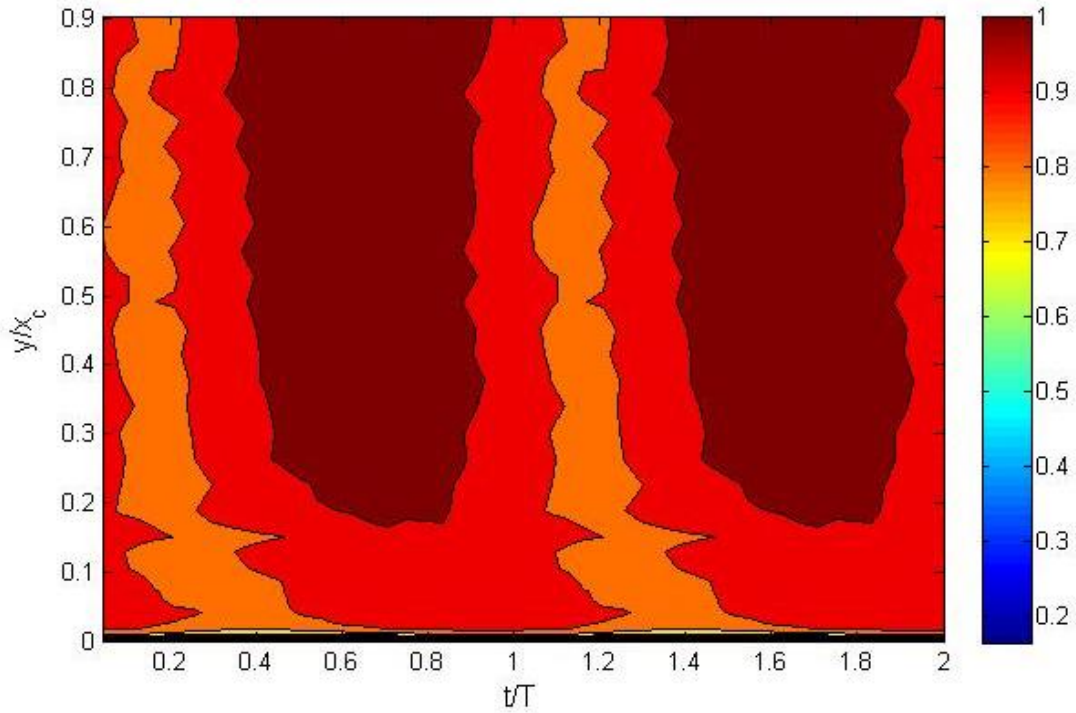

Figure 20 - u/u_∞ **over the period of a rod passing at different distances from the endwall**
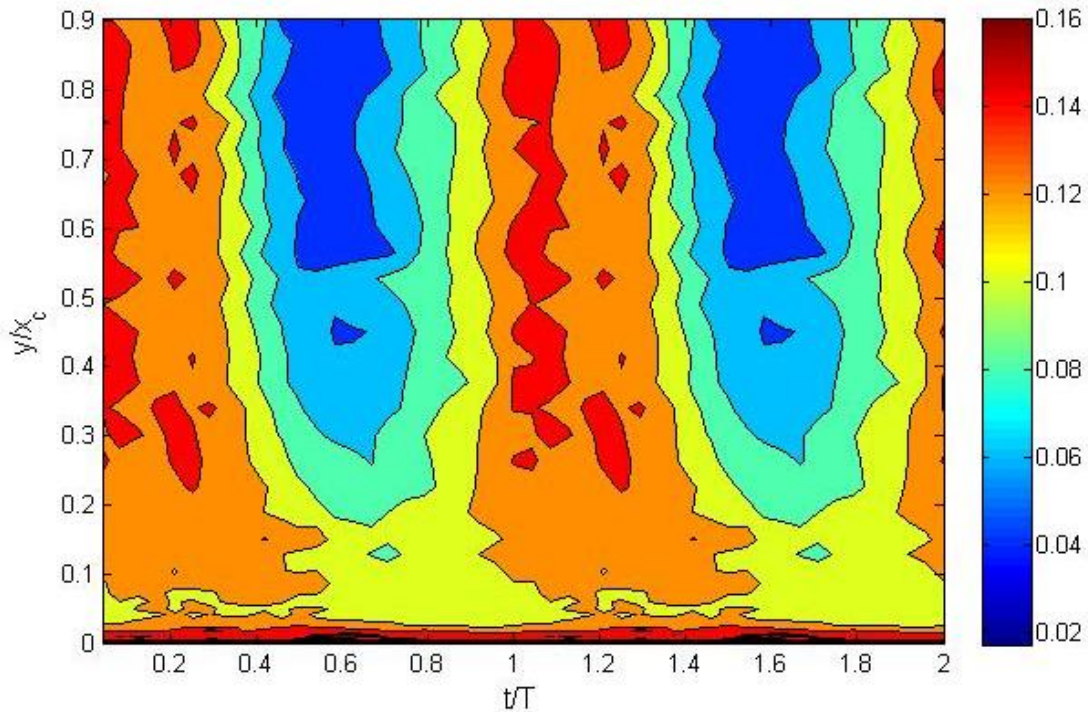

Figure 21 – u'/u_∞ **over the period of a rod passing at different distances from the endwall**

Downstream Velocity

        A hot wire velocity profile was also taken across the blade row $0.1x_c$ downstream of the cascade at the midspan. Figure 22 shows the velocity normalized by the mean of the exit velocity, u_2 across three passages for the case with wakes and the case without wakes. The velocity differs between the two main passages by approximately $0.03u_2$. The wakes increase the width of the boundary layer of the blades as can be seen by the wider velocity dips. Additionally the wakes cause the velocity to decrease by more downstream of the trailing edge of the blades. This velocity decrease downstream of the blades occurs because the turbulence of the wake causes the boundary layers on the blade to be thicker.
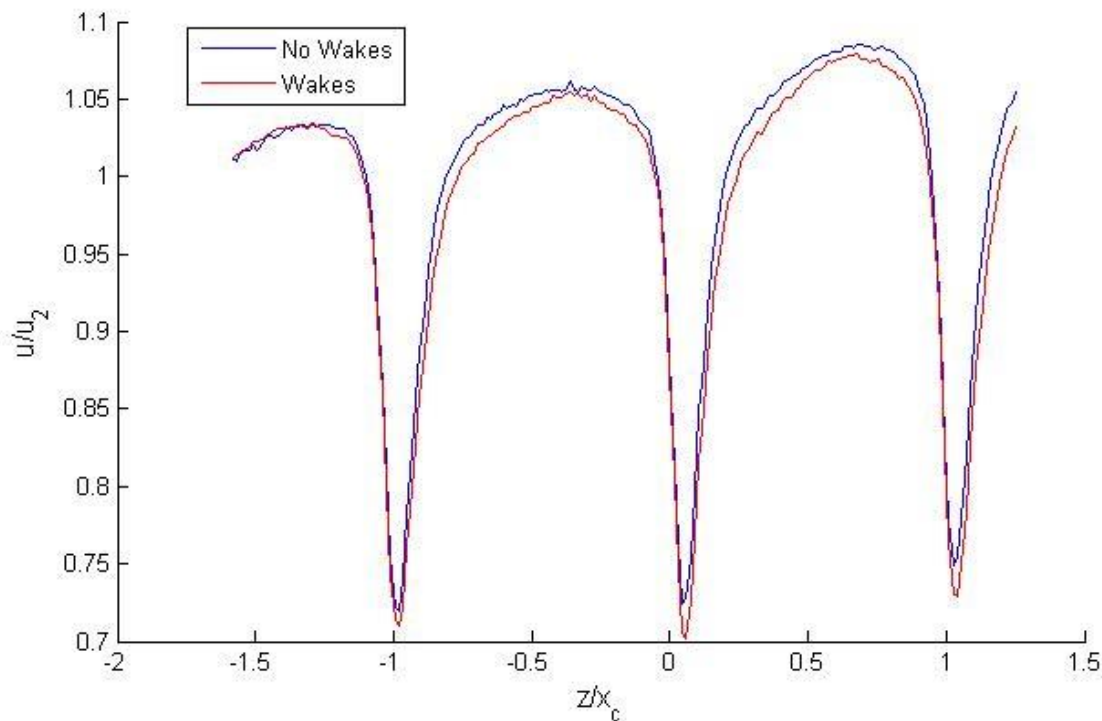
Figure 22 – u/u_2 downstream of the blade row

Total Pressure Loss

        Total pressure loss measurements were also made across the passages $0.1x_c$ downstream of the blades. A Kiel probe was positioned at the midspan of the blades. The probe captured the pressures across three passages. The loss coefficient was calculated for each point using (4). Figure 22 shows the loss coefficient over three passages with and without wake generation. The loss coefficient is highest directly behind the trailing edge of the blades. The loss coefficient is consistently higher for the case with wake generation. The wake generator creates vortices and other losses in the flow, increasing the loss coefficient. The width of the region of high pressure loss associated with the

location of the blade trailing edge increases with the introduction of wakes. Additionally higher losses due to the turbulence of the wakes are seen across the area of study.
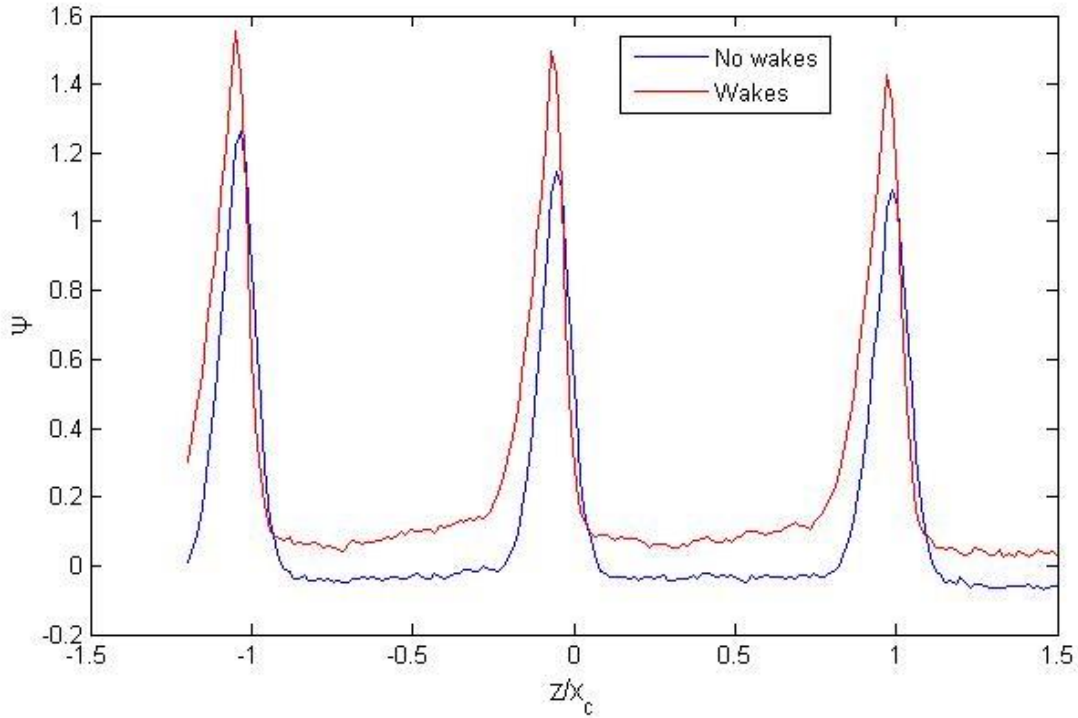

Figure 23 – Loss coefficient profile downstream of the blade row

Pressure loss coefficients were collected for a grid that included the middle passages and the 120 mm closest to endwall for cases with and without wakes. The data were plotted as contour maps. These grids show the pressure loss caused by the blade row as well as the pressure loss due to boundary layer flows. Figure 24 shows the loss coefficient, ψ, for the case without wake generation. The loss coefficient has a maximum value of 1.55 directly behind the trailing edge of the blades. The region of increased losses has a peak width of $0.42X_c$ at approximately $0.3X_c$ from the endwall. This may be the location of the passage vortex.

Figure 25 shows ψ for the case with wake generation. The wakes from the rods increase pressure losses by increasing the vortices in the flow. The wake generation increases the width of the area of high pressure drop downstream of the blades. Additionally the rods increase the overall pressure loss. The highest ψ is approximately 1.7 directly behind the trailing edge of the blade. The wakes increase the peak width of the region of loss to approximately $0.53X_c$ at a distance from the endwall of approximately $0.23X_c$. The vortices also increase the pressure loss between blade wakes. The addition of wakes increased the average pressure loss by 35% in the region bounded by $Y/X_{c=}$ -0.87 and the length of Z plotted.
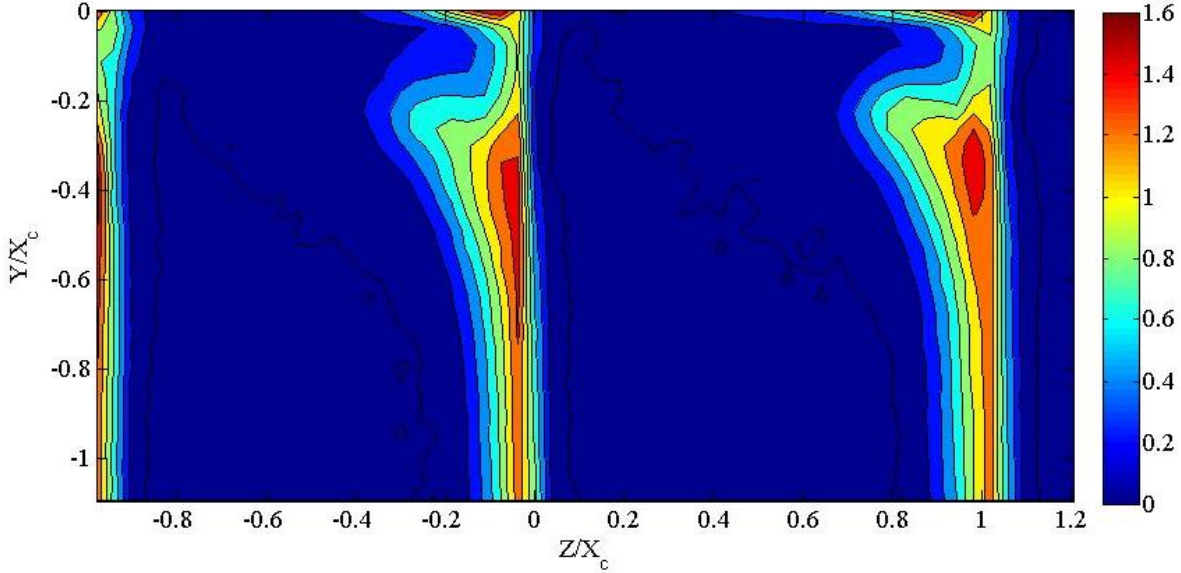
Figure 24 – ψ downstream of blades without wake generation at different distances from the endwall
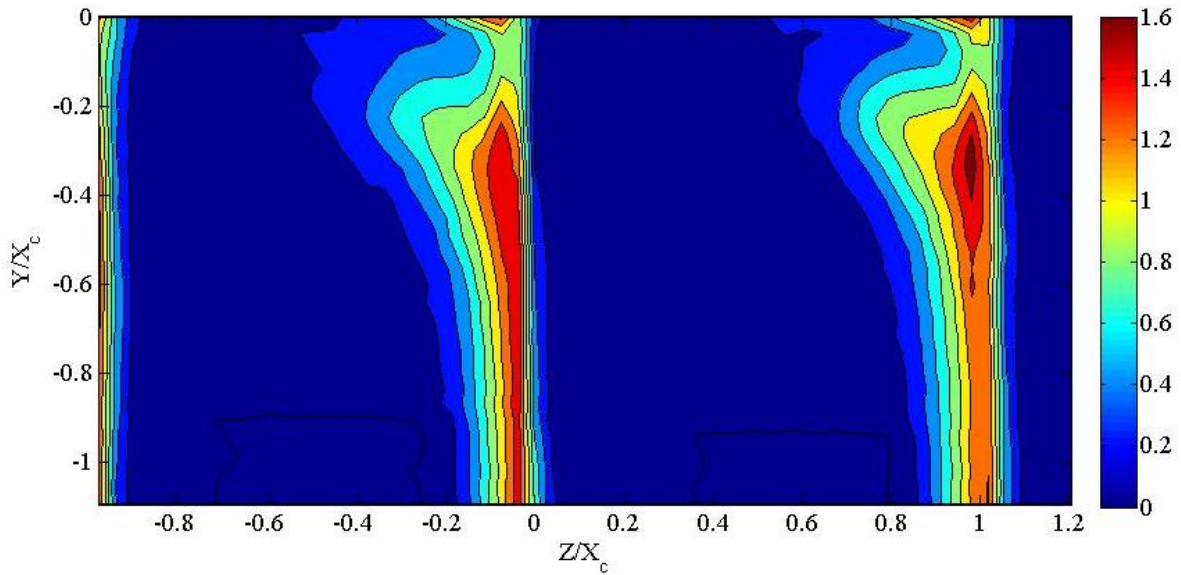

Figure 25 – ψ downstream of blades with wake generation at different distances from the endwall

The midspan profile was subtracted from the rest of the image for both cases. This shows the difference in pressure loss caused by the endwall flows. Figure 26 shows the midspan subtracted pressure loss grid for the case without wakes and Fig 27 shows the case with rods. The plots have a large region of high pressure loss centered at approximately -0.3 Y/X_c from the endwall. The circular shape and the location suggest this may be the passage vortex. PIV data will be compared to these plots to validate this conclusion.
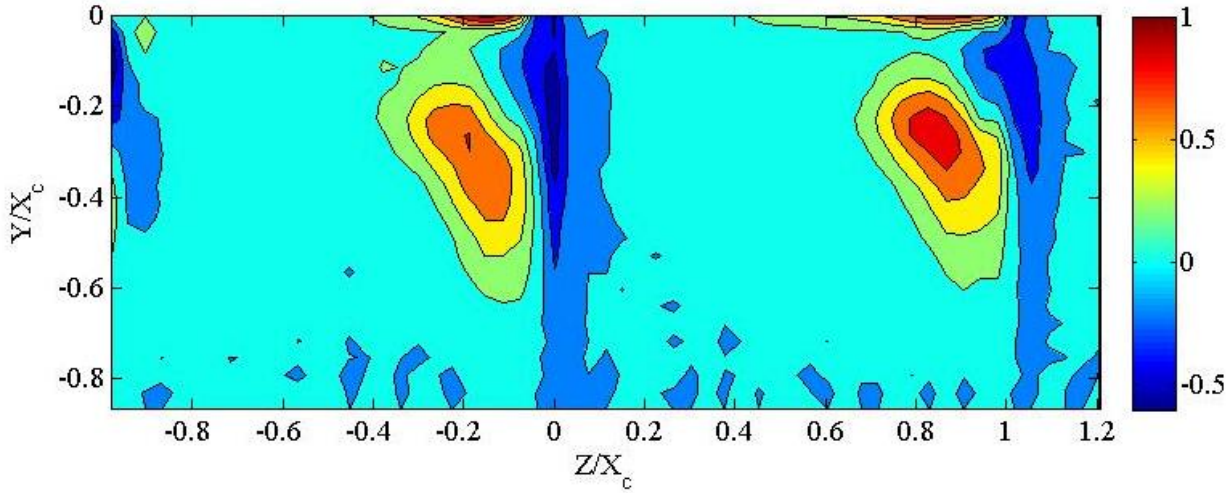
Figure 26 – The ψ for the case without rods with the midspan profile subtracted from the plot
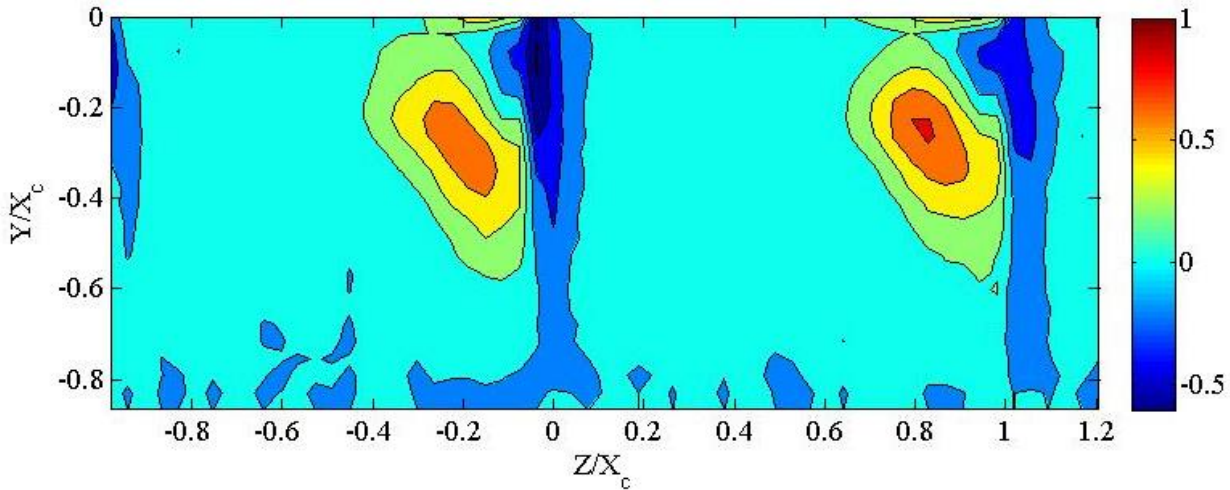

Figure 27 – The ψ for the case with rods with the midspan profile subtracted from the plot

Figure 28 shows the pressure loss grid for the case with a 2 mm tip gap without wakes. Figure 29 shows the pressure loss grid for the 2 mm tip gap case with wake generation. The midspan profile was not subtracted from the 2 mm or the 5 mm case because the loss center was evident without the subtraction. Similar to the previous case the wakes did not affect the magnitude or location of the loss core but increased the overall pressure loss. The wakes increased the average pressure loss by 8.8%. The pressure loss peaks at a value of 2.26 at approximately -0.05 Y/X_c. The increased pressure loss is caused by the tip gap vortex. The center of the loss core is closer to the endwall because the tip gap flows occur there. The tip gap flow increased the average pressure loss by approximately 99%.The increased pressure loss is caused by the tip gap flow.
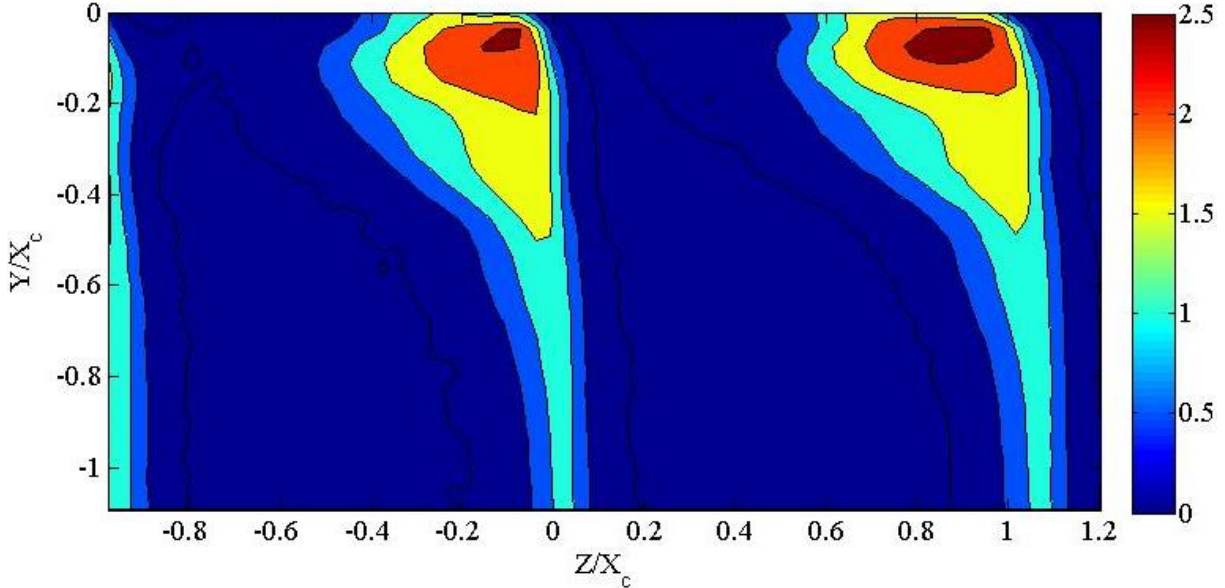
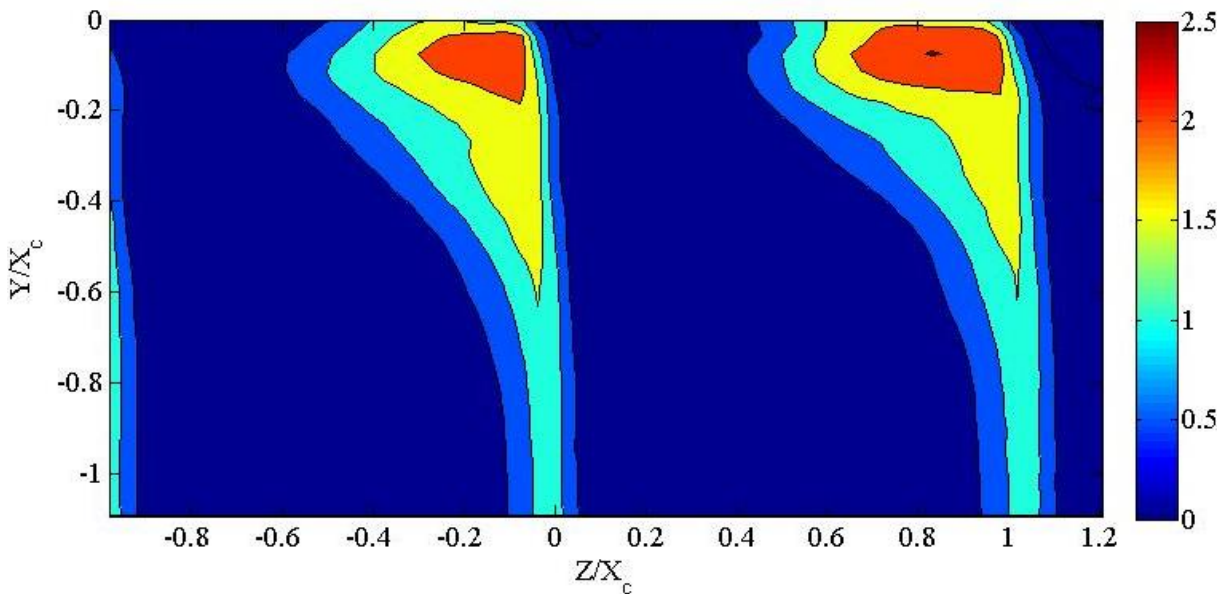**Figure 28 - The ψ for 2 mm tip gap case with no wakes**

Figure 29 - The ψ for 2 mm tip gap case with wakes

Figure 30 shows the pressure loss for the case with a 5 mm tip gap without wakes. Figure 31 shows the pressure loss for the 5mm case with wake generation. The greatest region of pressure loss is located at -0.075 Y/X_c from the endwall. The maximum pressure loss shifts from being centered at -0.11 Z/X_c from the blade's wake to being centered -0.38 Z/X_c from the blade's wake. The movement in the Z direction of the pressure loss is likely caused by the increased mass flow of air through the larger tip gap driving the center of the tip gap vortices further into the passage. Adding the 5 mm tip gap increased the average pressure loss by 120% from the case

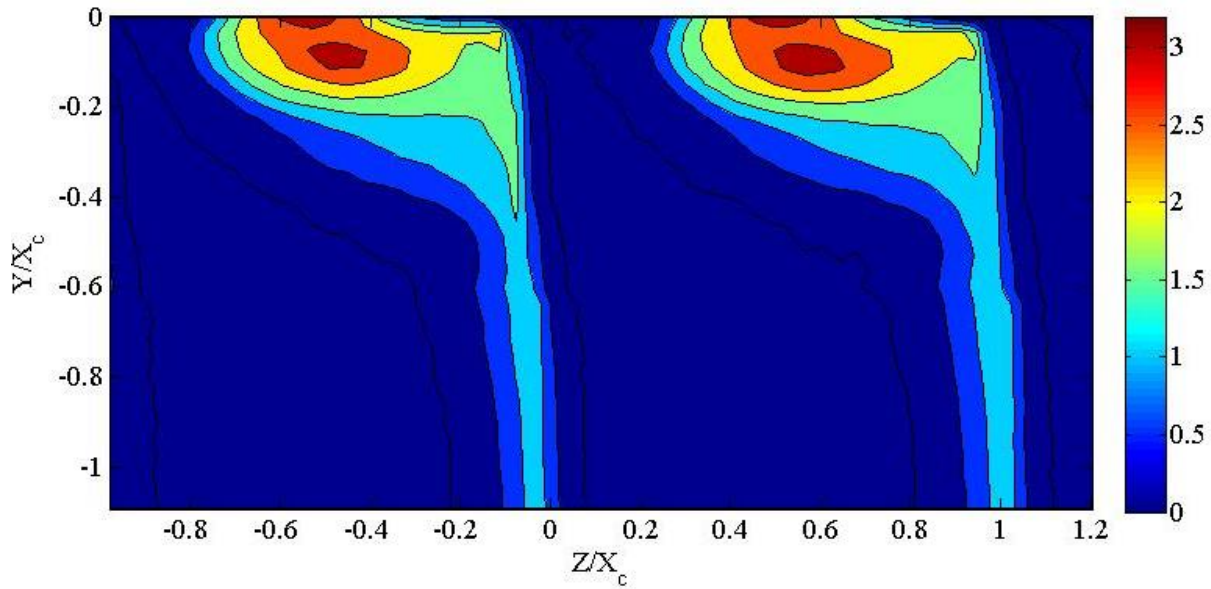without tip gap. The case with wakes had an average pressure loss increase of 17% from the steady case.

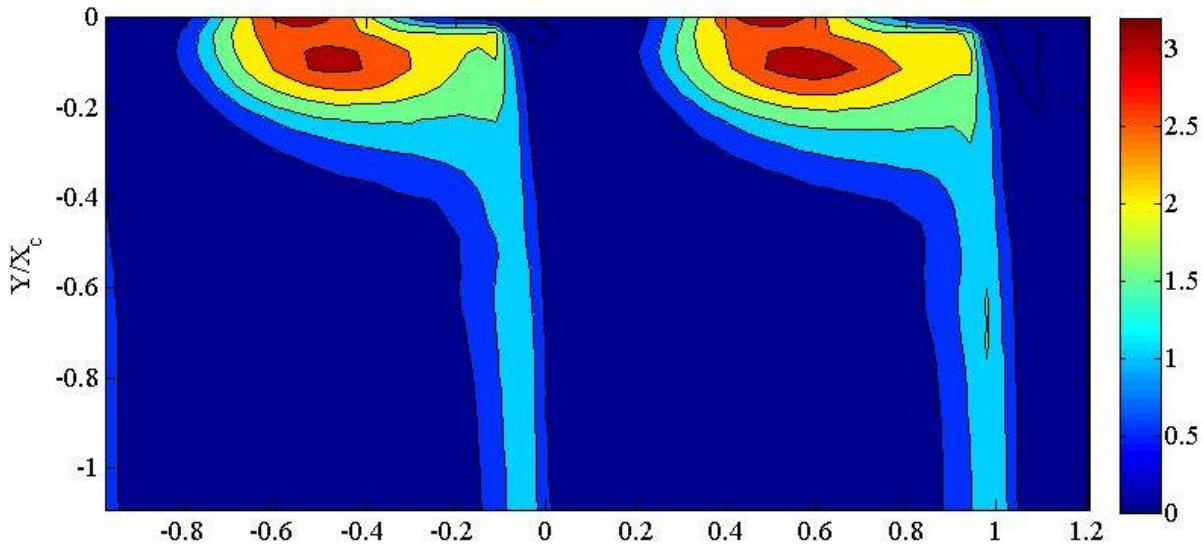

Figure 30 - The ψ for 5 mm tip gap case with no wakes

Figure 31 - The ψ for 5 mm tip gap case with wakes

Exit Velocity Field with no Tip Gap

The PIV system was used to determine the flow exit angle. The first plane analyzed, the 1 plane as shown previously in Fig 11, is perpendicular to the flow direction and tangent to the trailing edge of the blade of the pressure side of passage 1. The plane intersects the suction side of the blade upstream of the trailing edge. The PIV system was used to collect velocity fields

inside the passage. One thousand image pairs were collected and averaged for the steady cases presented. w is the velocity of the flow in the Z_2 direction. Figure 32 shows the averaged turbulence of the velocity in Z_2 direction, w', normalized by the inlet velocity u_1 for the case with no tip gap and no wakes. The Y axis is the vertical distance away from the ceiling of the tunnel with the moveable ceiling as the 0. The Z_2 direction is perpendicular to the flow direction, and the image is bounded by the pressure side of the passage on the left and the suction side of the passage on the right. w' reaches its maximum of 0.16 u_1 near the endwall in the boundary layer. There is also a circular region of high turbulence at $Y/X_c = -0.10$ and $Z_2/X_c = 0.375$. This region corresponds to the location of the passage vortex. The background w' varies from 0.04 to 0.06 u_1. There is a region of higher turbulence along the pressure side of the passage, which varies from 0.12 to 0.08 as the distance from the ceiling increases.
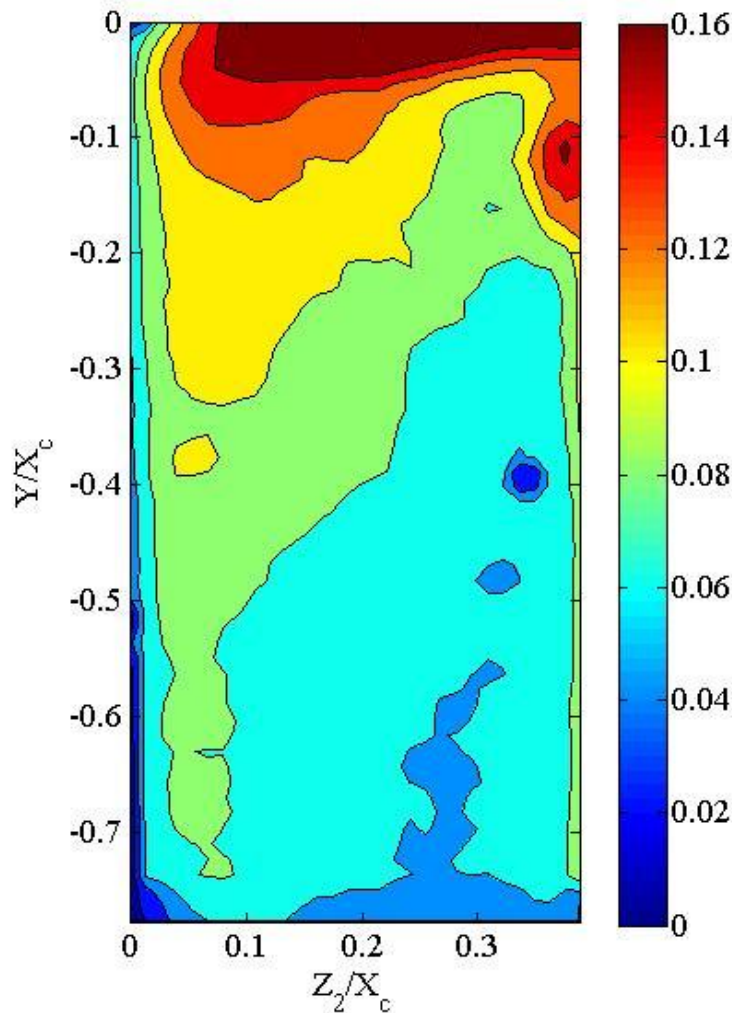

Figure 32 – w'/u_1 for the 1 plane perpendicular to the flow direction and tangent to the trailing edge of the pressure side of passage 1.

Figure 33 shows the vortices in a turbine passage. The largest vortex, the passage vortex is the pressure side leg of the horseshoe vortex that gains strength due to the endwall crossflow. The vortices along the endwall and blade surface are the corner vortices. The vortex above the

passage vortex is the suction leg of the horseshoe vortex. The vortices expand in size as they continue downstream.
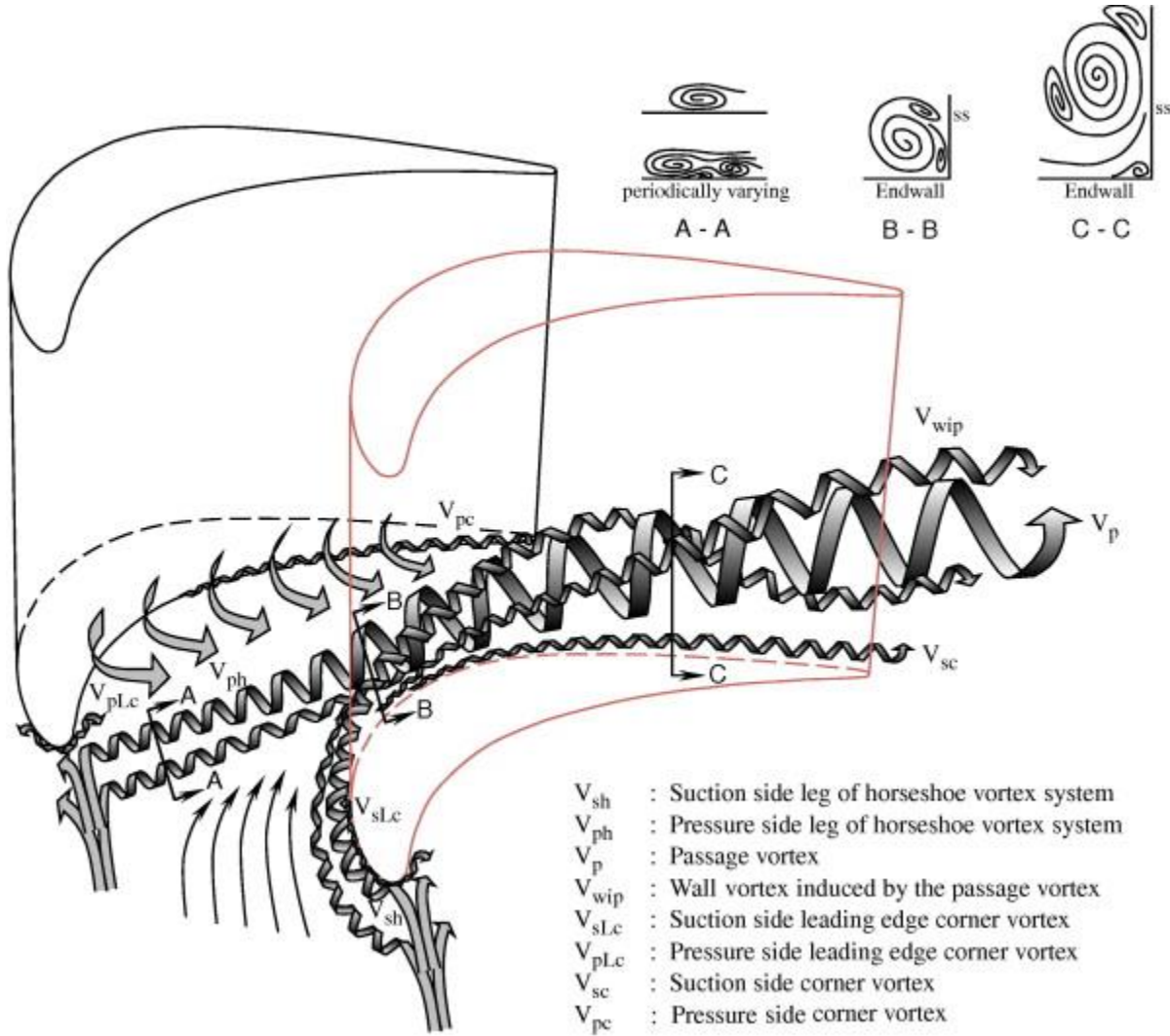

V_{sh}	:	Suction side leg of horseshoe vortex system
V_{ph}	:	Pressure side leg of horseshoe vortex system
V_{p}	:	Passage vortex
V_{wip}	:	Wall vortex induced by the passage vortex
V_{sLc}	:	Suction side leading edge corner vortex
V_{pLc}	:	Pressure side leading edge corner vortex
V_{sc}	:	Suction side corner vortex
V_{pc}	:	Pressure side corner vortex

Figure 33 – Vortices in a turbine passage. (Wang et al., 1997)

The velocity fields collected were used to calculate the swirl strength of the flow. The swirl strength is the imaginary part of the eigenvalues of the velocity gradient tensor. If the imaginary part is positive, it indicates that the flow has circular structure around local centers. The magnitude of the swirl strength represents the strength of the swirling motion. The swirl strength is not affected by background velocity and can detect a vortex that is not visible by looking at the velocity fields. The normalized swirl strength, λ, is the swirl strength, k, normalized by the inlet velocity, u_1, and the chord length, X_c as shown in (6):

(6)
$$\lambda = \frac{k \, X_c}{u_1}$$

Positive values of λ correspond to fluid circulating in the clockwise direction while negative values correspond to fluid rotating in the counter clockwise direction in the image plane. Figure 34 shows λ for the 1 plane and the velocity vectors. The highest swirl strength is λ=7.4 located at Y/X_c = -0.10 and Z_2/X_c = 0.375, which is the location of the circular region of high turbulence in Fig 32. This vortex is the passage vortex, which is created by the endwall cross flow and the pressure side of the horseshoe vortex, and its direction and location match the descriptions of the passage vortex. The vortex beneath the passage vortex is spinning counter clockwise and has λ = -2.37. Based on the vortex's rotational direction and relative strength, it could be one of two documented vortices. It could be the suction side of the horseshoe vortex, or it could be an induced vortex called the counter vortex. Induced vortices are caused by inertial effects of rotating fluid coming in contact with a solid boundary, in this case the suction side of the passage. The vortex centered at Y/X_c = -0.05 and Z_2/X_c = 0.1 with a swirl strength of 2.4 may be the corner vortex because of its location along the pressure side of the passage. The vortex centered at Y/X_c =-0.02 and Z_2/X_c = 0.37 is unidentified, but it persists in the cases with wake generation.
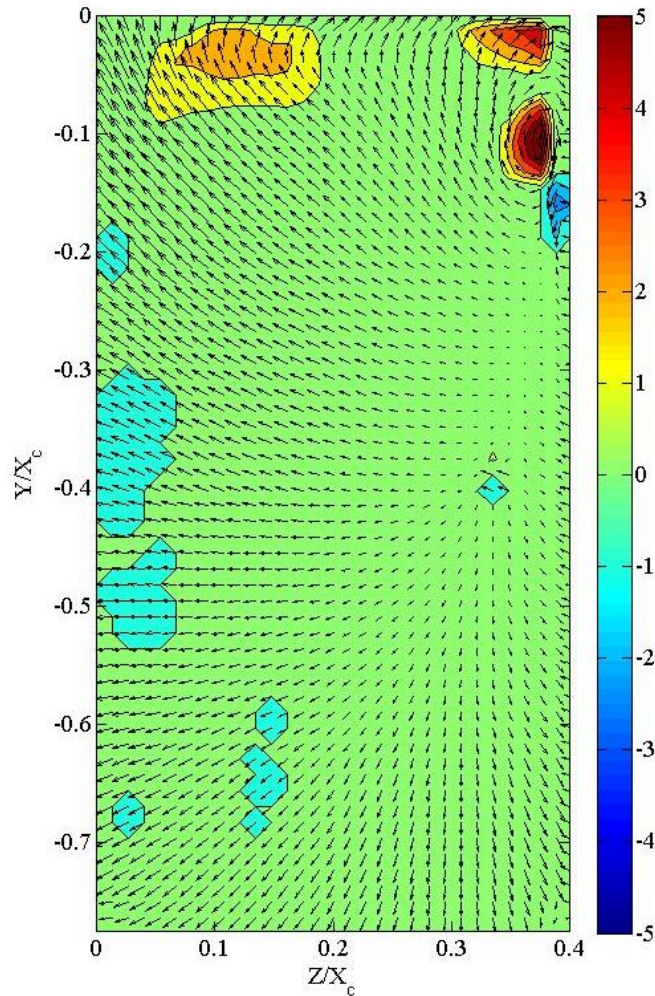

Figure 34 – λ for the 1 plane with no tip gap and steady flow.

The PIV system was also used to collect velocity fields when the wake system was running. The velocity fields were collected at evenly spaced phases over the period of the wake. One hundred image pairs were collected at each phase and averaged. Figure 35 shows the normalized turbulence, w'/u_1 at each of the ten phases, which are separated by intervals of 0.1 T. The 10 plots are read left to right with the first four phases on the first row, phases 5 through 8 on the second row and phases 9 and 10 on the third row. The color scale is the same from the steady case going from 0 to 0.16. Phase 2 is outside the wake and has a background turbulence of approximately 0.08u_1. The structure of the turbulence in the phase is similar to the turbulence of the steady case. The effects of the wake can be seen in phase 7. The turbulence is centered in the passage, and the background turbulence intensity varies between 0.14 and 0.16 u_1.
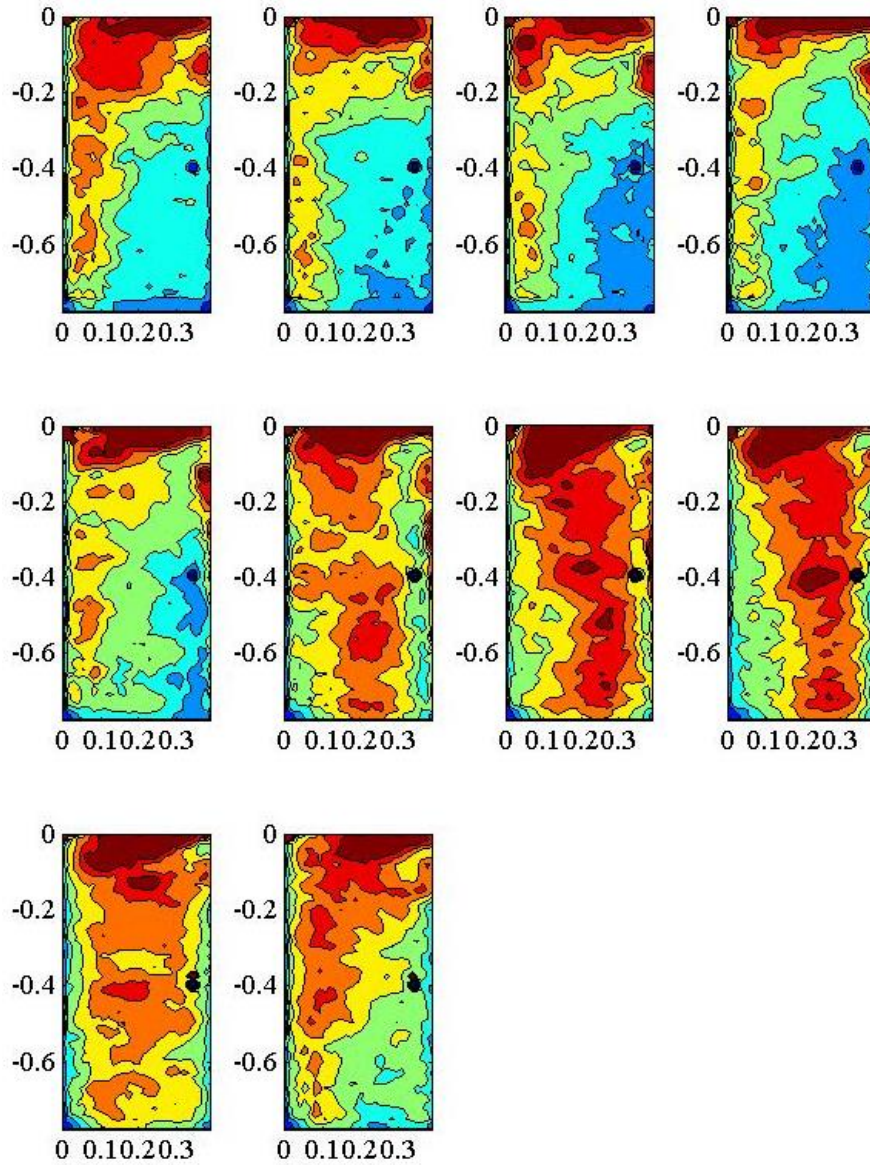

Figure 35 – w'/u$_1$ for 10 phases of the wake in the 1 plane. The phases are separated by a delay time of t =0.1T

Figure 36 shows λ for 10 phases of the wake's passage in the 1 plane. These phases line up with the turbulence plots above. The color scale is the same as steady swirl strength case in Fig 34 and goes from -5 to 5. The phases show that while the vortices move and respond to the wake passing, the structure of the flow does not greatly change and the vortices do not disappear as the wake passes. The passage vortex does not move in the Z_2 direction and is located at Z_2/X_c = 0.36. The passage vortex moves in the y direction. The center of the passage vortex is at Y/X_c = 0.08 in phase 9 and at Y/X_c =0.13 in phase 5. The strength of the passage vortex varies from λ=5.9 to λ=8.5. The highest swirl strengths are associated with phases 4, 5 and 6, the phases with the largest time elapsed from the wake's passage. The counter vortex or suction leg of the passage vortex shrinks from its maximum height of 0.10 X_c with a maximum λ=-3.75 in phase 5 to a height of 0.03 X_c with maximum λ=-2.0 in phase 8. The size of the corner vortex varies greatly over the 10 phases and λ varies from 2.4 to 4.3. The unidentified vortex above the passage vortex weakens as the wake passes. Figures 37 and 38 show the swirl strength and the vector fields outside of the wake and inside the wake respectively.
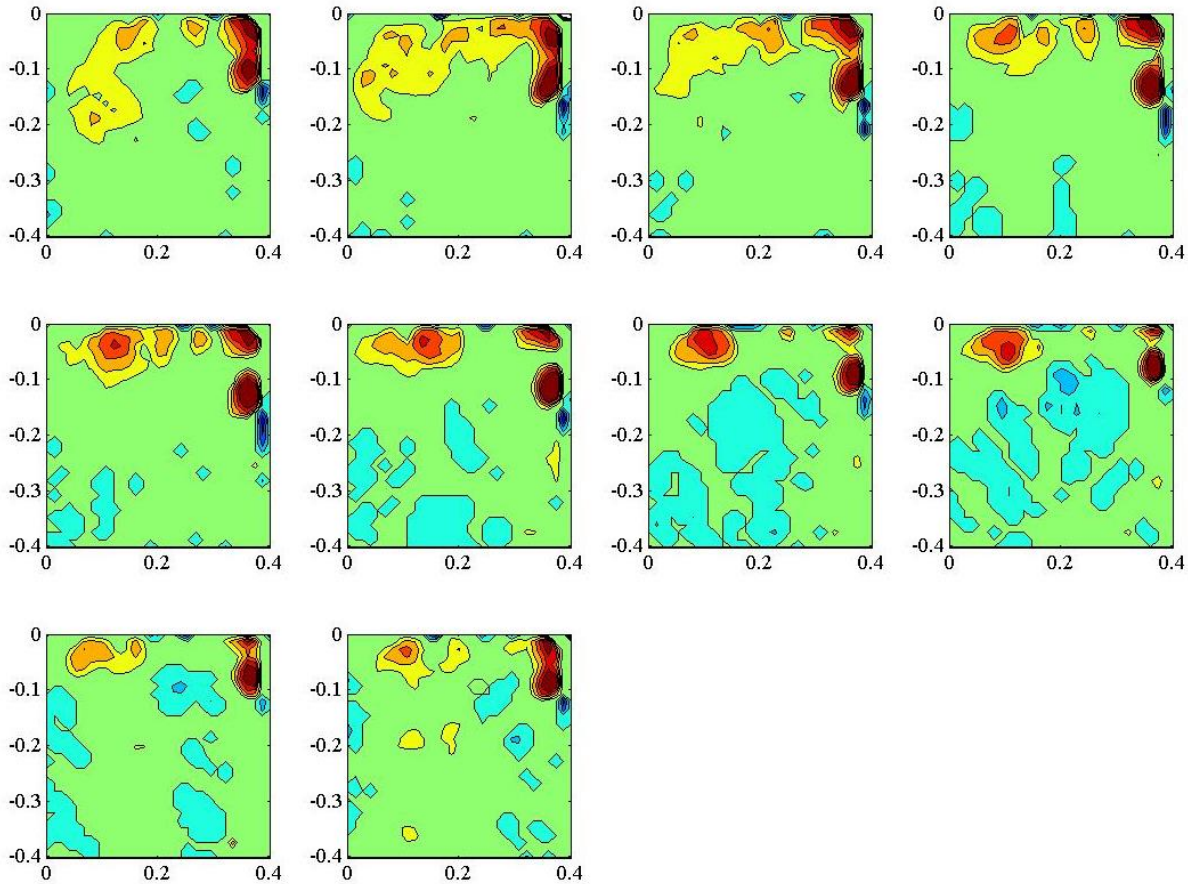

Figure 36 – λ for 10 phases of the wake in the 1 plane. The phases are separated by a delay t=0.1T
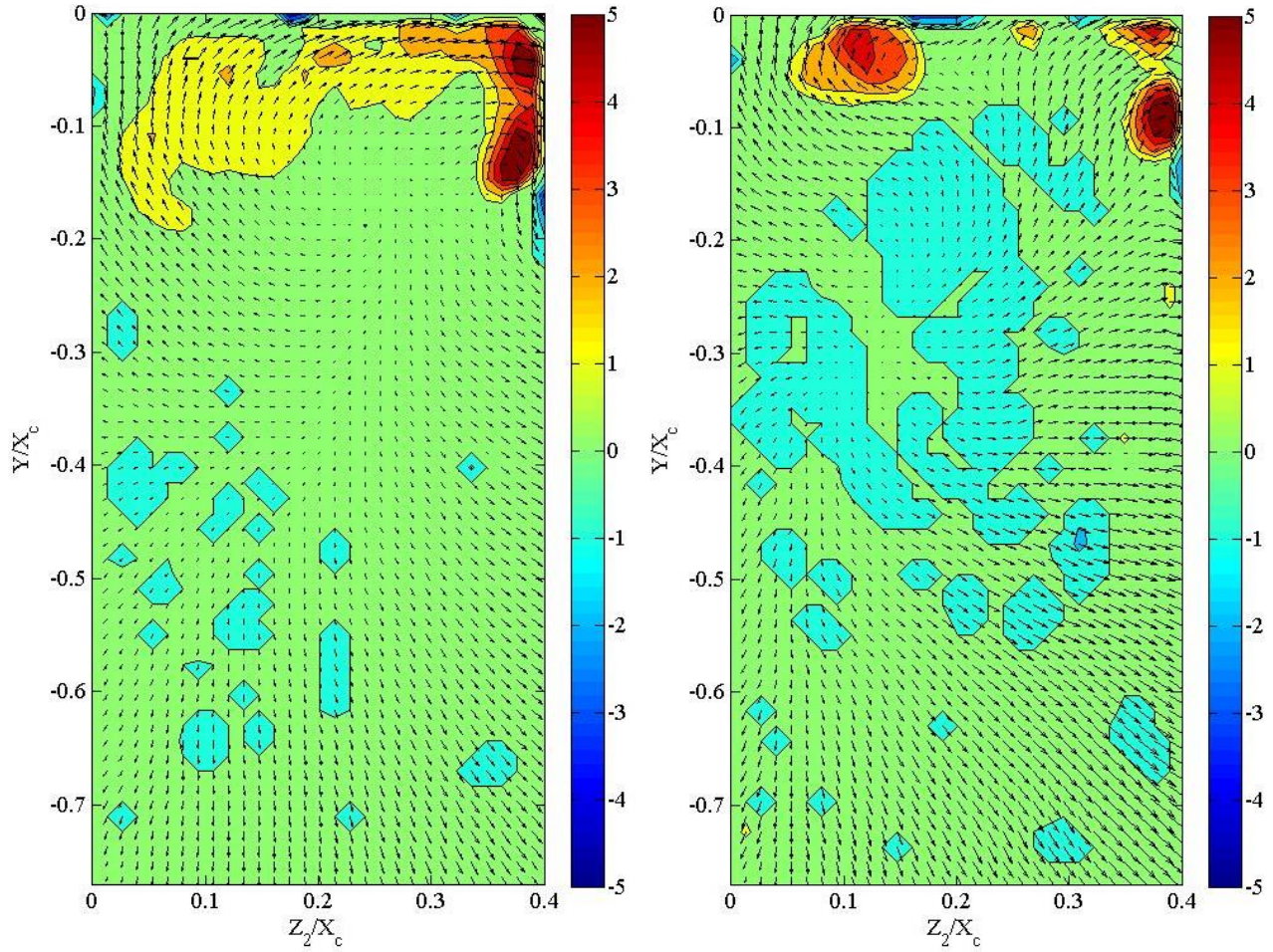
Figure 37 and 38 – λ in the 1 plane outside of the wake and inside of the wake with vector fields plotted

The 2 plane is perpendicular to the exit flow direction and tangent to the trailing edge of the suction side of passage 1. The 2 plane, as shown in Fig 12 shows the passage further downstream than the 1 plane. The vortices expand, and their rotational strength decreases. The measurements taken in the 1 plane, the steady measurements and the 10 phases of the wake, are repeated in the 2 plane. Figure 39 shows λ in the 2 plane with no wakes. The passage vortex, counter vortex and corner vortex are still visible. The passage vortex has expanded and decreased in strength with a maximum λ=2.97. The counter vortex has a maximum λ=-0.33. The corner vortex has a maximum λ=1.61. A new vortex located near the ceiling at Z_2/X_c =0.25 appears in the steady case and the cases with wakes. The swirl strength of the vortex is 1.61. The distance between the vortices has increased from the 1 plane.
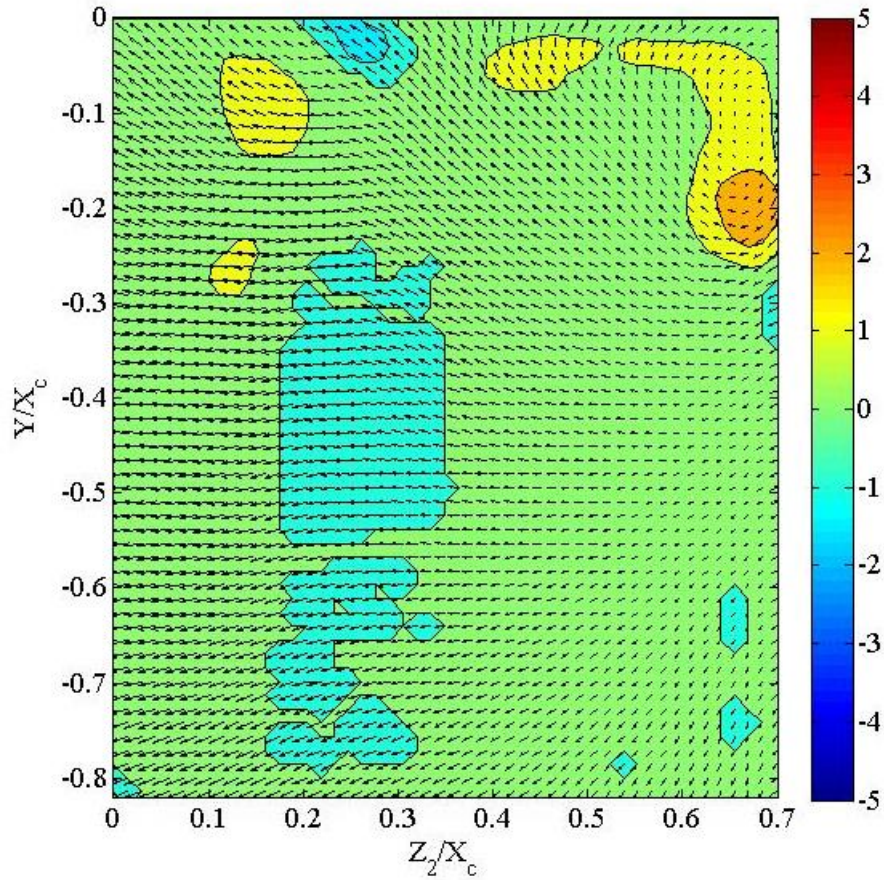
Figure 39 – λ for the steady case in the 2 plane with the vector field plotted

Figure 40 shows the normalized turbulence in the 2 plane at 10 phases of the wake's passage. The color levels are the same those in Fig 34 and range from 0 to 0.16 u_1. The average background turbulence intensity inside of the wake is approximately 0.11 u_1. The turbulence outside of the wake is approximately 0.04 u_1. The wake crosses the image plane in phase 1. The wake has moved out of the image plane by phase 6. The overall turbulence level created by the wake has decreased from the turbulence level seen in the 1 plane.
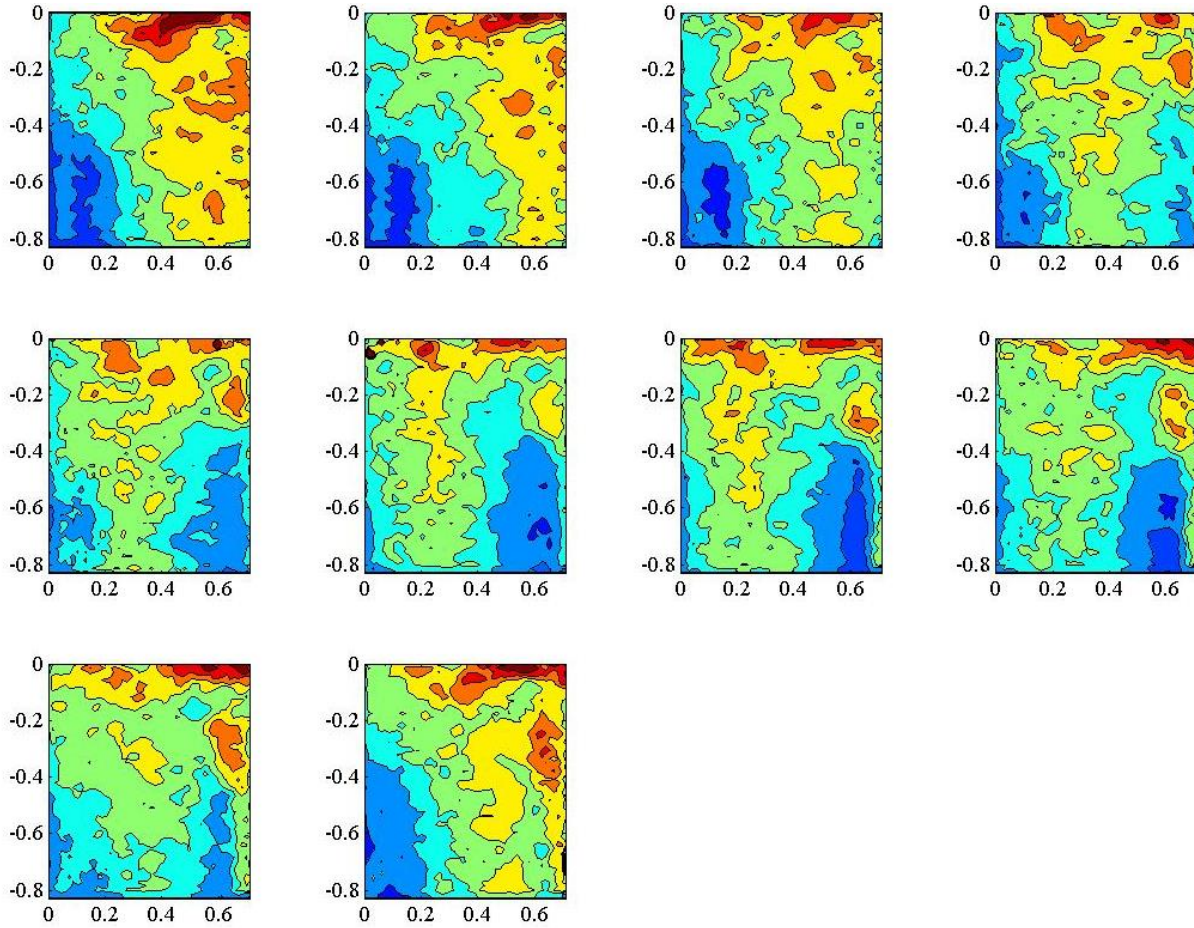
Figure 40 – w'/u_1 for 10 phases of the wake in the 2 plane. The phases are separated by a delay time of t =0.1T

Figure 41 shows the normalized swirl strength in the 2 plane at 10 phases of the wake's passage. The color limits are the same as those in Fig 34 and range from -5 to 5. The passage vortex does not move in the Z_2 direction. The passage vortex moves in the Y direction. The passage vortex is centered at Y/X_c = -0.16 during the phases inside of the wake and moves to Y/X_c = -0.23 outside of the wake. The passage vortex has a maximum λ = 3.6 in phase 1 and a minimum λ=2.0 in phase 5. The swirl strength of the passage vortex is generally higher in velocity fields affected by the wake and lower in phases outside of the wake. The vortex spinning the opposite direction beneath the passage vortex weakens to the point that it is not visible in phases 1, 2, 3, 9 and 10. The wake passes during these phases. The corner vortex is visible in all 10 phases and is located approximately at Z_2/X_c=0.16 and Y/X_c=0.13. The vortex spinning counter clockwise near the ceiling of the wind tunnel is consistently at Z_2/X_c=0.26 and Y/X_c=-0.015. This vortex was not seen in the 1 plane but is stronger than the corner vortex and has a maximum λ ranging from -1.5 to -2.0 through the 10 phases. Figures 42 and 43 show the swirl strength out of and in the wakes and the velocity fields in the 2 plane. Figure 42 has a similar structure to the steady case in the 2 plane.
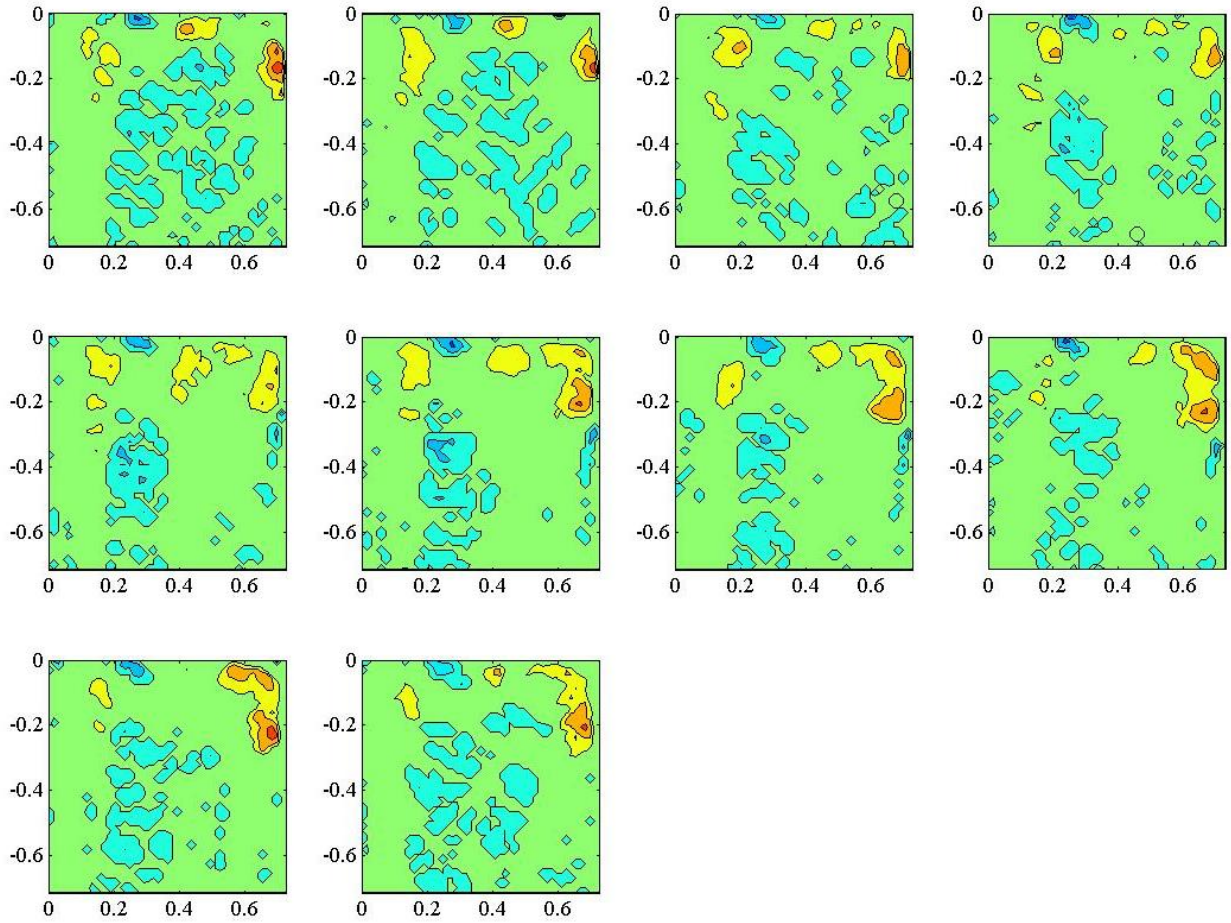
Figure 41– λ for 10 phases of the wake in the 2 plane. The phases are separated by a time delay of t=0.1T
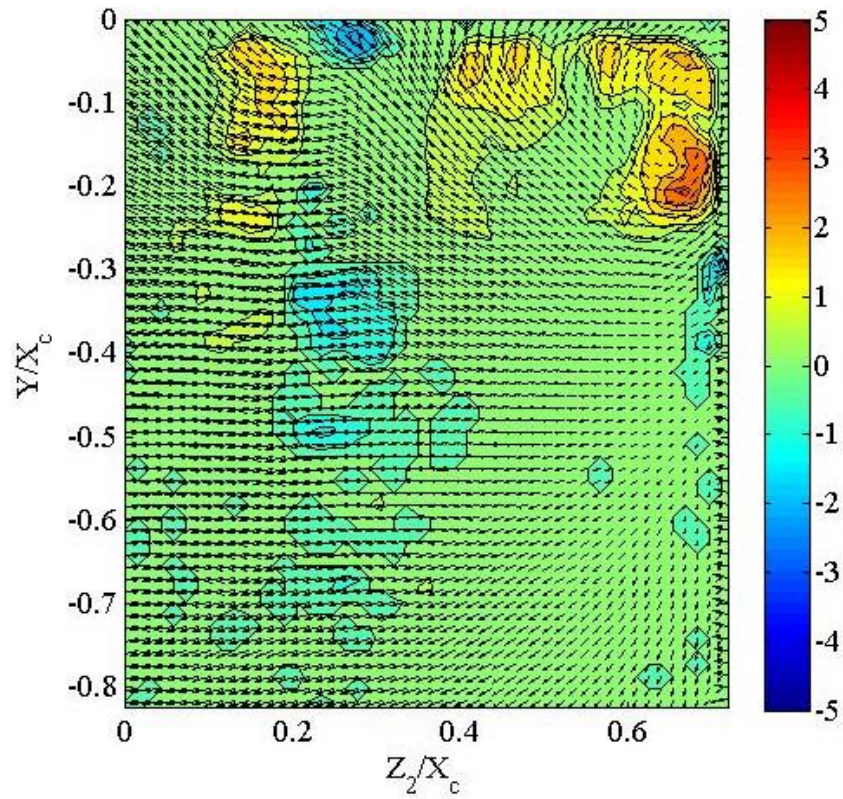
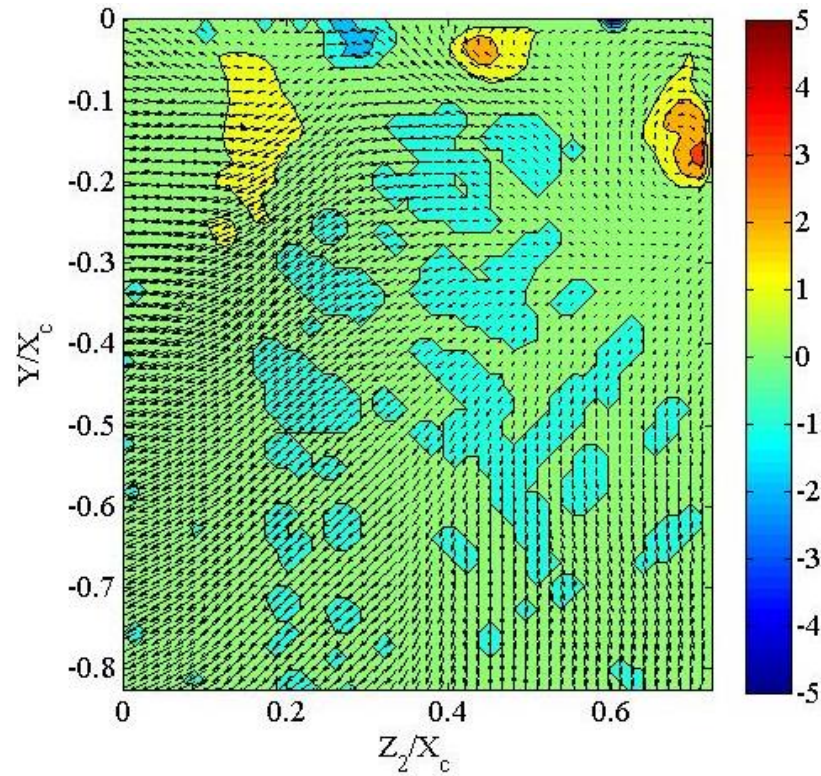**Figure 42– λ in the 2 plane outside of the wake**

Figure 43– λ in the 2 plane in the wake

The moveable ceiling of the wind tunnel was adjusted so that a tip gap of 2 mm was present. As shown in the pressure loss figures the tip gap allows flow from the high pressure side of the blade to flow through the gap to the low pressure side of the blade. This mass flow unloads the blade and creates a strong vortex. The velocity fields were collected in image planes 1 and 2 with steady flow and with wakes. The normalized turbulence and the swirl strength are plotted for the cases. Figure 44 shows the normalized turbulence for the steady case. The presence of the tip gap significantly increases the turbulence. The region of highest turbulence is the path the flow takes after leaving the tip gap. The surrounding circularly shaped turbulence rings correspond to the vortices created by the tip flow. The average turbulence in the darkest red portion at the center of the circular structure is approximately $0.42u_1$. The average turbulence of the region from the endwall to $Y/X_c = -0.35$ increased by 20% from the case with no tip gap. This region was chosen because it included all of the endwall flow effects as well as the effects from the tip gap vortex in both the 2 mm and 5 mm cases.

C
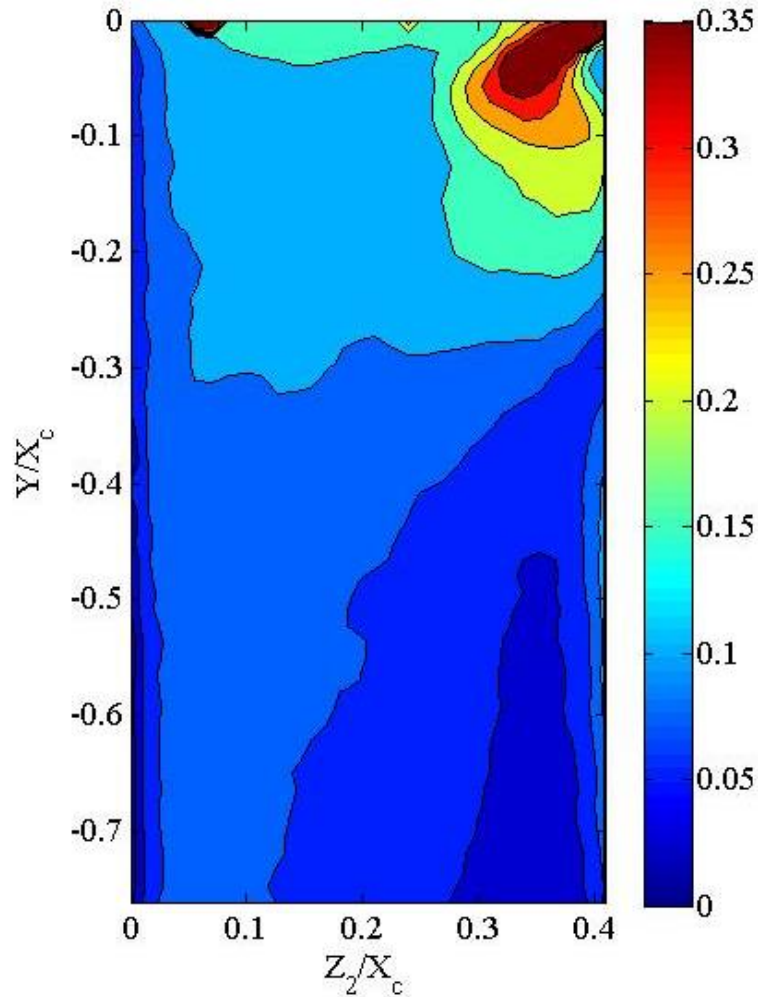
Figure 44 – w'/u_1 for the 1 plane with steady flow and a 2 mm tip gap

Exit Velocity Field with 2 mm Tip Gap

Figure 45 shows λ for the case with steady flow and a 2mm tip gap. The strongest vortex is no longer the passage vortex but the tip gap vortex, which spins counter clockwise. The tip gap vortex has a maximum λ=-13.1 which is nearly double the swirl strength from passage vortex in the case without tip gap. The tip gap vortex displaced the passage vortex which is now likely centered at Z_2/X_c=0.312 and Y/X_c=-0.015. The passage vortex has a maximum λ= 7.1 This similar to the strength of the passage vortex in the 1 plane with no tip gap. The vortex centered at Z_2/X_c=0.31 and Y/X_c=-0.18 has a maximum λ=4.3.
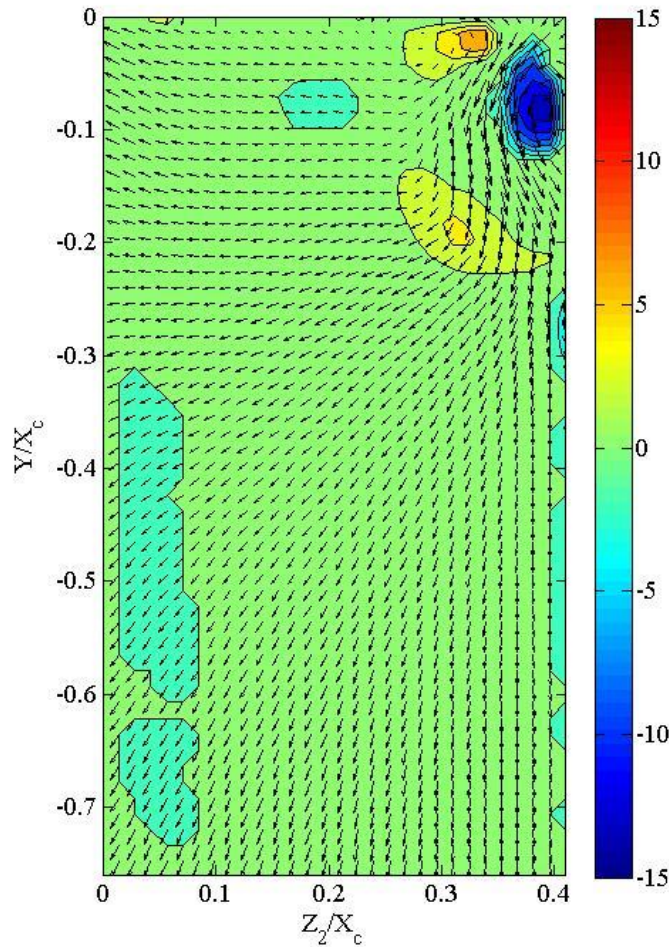

Figure 45 – λ for the steady case with 2mm tip gap in the 1 plane with the velocity field plotted

Figure 46 shows the normalized turbulence for the case with 2 mm tip gap at 10 phases. The color limits are set at 0 to 0.16. The range corresponds to that used in the case with no tip gap. The lower range causes a large area of turbulences of varying strengths to appear to be the same level. This range was selected because the wake can easily be seen passing in the lower half of the plots. The maximum turbulence seen is approximately $0.4u_1$. Phase 1 is outside of the wake as can be seen by the region of low turbulence of $0.06u_1$ near the suction side of the

passage. Phase 6 has the largest area of high turbulence and therefore is designated as the wake passing.
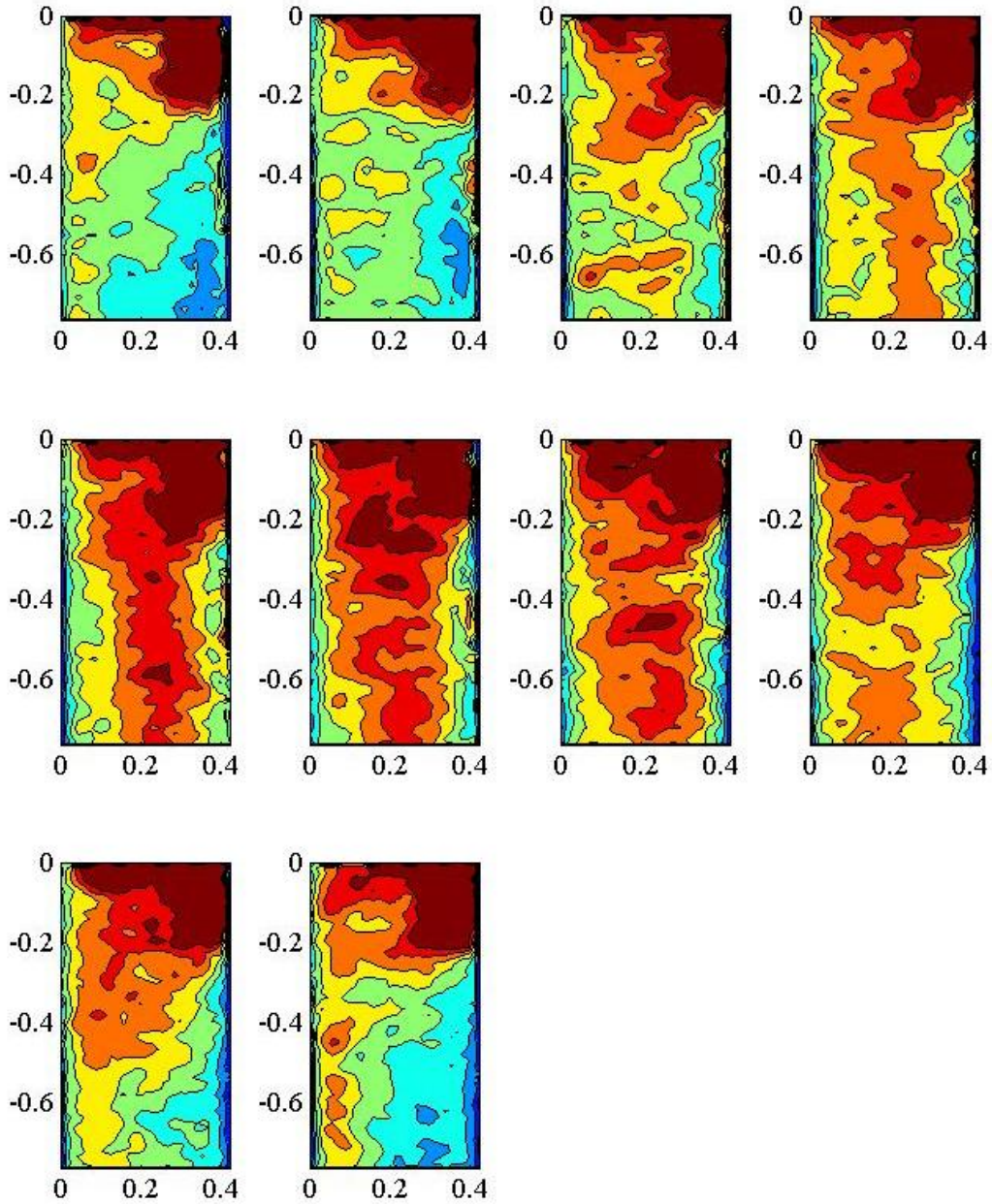

Figure 46 – w'/u_1 for the 10 phases of the wake in the 1 plane with a 2mm tip gap. The phases are separated by a delay time of t =0.1T

Figure 47 shows the normalized swirl strengths that correspond with the phases of turbulence in Fig 46. The color limits are -20 to 20 the same color limits used in Fig 45. The strength and the tightness of the tip gap vortices in the 1 plane prevents the wake from affecting its location or strength. The tip gap vortex is centered at Z_2/X_c=0.38 and Y/X_c =-0.085. The vortex has a constant width of 0.056 X_c and a height of .093 X_c in all 10 phases. The highest

swirl strength is $\lambda=-13.8$. The vortex at the endwall centered at $Z_2/X_c = 0.0325$ maintains a near constant shape and center in all phases. The passage vortex was relatively unchanged by the wake in the case without tips gaps. Thus it is not surprising that the passage vortex is consistent in the case with tip gap. The moved passage vortex has a maximum normalized swirl strength of $\lambda = 7.2$. The weaker vortex beneath the tip gap vortex centered at $Z_2/X_c=0.3$ and $Y/X_c = -0.2$ is affected by the wake and its maximum λ ranges from 3.5 to 4.7 through the 10 phases. Figures 48 and 49 show λ and the velocity fields for the cases outside and inside the wake respectively. The velocity fields show the strength and tightness of the tip gap vortex compared to the strength of the passage vortex seen in the case without tip gap.
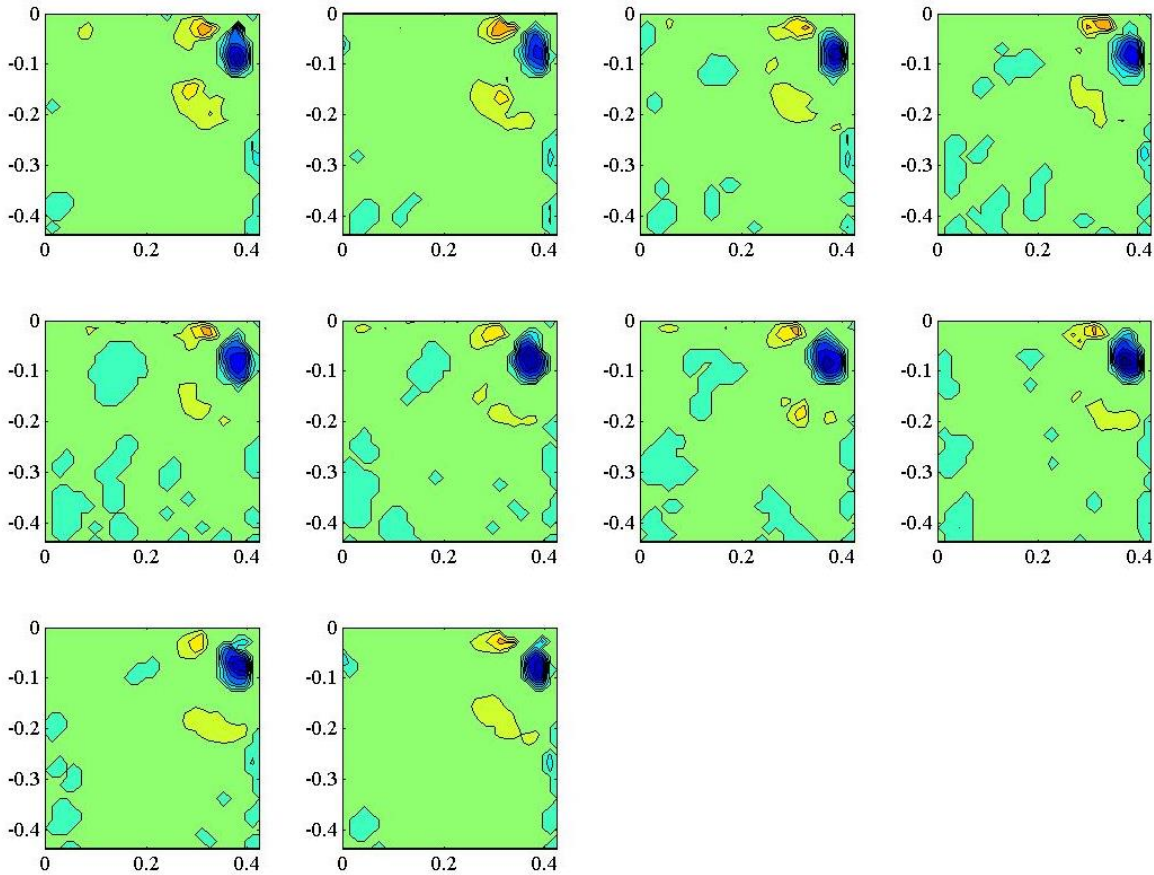

Figure 47 – λ for the case with 2 mm tip gap at 10 phases of the wake in the 1 plane. The phases are separated by a time delay of t=0.1T
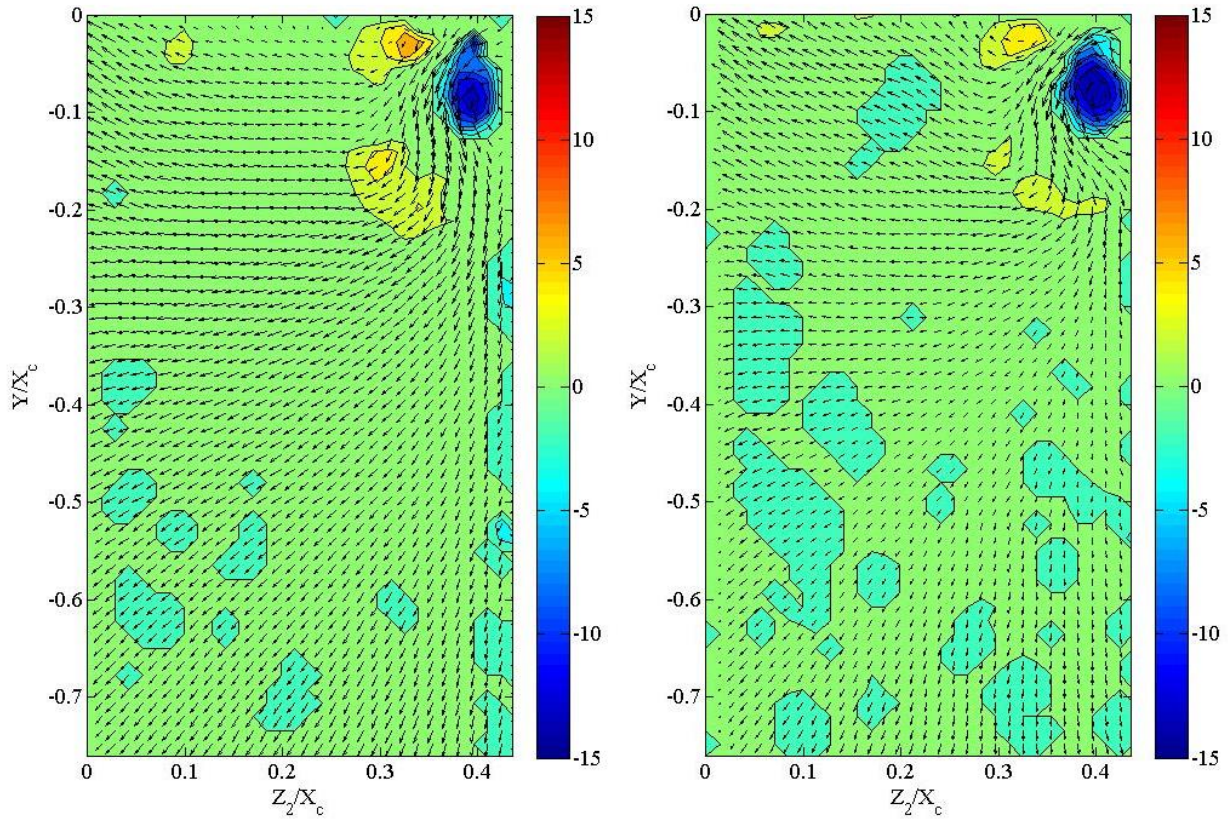
Figure 48 and 49 – λ for the case with 2mm tip gap in the 1 plane outside of the wake and inside of the wake. The velocity fields are plotted

The tip gap vortex expands and dissipates as it travels downstream. Figure 50 shows the swirl strength and velocity vectors for the steady case in the 2 plane. The tip gap vortex has decreased in strength and the maximum magnitude of $\lambda = -4.95$. The swirl strength of the tip gap vortex has decreased by 62% from the 1 plane. The tip gap vortex has expanded and has an approximate diameter of $0.17X_c$. The vortices to the left of and below the tip gap vortex have decreased in strength to $\lambda=1.37$ and $\lambda=1.41$. The vortex thought to be the passage vortex has decreased in swirl strength by 81% from the 1 plane. In comparison the passage vortex decreased in swirl strength by approximately 60% from the 1 plane to the 2 plane in the case without tip gap. The expansion of the tip gap vortex may weaken the passage vortex.
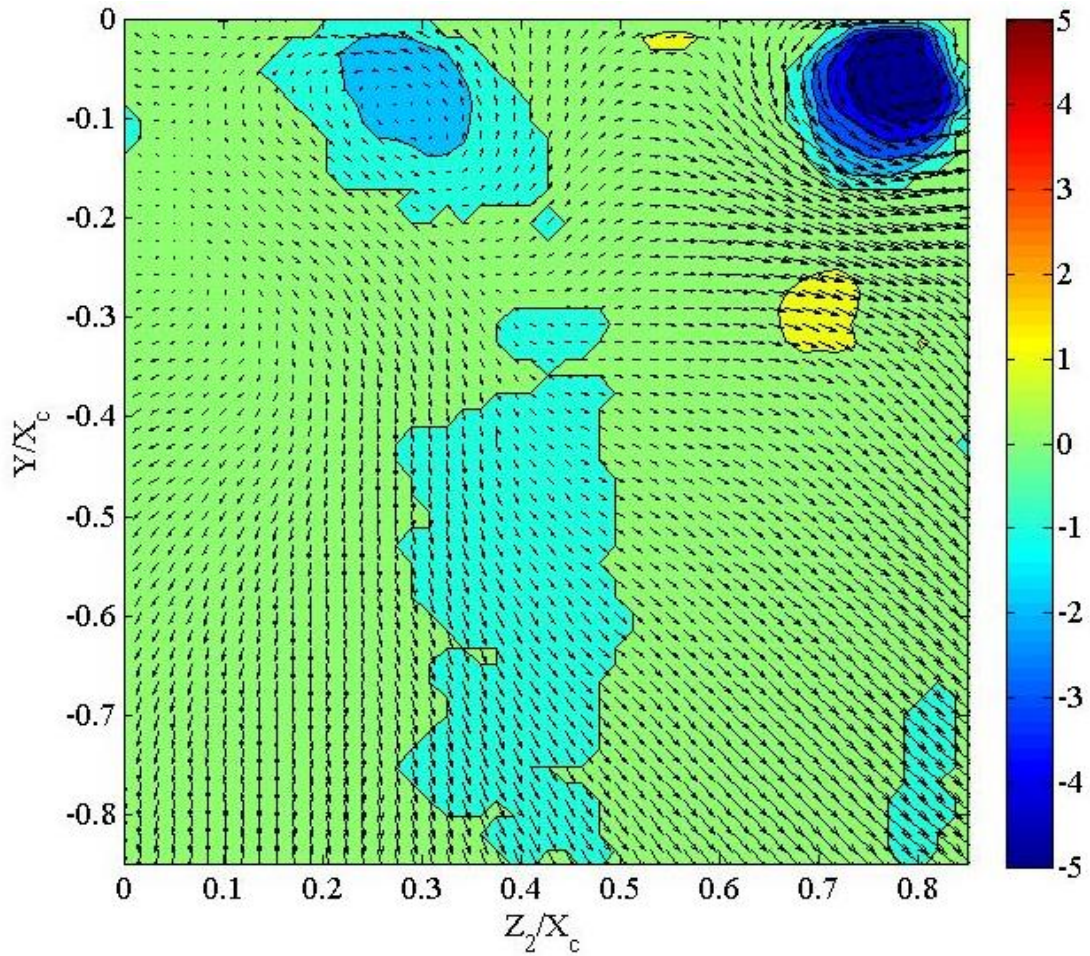
Figure 50- λ and the velocity fields in the 2 plane for the case with 2 mm tip gap and no wakes.

Figure 51 shows the normalized turbulence in the 2 plane for the case with a 2 mm tip gap and wakes. The figure shows the 10 evenly spaced phases of the wake. As with the previous cases the color limits are the same as those in Fig 35 and are set at 0 and 0.16 u_1 in order be able to clearly see the passage of the wake in the lower portion of the figure. Phase 5 is outside of the wake and has the lowest midspan turbulence intensity with a value of approximately 0.06 u_1 on the suction side of the passage. Phase 10 is inside of the wake and has a midspan turbulence intensity of approximately 0.11 u_1. The maximum turbulence is approximately $0.30u_1$.
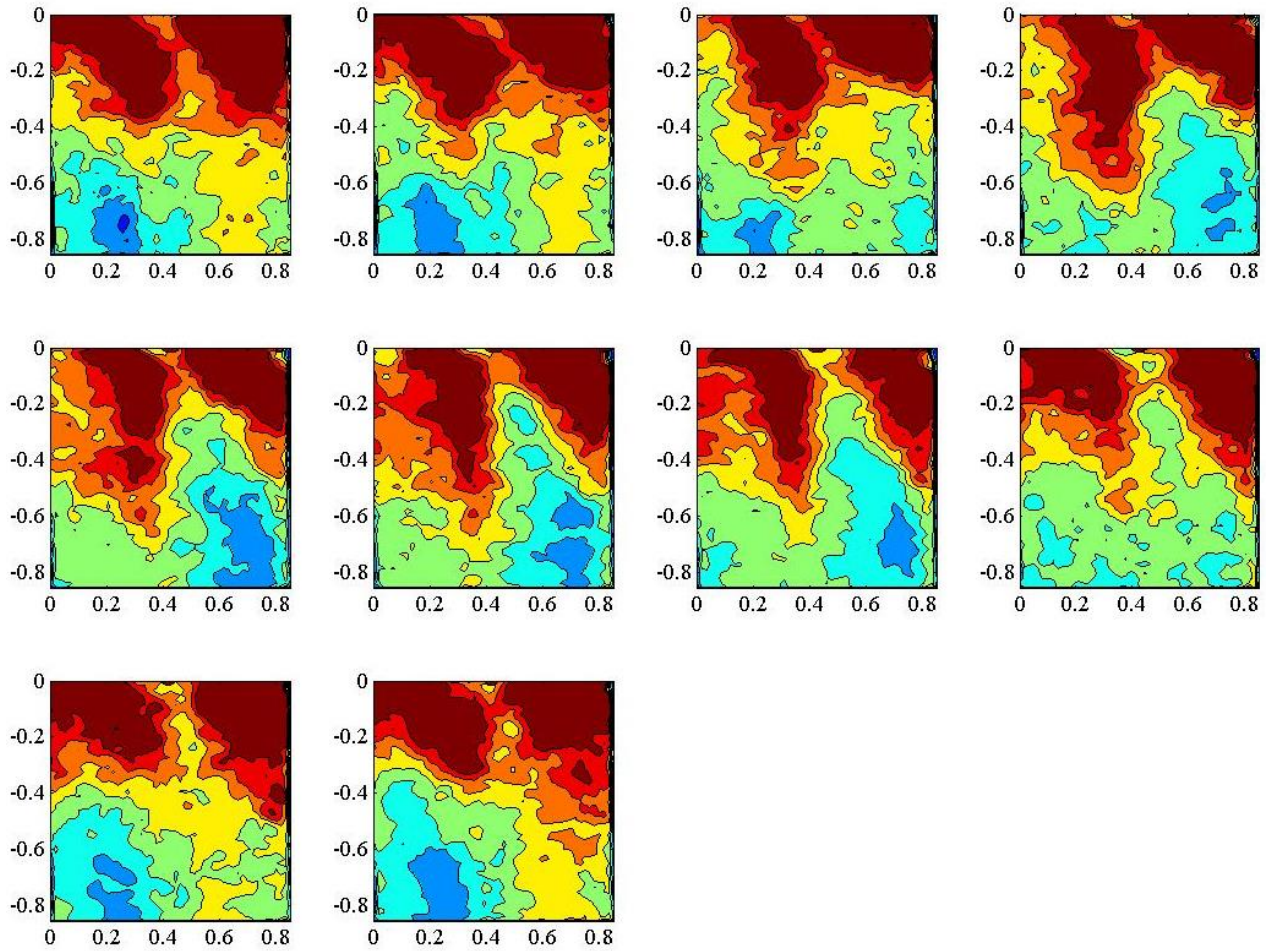
Figure 51 – w'/u_1 in the 2 plane for the case with a 2 mm tip gap and wakes. The phases are separated by a time delay of t=0.1T

Figure 52 shows λ for the 10 phases of the wake in the 2 plane. The color limits are -5 to 5 and are the same as those in Fig 50. The maximum λ for the tip gap vortex is approximately -7.0 in phase 9. The average value of λ for the center of the tip gap vortices for phases outside of the wake, phase 4 through 8, is approximately -4.5. The average value of λ for the center of the tip gap vortices for phases in the wake, phase 1 through 3 and 9 and 10, is approximately -3.3. The turbulence of the wake appears to weaken the tip gap vortex. The tip gap vortex changes size with a minimum diameter of approximately 0.11 X_c in phase 9 and a maximum diameter of approximately 0.21 X_c in phase 4. Figure 53 and Fig 54 show the swirl strength and velocity field for phases outside and inside the wake respectively. The change of size of the tip gap vortex caused by the wake's passage as well as the expansion and dissipation of the vortex from the 1 plane are clearly shown in the figures.
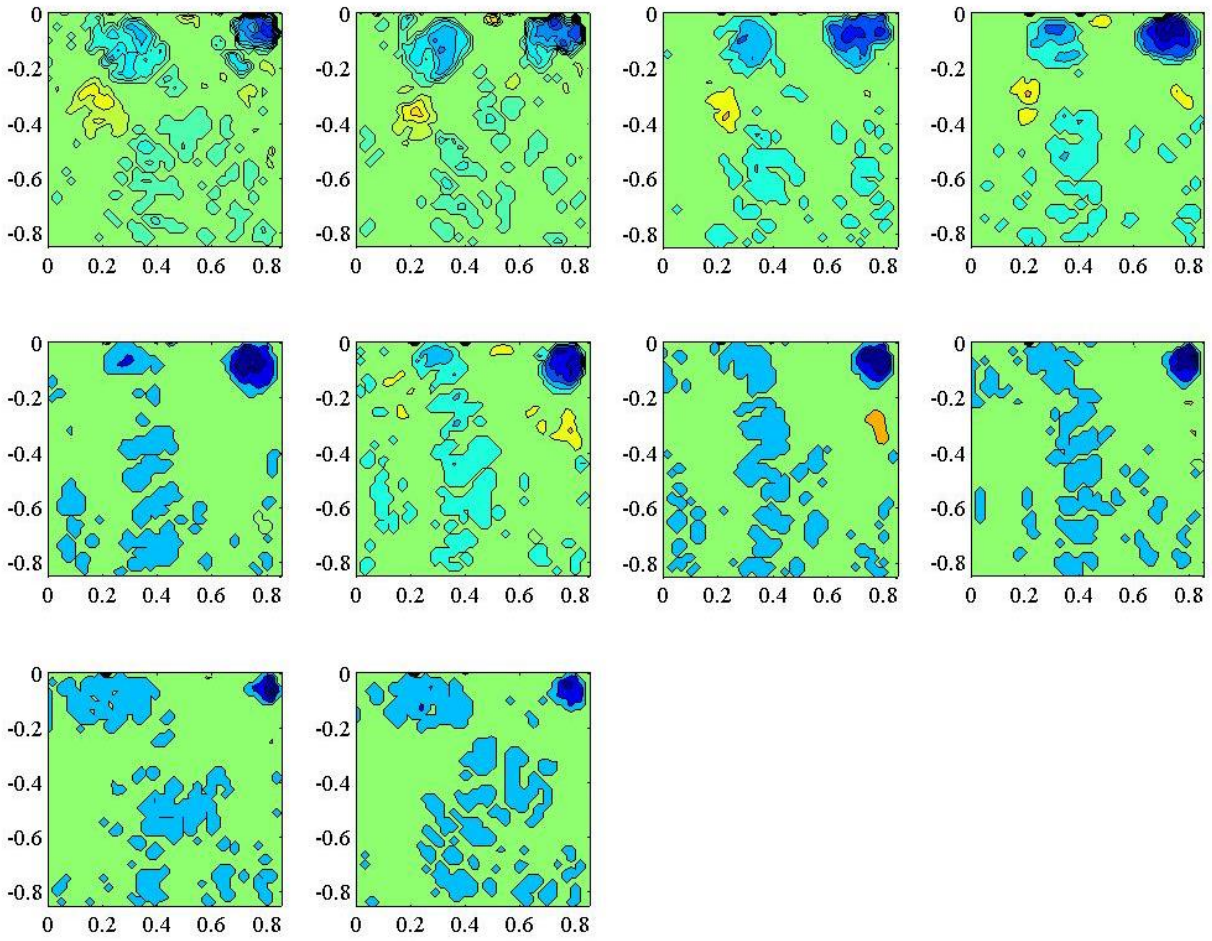
Figure 52 – λ in the 2 plane for the case with a 2 mm tip gap and wakes. The phases are separated by a time delay of t=0.1T
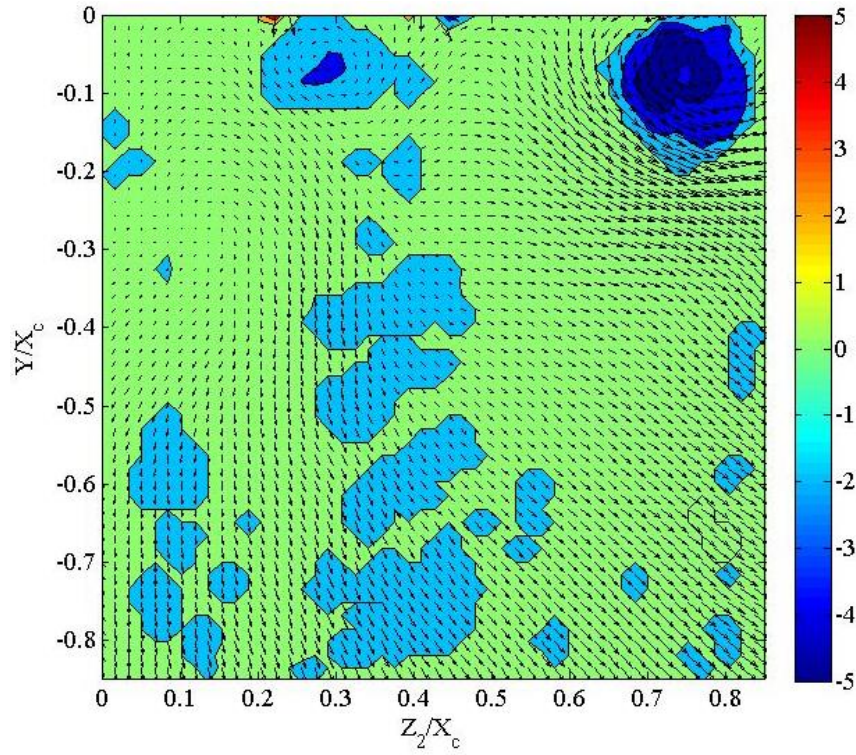
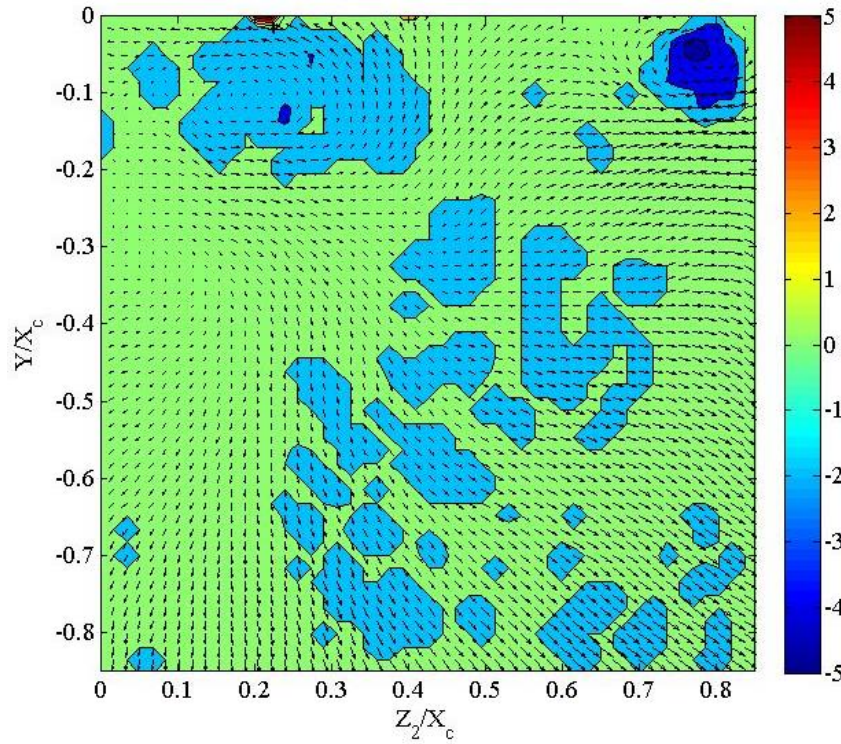**Figure 53- λ and the velocity field in the 2 plane for the case with 2 mm tip gap outside of the wake**

Figure 54- λ and the velocity field in the 2 plane for the case with 2 mm tip gap in the wake

Exit Velocity Field with 5 mm Tip Gap

The moveable ceiling of the wind tunnel was adjusted so that a tip gap of 5mm was present. As shown in the pressure loss figures the tip gap allows flow from the high pressure side of the blade to flow through the gap to the low pressure side of the blade. This mass flow unloads the blade and creates a strong vortex. The velocity fields were collected in image planes 1 and 2 with steady flow and with wakes. The normalized turbulence and the swirl strength are plotted for the cases. The 5 mm case allowed more flow though the tip gap creating larger losses and higher turbulence. Figure 55 shows the normalized turbulence for the steady case. The presence of the tip gap significantly increases the turbulence. The region of highest turbulence is the path the flow takes after leaving the tip gap. The surrounding circularly shaped turbulence rings correspond to the vortices created by the tip flow. The turbulence reaches a maximum of approximately 0.60 u_1 near the tip gap. The average turbulence in the darkest red portion at the center of the circular structure is approximately $0.43u_1$. The average turbulence of the region from $Y/X_c = 0$ to $Y/X_c = -0.35$ increased by 38% from the case with no tip gap and by 15% from the case with a 2 mm tip gap.
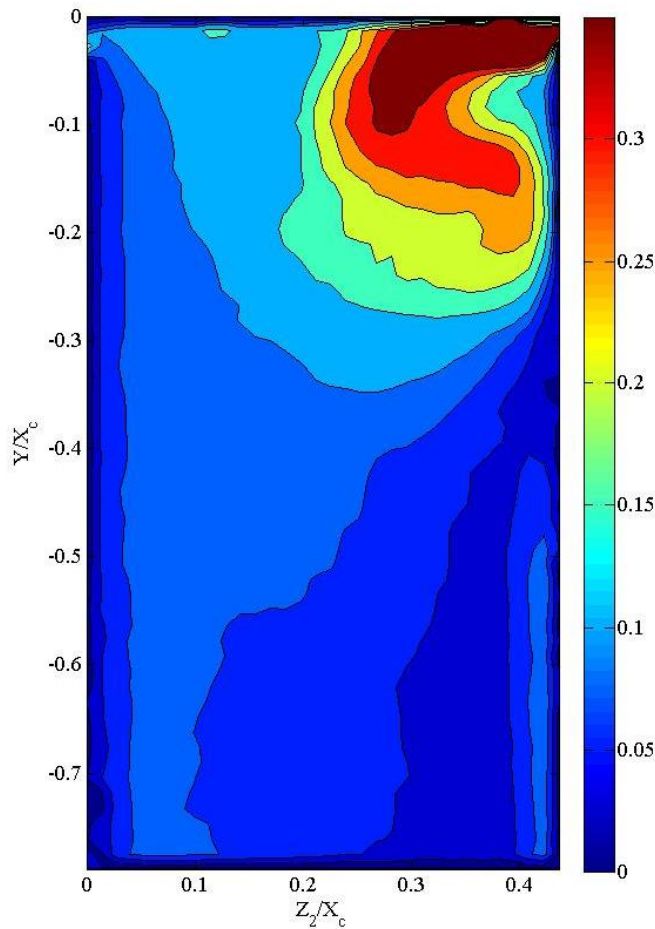

Figure 55 – w'/u$_1$ in the 1 plane for the case with steady flow and a 5mm tip gap

Figure 56 shows λ in the 1 plane for the case with steady flow and a 5 mm tip gap. The swirl strength reaches a maximum value of λ=-21.5 at $Z_2/X_c = 0.37$ and $Y/X_c= 0.14$. Increasing the tip gap from 2 mm to 5 mm increased the maximum λ by 64%. The passage and the induced vortices are no longer significant compared to the tip gap vortex.
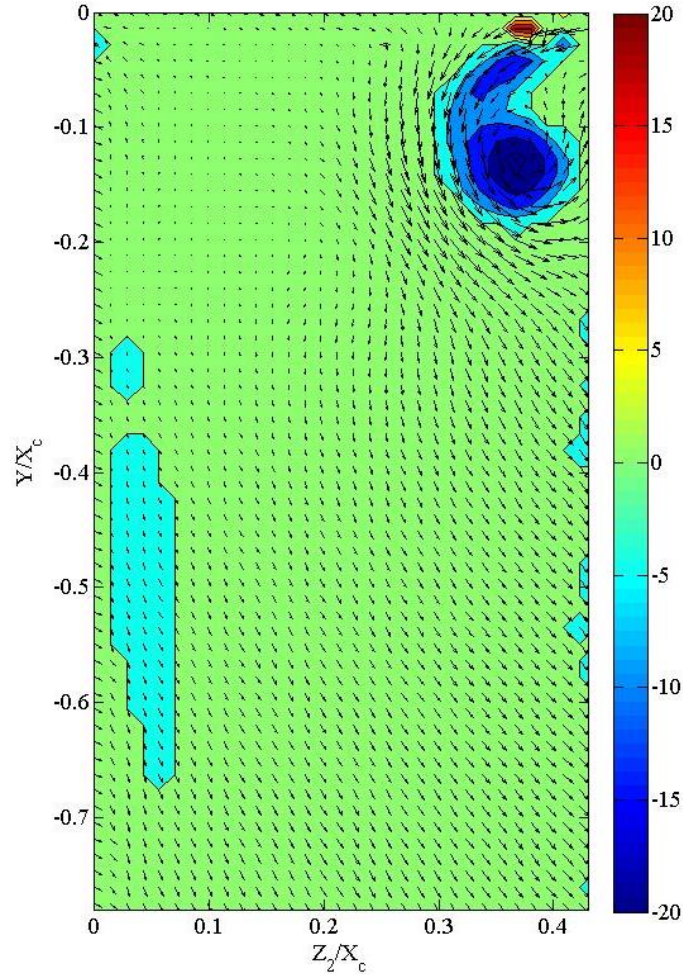

Figure 56 – λ and the velocity field in the 1 plane for the case with steady flow and 5 mm tip gap.

Figure 57 shows the normalized turbulence for the case with 5 mm tip gap at 10 phases. The color limits are those used in Fig 35 and are set at 0 to 0.16. The range corresponds to the range used in the case with no tip gap. The lower range causes a large area of turbulences of varying strengths to appear to be the same level. This range was selected because the wake can easily be seen passing in the lower half of the plots. Phase 2 is outside of the wake as can be seen by the region of low turbulence of $0.05u_1$ near the suction side of the passage. Phase 7 has the largest area of high turbulence and therefore is designated as the wake passing.
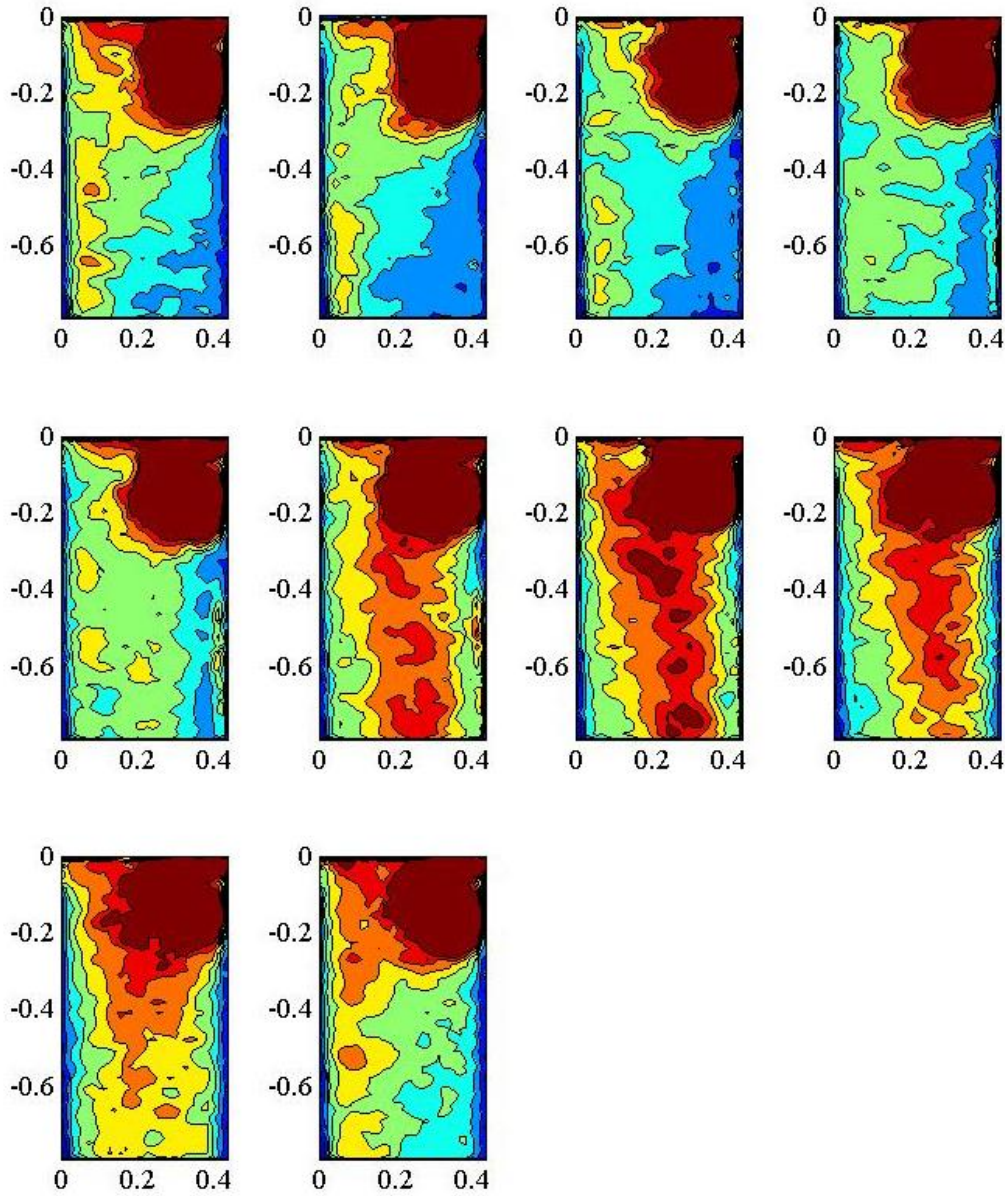
Figure 57- w'/u_1 in the 1 plane for cases with 5 mm tip gap and wakes. The phases are separated by a time delay of t=0.1T

Figure 58 shows the normalized swirl strength in the 1 plane with a 5 mm tip gap over 10 phases. The color limits are set at -20 and 20, the same as the steady flow case. The tip gap vortex is unaffected by the wake and is centered at $Z_2/X_c = 0.37$ and $Y/X_c = -0.14$. The tip gap vortex size does not change as the wake passes and the maximum normalized vorticity only varies from $\lambda=-21$ to $\lambda=-25$. No other vortices of the same magnitude appear and the small spots that do appear are not constant and are insignificant compared with the tip gap vortex created by a 5 mm tip gap.
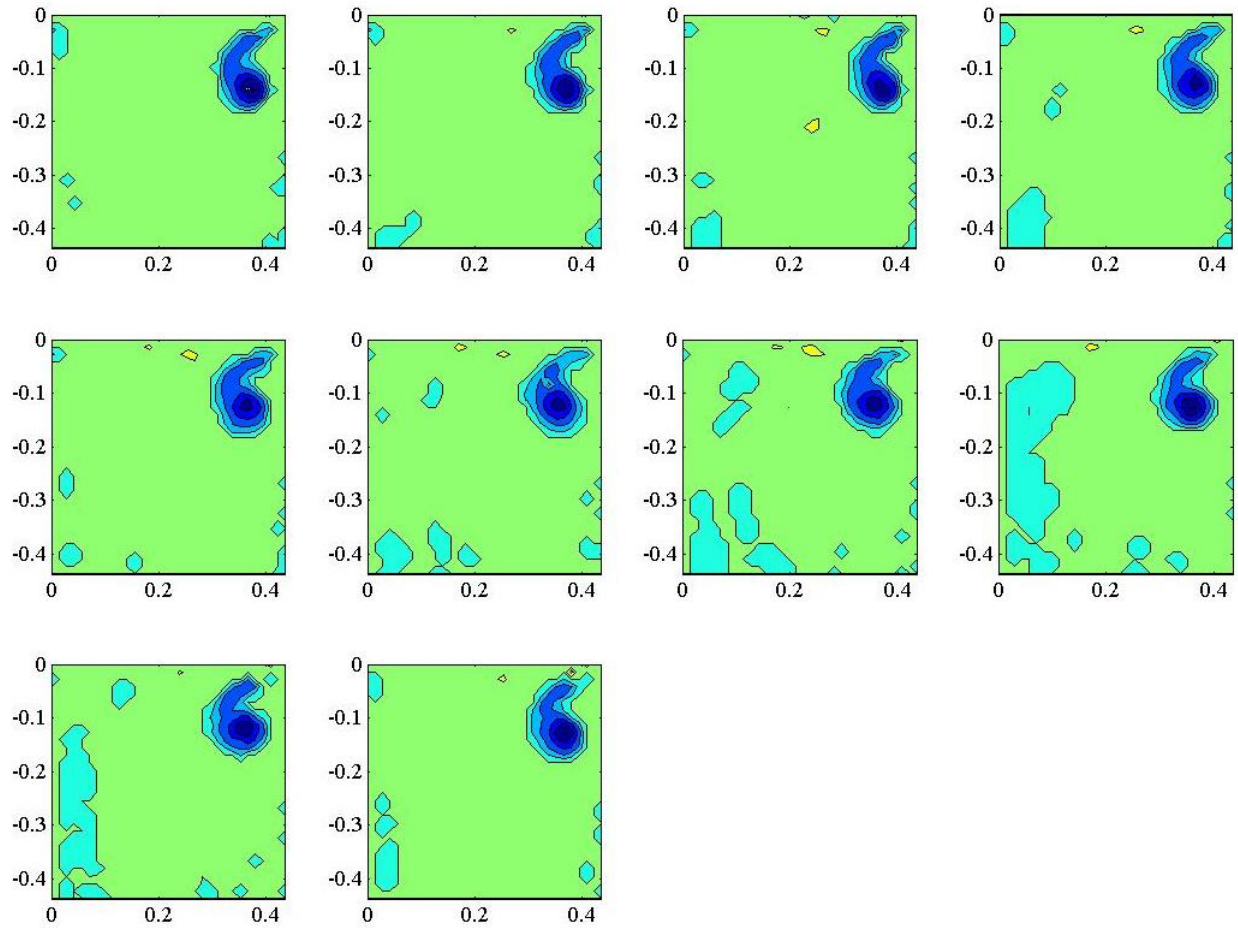
Figure 58- λ in the 1 plane for cases with 5 mm tip gap and wakes. The phases are separated by a time delay of t=0.1T

The tip gap vortex expands and dissipates as it travels downstream. Figure 59 shows the swirl strength and velocity vectors for the steady case in the 2 plane with 5 mm tip gap. The tip gap vortex has decreased in strength and the maximum λ= -5.01. The average λ for the central level of the swirl strength is approximately -4.3. The swirl strength of the tip gap vortex has decreased by 76% from the 1 plane. The tip gap vortex has expanded and has an approximate height of $0.20X_c$ and an approximate width of $0.32 X_c$. Vortices to the left of and below the tip gap vortices have appeared with an approximate strength of λ=2.2 and λ=1.41. These vortices were not visible in color scale set for the 1 plane.
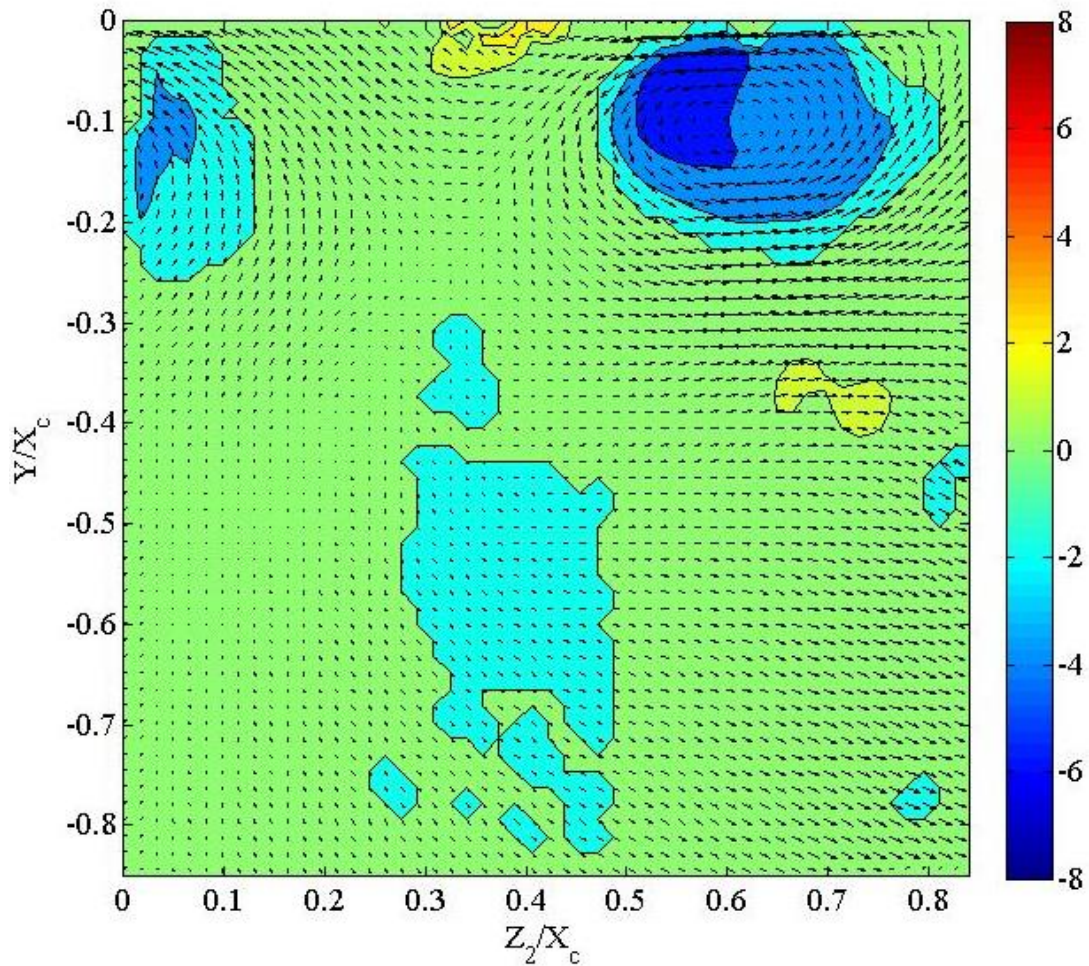
Figure 59- λ and the velocity field in the 2 plane with steady flow and a 5 mm tip gap

Figure 60 shows the normalized turbulence in the 2 plane for the case with a 5 mm tip gap and wakes. As before the figure shows the 10 evenly spaced phases of the wake. As with the previous cases the color limits are set at 0 and 0.16 u_1 in order be able to clearly see the passage of the wake in the lower portion of the figure. Phase 8 is outside of the wake and has the lowest midspan turbulence intensity with a value of approximately 0.04 u_1 on the suction side of the passage. Phase 2 is inside of the wake and has a midspan turbulence intensity of approximately 0.11 u_1.
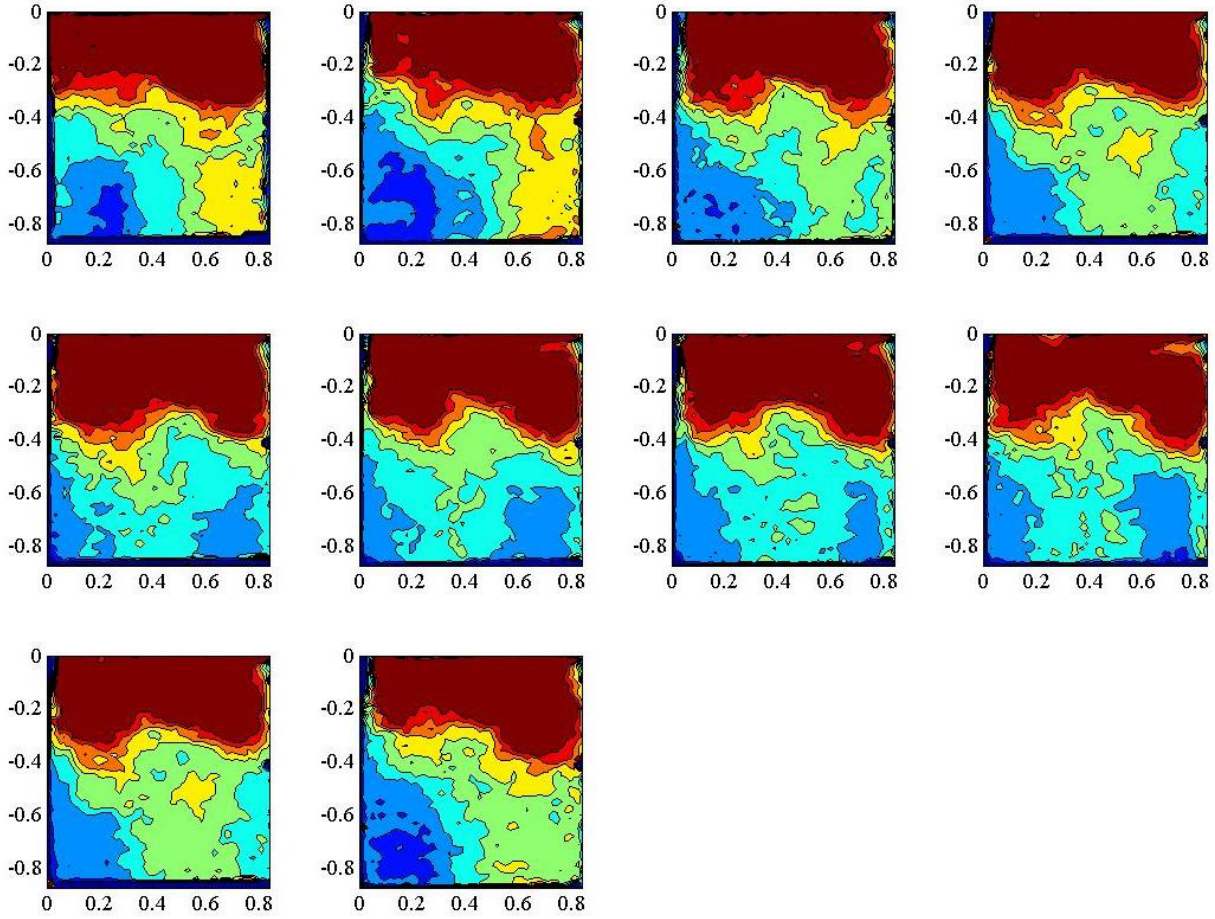
Figure 60 – w'/u_1 in the 2 plane for the case with a 2 mm tip gap and wakes. The phases are separated by a time delay of t=0.1T

Figure 61 shows λ for the 10 phases of the wake in the 2 plane. The color limits are -8 to 8 and are the same from Fig 59. The maximum λ for the tip gap vortex is approximately 5.5 in phase 5. The tip gap vortex changes size. The smallest tip gap vortex, which occurs in phase 3, has a height of approximately 0.19 X_c and a width of 0.24 X_c. The largest vortex, occurring in phase 8, has a height of 0.22 X_c and a width of 0.31X_c. Figure 62 and Fig 63 show the swirl strength and velocity field for phases outside and inside the wake respectively. The change of size of the tip gap vortex caused by the wake's passage as well as the expansion and dissipation of the vortex from the 1 plane are clearly shown in the figures.
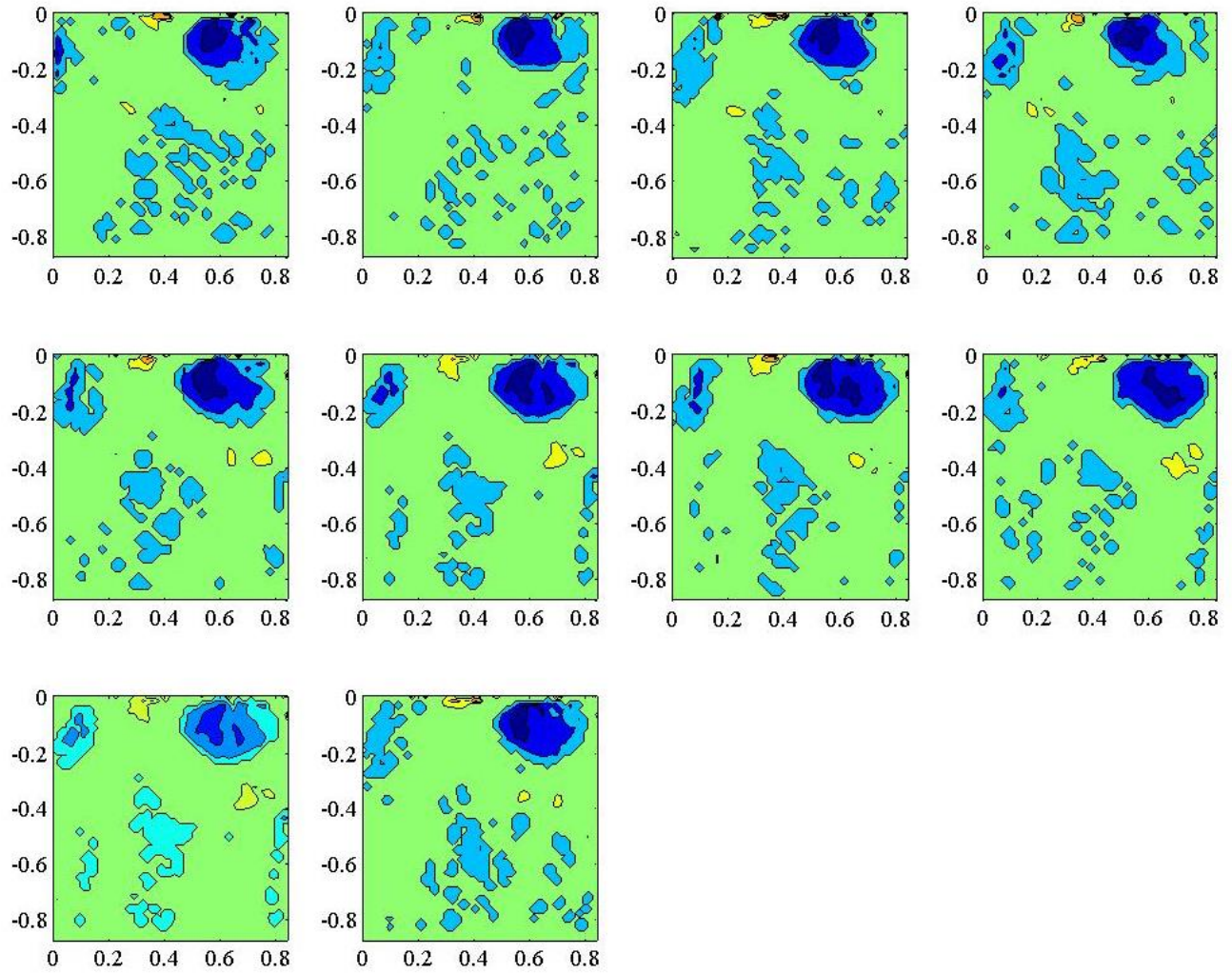
Figure 61 – λ in the 2 plane for the case with a 2 mm tip gap and wakes. The phases are separated by a time delay of t=0.1T
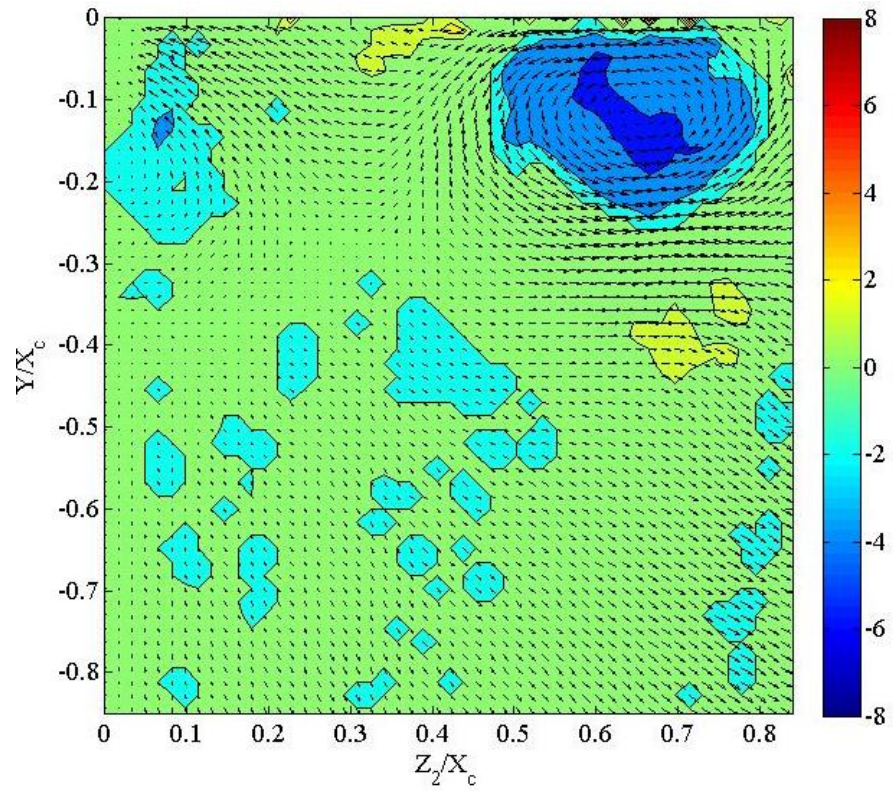
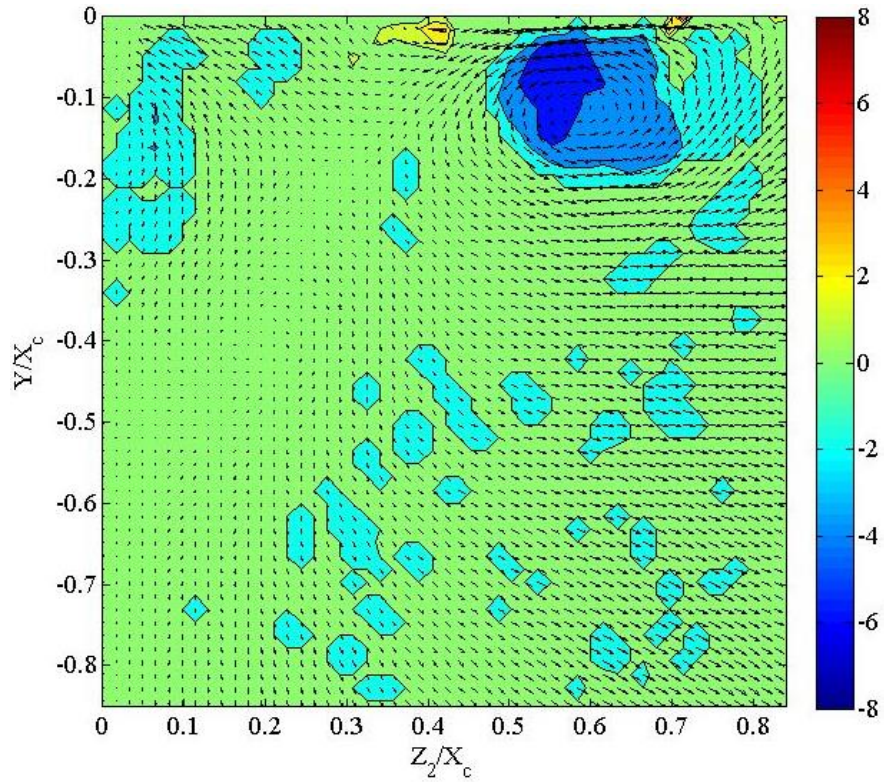**Figure 62 – λ and velocity field in the 2 plane for the case with a 5 mm tip gap outside of the wake**

Figure 63 – λ and velocity field in the 2 plane for the case with a 5 mm tip gap in the wake

57

Velocity Field and Pressure Loss Comparisons

        The PIV system was used to capture the velocity fields in the 3 plane parallel to the blade exit row where the pressure loss grids were taken. The swirl strength was calculated and the velocity field and swirl strength were compared directly to the pressure loss with the midspan profile subtracted. Figure 64 shows the velocity field overlaid on the pressure loss with no tip gap. Figure 65 shows the velocity overlaid on the swirl strength in the plane parallel to the blade exit row. The center of the passage vortex is above the region of high pressure loss. The velocities associated with the vortex increase as the distance from the center increases. These higher velocity areas that circle the vortices create the larger loss.

Figure 64 ψ and the velocity fields from the plane parallel to the blade exit row for the case with no tip gap.
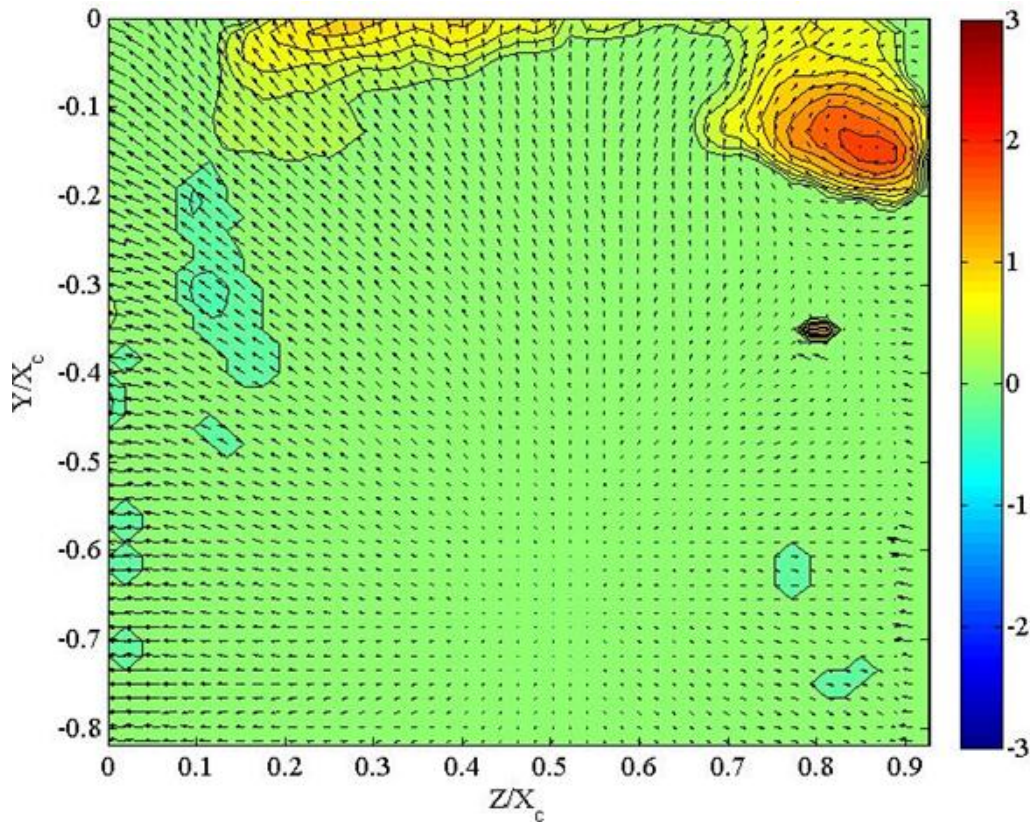
Figure 65 λ and the velocity fields from the plane parallel to the blade exit row for the case with no tip gap.

The pressure loss shown in Fig 66 is caused by the tip gap flow from the 2 mm tip gap, which can be clearly seen as the vortex spinning in the counter clockwise direction. The center of the vortex is above the center of the loss core because the higher velocity areas of rotating flow create higher pressure losses. Figure 67 shows swirl strength for the same region for comparison.
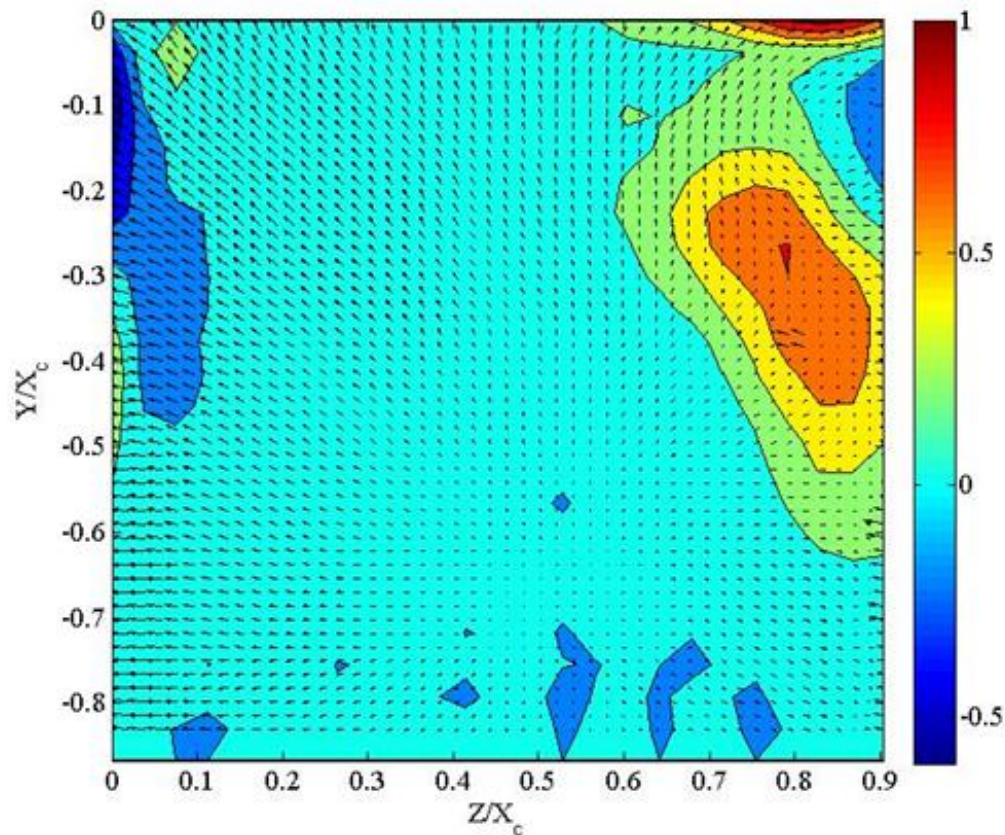
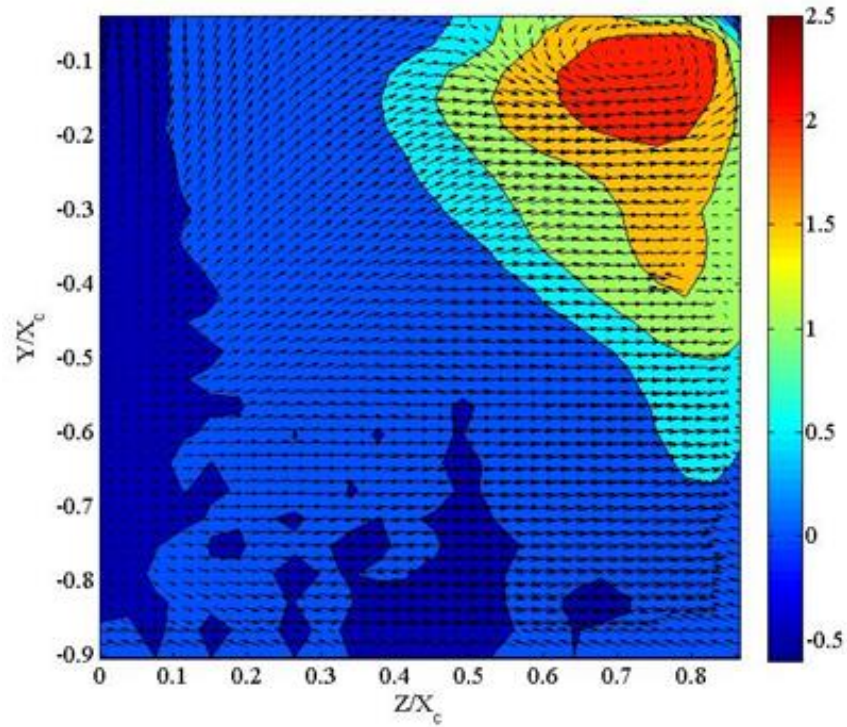**Figure 66 ψ and the velocity fields from the plane parallel to the blade exit row for the case with a 2 mm tip gap.**
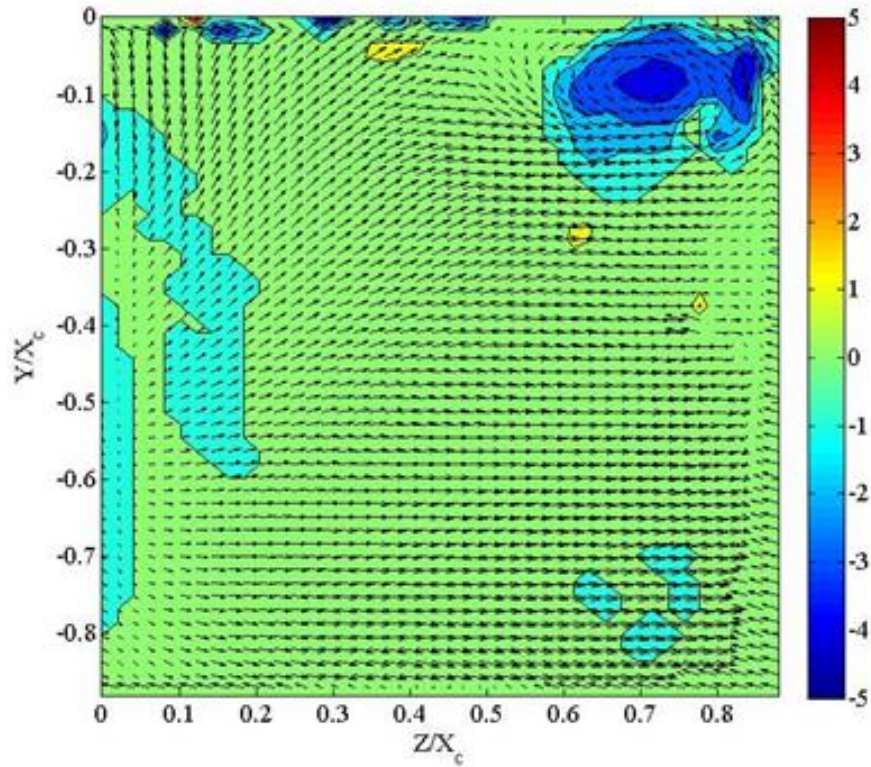

Figure 67 λ and the velocity fields from the plane parallel to the blade exit row for the case with a 2 mm tip gap.

The 5 mm tip gap case created the largest and highest region of pressure loss. The increased mass flow over the tip pushed the tip gap vortices further into the passage. Figure 68 shows the pressure loss core for the 5 mm case and Fig 69 shows λ. The location of the vortex which can be seen from the velocity field and from the swirl strength plot match the location of high pressure loss. Table 2 compares the effects of tip gap and wakes on the pressure loss. The steady flow case with no wakes is used as the base line. The 2mm tip gap increased the pressure loss by 98% from the case with no tip gap and the 5mm case increased the pressure loss by 120.1% from the case with no tip gap. The effect of the wakes on the pressure loss was much smaller than the effect of the tip gaps. The tip gap vortex was the leading cause of loss in this study.
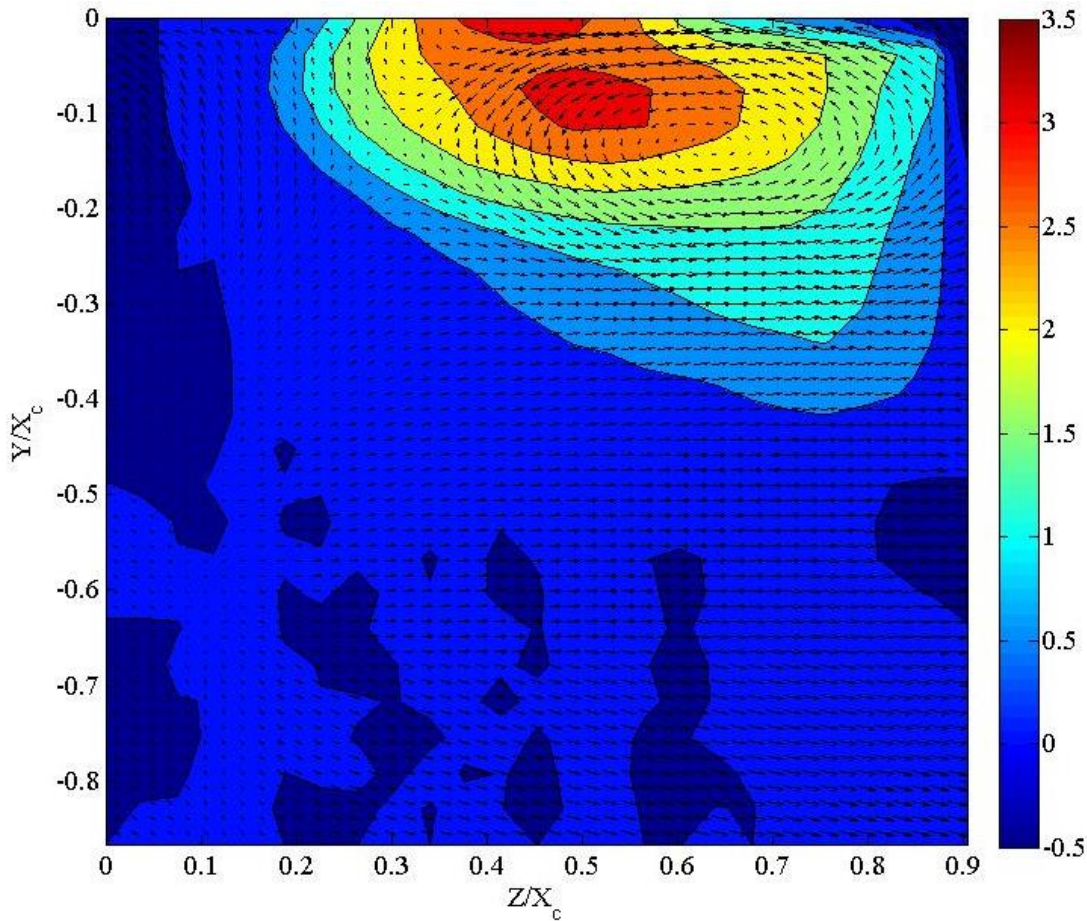
Figure 68 ψ and the velocity fields from the plane parallel to the blade exit row for the case with a 5 mm tip gap.
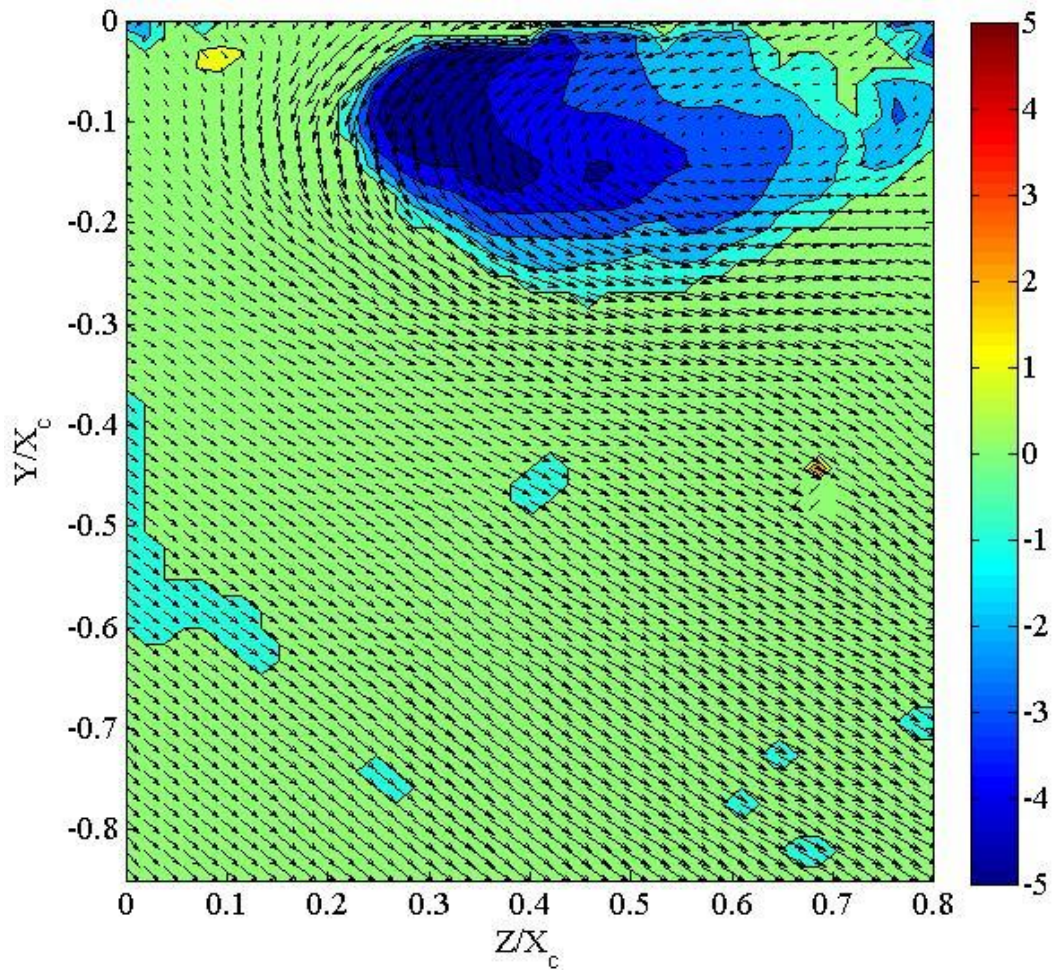
Figure 69 λ and the velocity fields from the plane parallel to the blade exit row for the case with a 5 mm tip gap.

Table 2-Comparison of ψ for different cases

Case	Average ψ for Steady flow	Average ψ for wakes	% increase from steady flow to wakes	% increase from no tip gap with steady flow	% increase from no tip gap with wakes
0 mm tip gap	0.243	0.327	34.7	N/A	N/A
2 mm tip gap	0.482	0.525	8.84	98.7	60.5
5 mm tip gap	0.535	0.626	17.15	120.1	91.7

Conclusions

The pressure measurements along the blades and the inlet velocity measurements were used to characterize the conditions in the experimental apparatus. The dynamic pressure

measurements taken at taps along the blades show that the flow through the two center passages is similar. The outer passages were present to make the conditions in the center two passages similar to those in a turbine passage. Testing the similarity of the center passages serves as a way to ensure that the flow in the center of the apparatus is unaffected by the wake generator axels and the sides of the tunnel. Additionally, the pressure measurements along the profile of the blades show that the flow does not separate from the blades. The dynamic pressure measured from the taps at the tips of the blades is lower than the dynamic pressure measured from the midspan taps. The lower dynamic pressures indicate that the velocity of the flow is slower in the boundary layer as expected. The ceiling was adjusted to create a 2 mm and 5 mm tip gap. The tip gap affected the pressure measured from the taps near the tips of the blades. There was no change in the midspan pressures. Finally, the pressure was measured along the blades when the wake generation system was running. The added turbulence from the wakes did not change the pressures along the blades for any of the cases. In order to see the effects of the wakes hot wire data were acquired.

The hot wire profiles were taken upstream of the blades and downstream of the rods. The hot wire profiles measured the inlet velocity from ceiling of the tunnel into the freestream of the flow. The hot wire profiles at the inlet of the passage show that the endwall boundary layer thickness is approximately 0.41 X_c. The turbulence reached a maximum at the near wall shear peak as expected and then decreased to the freestream value of 4% of the inlet velocity. The hot wire probes were used to measure the effects of the wake generation system because they measure the instantaneous velocity of the flow. The data from the hot wire were phase averaged so that the velocity inside the wake of the rod could be compared to the velocity outside of the wake. The velocity is lower in the wake than the velocity outside of the wake. Conversely, the turbulence at the inlet of the passages is highest in the wakes, and the turbulence outside of the wakes matches the turbulence from the case with steady flow. This shows that the flow returns to a lower state of turbulence similar to the case without wakes in between the passing of the wakes.

The pressure loss was measured downstream of the blades. The pressure loss is directly related to the aerodynamic losses. A pressure loss profile was measured downstream of the blades at the midspan. The pressure loss profile shows peaks behind the trailing edges of the blades. The pressure loss profile for the case without wakes was compared to the pressure loss profile with wakes. The pressure profile downstream of the blades shows that the rods increase the loss coefficient in the passages as well as downstream of the trailing edges of the blades. The turbulence introduced by the wake generation system increase the width of the loss peak caused by the trailing edge of the blade. Additionally the pressure loss was higher throughout the passage for the case with wakes.

A pressure loss grid was taken downstream of the blades from the endwall to the freestream. The pressure loss map showed a circular region of pressure loss where the passage vortex was located. The addition of wakes increased the overall pressure loss but did not move the circular region of high pressure loss. The addition of wakes to the case with no tip gap increased the pressure loss by 34.7%. The ceiling was adjusted to create a 2 mm tip gap and the pressure loss was measured. The region of high pressure loss moved and strengthened. The region of high pressure loss is associated with the location of the tip gap vortex. The presence of the 2 mm tip gap increased the pressure loss from the case without tip gap by 98.7%. The apparatus was adjusted to create a 5 mm tip gap and the pressure loss was measured. The region

of high pressure loss was larger, higher, and had shifted further into the passage due to the increased mass flow through the tip gap. The presence of the 5 mm tip gap increased the pressure loss from the case without tip gap by 120.1%. The tip gap vortex was the largest source of pressure loss and its effects were significantly larger than those of the wakes or the passage vortex.

PIV was used to map instantaneous velocity fields inside the passage of a turbine. These velocity fields showed the locations of vortices. The location of the vortices was found mathematically using swirl strength as a metric. The PIV data also showed how vortices reacted to the wake's passage. The PIV data showed that while the passage vortex responded to the passage of the wake, moving 0.05 X_c in the vertical direction, the structure of the flow in the passage never changed. This showed the locations and strengths of vortices were essentially stable and resistant to the effects of periodic turbulence. Additionally, the passage, counter and corner vortices were documented in the tests. The weaker portions surrounding the area of high swirl of the vortices disappeared during the passage of the wake. The velocity fields were collected in 2 planes perpendicular to the flow. The vortices expanded and moved relative to each other as they proceeded downstream from the 1 plane to the 2 plane. The tip gap vortices created by the 2 mm tip gap and the 5 mm gap showed that the tip gap vortices were much stronger than the passage vortex. The tip gap vortex displaced the passage vortex for both the 2 mm and 5 mm cases. Due to the strength of the vortices in the 1 plane, the tip gap vortex was completely unaffected by the wake passing. The tip gap vortex expanded and elongated from the 1 plane to the 2 plane and its strength was affected by the passing of the wake. Finally, velocity fields were measured in the plane where the pressure loss data were taken. The location of the passage vortex for the case with no tip gap and the tip gap vortex for the other two cases correlated to the region of high pressure loss. This shows that the pressure loss was a direct result of the aerodynamic loss caused by vortices.

In summation, this study showed that pressure losses associated with the effects of the tip gap vortex were the most significant source of loss. The locations and strength of vortices did not significantly change as a result of the turbulence from wakes passing. The magnitude of the pressure loss caused by the tip gap vortex shows research efforts should focus on decreasing the mass flow through the tip gap. A lower mass flow would create a weaker tip gap vortex and therefore create less pressure losses, creating a more efficient turbine design. Research into the effects of squealer tips will be conducted in the experimental apparatus used in this study. Squealer tips are turbine blade tips with small cavities cut into the tip of the blade. The concept behind the squealer tip is that flow will decelerate when it enters the cavity decreasing the overall mass flow. The effects of the squealer tips will be compared by using the data in this study as a baseline. The new study will show pressure loss changes as well as changes in the location and strength of the tip gap vortex. Ultimately this could lead to the implementation of better turbine tip designs and more efficient gas turbine engines.

References

Behr, T., 2007, "Control of Rotor Tip Leakage and Secondary Flow by Casing Air Injection in Unshrouded Axial Turbines," Doctor of Sciences Thesis, ETH Zurich.

Bindon, J. P.,1989. "The measurement and formation of tip clearance loss," *ASME Journal of Turbomachinery*, Vol.111, pp. 257–263.

Cengel, Y. A. and Boles, M.A., 2002, "Thermodynamics: An Engineering Approach," McGraw Hill, Ed. 4, p. 471

Dantec Dynamics, Particle Image Velocimetry measurement principles, 10 Jan. 2012, < http://www.dantecdynamics.com/Default.aspx?ID=1049>.

Denton, J.D., 1993, "Loss Mechanisms in Turbomachines," *ASME J. Turbomachinery*, Vol. 115, pp. 621-656.

European Commission, 2004, Turbine Aero-Thermal External Flows 2, 7 Jan. 2012, < http://ec.europa.eu/research/transport/projects/items/tatef_2_en.htm>.

Halila, E.E., Lenahan, D.T., and Thomas, T.T., 1982, "Energy Efficient Engine High Pressure Turbine Test Hardware Detailed Design Report," NASA CR-167955.

Harvey, N.W., 2004, "Aerothermal Implications of Shroudless and Shrouded Blades," VKI Lectures Series 2004-02, "Turbine Blade Tip Design and Tip Clearance Treatment".

Langston , L.S., 1980, "Crossflows in a Turbine Cascade Passage," *ASME J. Engineering for Power*, Vol. 102 pp. 866–874.

Hodson, H.P., and Howell, R.J., 2005, "Bladerow Interactions, Transition, and High-Lift Aerofoils in Low-Pressure Turbine," *Annual Review of Fluid Mechanics*, Vol. 37, pp. 71-98.

Payne, S.J., Ainsworth, R.W., Miller, R.J., Moss, R.W., and Harvey, N.W., 2003, "Unsteady loss in a high pressure turbine stage", *Int. J. Heat and Fluid Flow*, Vol. 24, pp. 698–708.

Pratt and Whitney, 2002, Cutaway – PW4000-112" Engine, 3 Jan. 2012, <http://www.pw.utc.com/presskit/images/pw4000112_cutaway_high.jpg>.

Sharma, O.P., Renaud, E., Butler, T.L., Milsaps, K., Dring, R.P., and Joslyn, H.D., 1988, "Rotor-Stator Interaction in Multistage Axial Flow Turbines," AIAA Paper 88-1033.

Volino, R.J., 2010, "Effect of Unsteady Wakes on Boundary Layer Separation on a Very High Lift Low Pressure Turbine Airfoil," ASME paper GT2010-23

Wang, H.P., Olson, S.J., Goldstein, R.J. and Eckert, E.R.G., 1997 "Flow visualisation in a linear turbine cascade of high performance turbine blades," *ASME Journal of Turbomachinery*, Vol. 119, No. 1, pp. 1-8.